SYNTHESIS OF MODIFIED POLYVINYL ALCOHOL AND CARBON NANOTUBE COMPOSITE MEMBRANE FOR THE PURIFICATION OF WATER

KWENA SELBY MAPHUTHA

A thesis submitted to the Faculty of Engineering and the Built Environment, University of the Witwatersrand, in fulfilment of the requirement for the Degree of Doctor of Philosophy in Engineering.

Johannesburg,

2014

DECLARATION

I declare that this thesis is my own, unaided work. It is being submitted for the degree of Doctor of Philosophy in the University of Witwatersrand, Johannesburg. It has not been submitted before for any degree or examination in any other University.

_____

(Signature of candidate)

_____ Day of _____

ABSTRACT

Water is one of the most important resources we have on earth and finding ways to maintain it is important. It has been found that the main pollutant discharge to water sources is oily wastewater which is produced by a lot of different industries. The aim of this thesis was to produce a membrane that can remove synthetic oil from water at reasonable flow rates. Since membranes are generally fragile, the mechanical properties of the membrane are enhanced by the addition of carbon nanotubes (CNTs). Carbon nanotubes are cylindrical graphite sheets that are produced from a carbon source (such as acetylene) and, depending on the method of production, a metallic catalyst. One of the most commonly used catalysts is ferrocene which is relatively cheap and easy to produce. Thus in this study an attempt was made to produce carbon nanotube by using ferrocene as both the carbon source and the catalyst. This was done in a chemical vapour deposition reactor (CVD) at temperatures between 800^{o}C and 950^{o}C. The product was analysed using transmission electron microscopy and Raman spectroscopy. It was found that CNTs are produced at all the tested temperatures and that at higher reaction temperatures, there was less adherence of the product to the walls of the reactor. Raman spectroscopy of the samples showed that MWCNTs were produced. Membrane filtration has been established as a widely used method for water purification and various filtration techniques are capable of removing synthetic oil from water. There are 2 major problems with membranes, which are fouling and concentration polarization. The fouling was addressed by using polyvinyl alcohol, which is highly hydrophilic in nature, as the top layer in a thin film composite membrane and thus by using it as the layer that comes into contact with the solution fouling can be

decreased. The bottom layer of the thin film composite membrane was a polysulfone membrane. Concentration polarization was looked at by conducting a study which determined whether concentration polarization can be decreased by increasing turbulence over the membrane. A representation of a singular tube in a tubular module, a polysulfone membrane (ultrafiltration membrane) and twisted tape were used for the tests. The twisted tape was used to induce turbulence in the tube. The addition of a twisted tape to the tube increased the stable flux by 72% and it reduced the rate at which the flux decreased from -14.99 to -5.51 L/(hm^2)/min. Carbon nanotubes were added to the polysulfone layer in order to increase the mechanical strength of the bottom support layer of membrane. The membrane structure was characterised by scanning electron microscopy and BET analysis. Increasing the CNT concentration in the membrane increased the pore sizes and the number of pores. The BET analyses showed that there is a 46% increase in the pore size between 0% CNT and 5% CNT concentrations and a 68% increase in pore size from 0% to 10% CNT concentration increase. The addition of CNTs to the polymer matrix also had an effect on the mechanical strength of the membranes with a peak mechanical strength increase obtained at a CNT concentration of 7.5%. At the concentration of 7.5% CNT in the polymer composite, a 119% increase in the ultimate tensile strength, 77% increase in the Young's modulus and 258% increase in the membrane toughness were seen indicating the suitability of the membrane in practical applications. Increasing the trans-membrane pressure decreased the membrane rejection of oil but increased flux. There is a trade-off between achieving high flux by increasing the trans membrane pressure and running the risk of filtrate breakthrough in any membrane system, especially if the filtrate can change shape, as is the case in this system where oil is used. In the same way, increasing the CNT

concentration in the membrane decreased rejection but increased membrane flux. Because an increase in the CNT concentration led to an increase in the pore sizes of the membrane it was inevitable that the rejection decreased as the oil made it through the membrane. An artificial neural network was then generated in order to model the filtration of oil from water. Encog is a framework for java and .Net and it contains classes that can be used to create an artificial neural network (ANN) and this was used to create the network. The network generated was a 3 layer feedfoward network with 1 output, 13 hidden neurons and 3 input neurons. The training error of the network was found to be 0.99% and the evaluation error was 0.92% which means this network can approximate the system quite closely. The network was transferred to Matlab where it was trained using the Levenberg-Marquardt method and the results obtained showed that the network describes the data well. A grid search method was then implemented to determine the best combination of CNT concentration and pressure. It was found that the best range to operate is at CNT concentrations between 5 and 8% and pressures between 1 and 4 bar.

DEDICATION

This thesis is dedicated to my family who have stood by me throughout everything.

ACKNOWLEDGEMENTS

The work presented in this thesis was made possible due to the assistance of a number of people and institutions. I would like to express my sincere gratitude to the following:

My family for their unconditional love and support.

Prof. S.E. Iyuke for his support throughout my research.

The NRF and Centre of Excellence – Strong Materials for funding my research.

I would also like to thank Sasol Ltd. for their financial support during my postgraduate studies.

The Wits Microscopy Unit.

CONFERENCES AND PUBLICATIONS

Presentation:

Synthesis of modified polyvinyl alcohol and carbon nanotube composite membrane for the purification of water, Saiche Conference, 16 – 19 September 2012, Central Drakensberg, KwaZulu Natal, South Africa.

Publications:

Yah, C. S., Simate, G. S., Moothi, K., Maphutha K. S. & Iyuke, S. E., 2011, 'Synthesis of Large Carbon Nanotubes from Ferrocene: The Chemical Vapour Deposition Technique', Trends in Applied Sciences Research 6, 1270 – 1279.

Maphutha, S., Moothi, K., Meyyappan, M. & Iyuke, S. E., 2013, 'A carbon nanotube-infused polysulfone membrane with polyvinyl alcohol layer for treating oil-containing waste water', Scientific Reports 3, 1509 - 1515.

Table of Contents

LIST OF FIGURES

LIST OF TABLES

NOMENCLATURE

WHO – World Health Organisation

UNICEF – United Nations Children's Fund

ANN – Artificial neural network

CP - Concentration polarisation

CNT – Carbon nanotube

PSF – Polysulfone

PVA - Polyvinyl alcohol

CVD - Chemical Vapour Deposition

MWCNTs - Multi-wall carbon nanotubes

SWCNTs - Single wall carbon nanotubes

$\vec{C}$ - Chiral vector

$\vec{a}_1, \vec{a}_2$ - Unit cell vectors

a - Length of the unit cell vector

acc - Carbon-carbon bond length (0.1421 nm)

nm – Nanometre

D - Diameter of the nanotube

c - Circumferential length

G_0 - One unit of the conductance quantum

e - Charge on one electron

h - Plank's constant

LPG – Liquid petroleum gas

TEM - Transmission Electron Microscope

IR – Infra red

SWNT - Single wall nanotube

RBM - Radial breathing mode

CNF - Carbon nanofibres

DMF – Dimethylformamide

MA – Maleic acid

SEM - Scanning electron microscope

F - Flux

A - Effective membrane area

V - Volume of permeate

R - Rejection

C_f – Feed concentrations

C_p - Permeate concentrations

y_j - Output for every unit

w_{nj} - Connection between the units denoted

s_n - Effective input from external inputs

σ - Activation function

b_j - Bias for each unit

γ - Positive constant representing the learning rate

d_k - Activation provided by the "teacher"

LMS - Least mean square

E - Error function

Rprop - Resilient backpropagation

GUI - Graphic user interface

RDMM - Rotating disk membrane module

ΔP – Hydraulic pressure difference

$\Delta \Pi$ - Osmotic pressure difference

R_m – Membrane resistance

k - Mass transfer coefficient

J - Permeate flux

J_∞ - Limiting flux

Re - Reynold's number

v - Velocity of the fluid

D_p - Diameter of the tube

ρ - Density of the fluid

μ - Viscosity

D_{TP} – Tape diameter

L_e - Twist length

δ_{tp} - Thickness of the tape

v_{ac} - Actual velocity

TMP – Trans-membrane pressure

CHAPTER 1

1. Introduction

1.1. Background

Water is one of the most important resources on earth and it is needed by everybody for the most basic means of survival. And yet many people do not have access to clean water in some parts of the world. Some of the statistics on the water situation are given below:

- Nearly a billion, 884 million people do not have access to clean and safe water. 37% of those people live in Sub-Saharan Africa. (WHO/UNICEF, 2010)
- 1 in 8 people world-wide do not have access to safe and clean drinking water. (WHO/UNICEF, 2010)
- Nearly 1 out of every 5 deaths under the age of 5 worldwide is due to a water-related disease. (WHO/UNICEF, 2009)
- By investing in clean water alone, young children around the world can gain more than 413 million days of health! (WHO, 2004)
- The United Nations estimates that Sub-Saharan Africa alone loses 40 billion hours per year collecting water; the same as an entire year's labor in all of France! (United Nations Development Programme, 2009)

Due to the statistics presented it is necessary to purify and recycle the water used. High volumes of wastewater in the form of oil-water emulsions are produced in various industries such as oil fields, petrochemical, metallurgical, pharmaceutical and others

(Siriverdin and Dallbauman, 2004). Oil concentrations in wastewater generated in the above industries range from 50–1000 mg/L (Chakrabarty et al., 2008) however, the acceptable discharge limit is only 10-15 mg/L (Bevis, 1992). Microfiltration (Abadi et al., 2011), ultrafiltration (Chakrabarty et al., 2010), nanofiltration and reverse osmosis (Mondal and Wickramasinghe, 2008) have all been successfully used in the separation of oil from water. Nanofiltration was the chosen filtration technique in this work because it operates at ranges between ultrafiltration and reverse osmosis thus having distinct advantages such as low operating pressures, high flux, high retention of multivalent ions and organic molecular above 300 (Hilal et al., 2004). The two major problems with membrane filtration are fouling and concentration polarization. Fouling is the adhesion (adsorption) of substances on the surface and/or inside the membrane pores thereby decreasing the flux through the membrane (Sablani et al., 2001). Concentration polarisation (CP) is a phenomenon that affects membrane flux negatively and it occurs when a solution comes into contact with the membrane surface and the solute builds up on the surface of the membrane and if left in contact with the membrane long enough it will lead to fouling (Guo et al., 2012). CP is also referred to as reversible fouling as there is no physical adhesion of the solute on the membrane. Fouling can be decreased by using hydrophilic membranes (Van der Bruggen et al., 2008). Polyvinyl alcohol (PVA) can be used as the barrier layer in a thin film composite (TFC) membrane because of its hydrophilic and good film forming characteristics (Hirai et al., 1989; Ibrahim and Abo-Shosha, 1993). Zhou et al. (2014) states that the substrate of the TFC should have sufficient mechanical, chemical and thermal stability to withstand industrial operations. In this work it was decided to use carbon nanotubes (CNTs) to increase the mechanical

strength of the substrate. Carbon nanotubes exhibit mechanical properties such as potentially having up to 5 times the elastic modulus (~ 1 TPa) and almost 100 times the tensile strength (~ 150 GPa) of high strength steels (Zhao et al., 2007) and studies have been done showing the transference of thermal (Bagchi and Nomura, 2006), electrical (Valentini et al., 2003) and mechanical (Coleman et al., 2006a) properties of carbon nanotubes (CNTs) to polymer composites. Any technique in which the formation of the solute layer is disrupted and which promotes fluid mixing along the flow path can decrease CP. The different methods that have been used to increase flux in a membrane by disrupting solute layer formation are the rotating filter (Kroner and Nissinen, 1988), adding baffles to a tubular module (Finnigan and Howell, 1989), by pulsating the flow (Bertram et al., 1993) and by inducing rotational flow (Millward et al., 1995). There is a need to model the filtration process in order to predict the decline of flux (caused by CP and fouling) during filtration. There are models that exist that can model the flux decline in membranes by using parameters such as particle size, zeta potential, temperature, pH, shear rate, transmembrane pressure etc. (Bowen and Jenner, 1995). The accuracy of these models is decreased by the lack of information on the phenomena occurring during the filtration process and assumptions that lead to discrepancies between the theoretical prediction and the experimental results. There is therefore a need for empirical models that are built from experimental data and can be used to predict membrane operations. Artificial neural networking is one of these modelling techniques and they have already been used in a number of membrane filtration processes (Goloka and Chittaranjan, 2006, Chen and Kim, 2006, Shetty and Chellam, 2003). Artificial neural networks (ANN) are basic models based on the neural

structure of the brain. The basic processing element in a neural network is a neuron. Like a biological neuron which accepts signals from multiple sources, it combines the information and applies an operation to it and then outputs the result. Figure 1-1 shows a simplified schematic of a biological neuron.

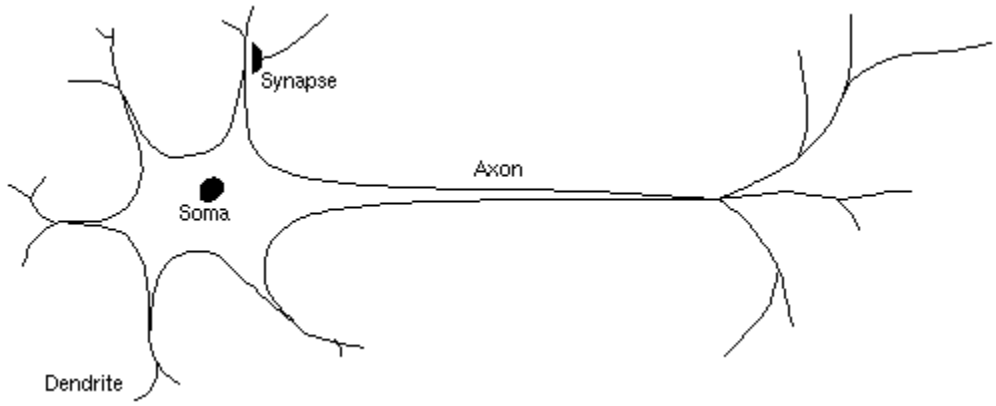

Figure 1-1: Schematic representation of major parts of a neuron (Dennis, 1997).

The dendrites accept input from synapses of other neurons, the soma processes the input signals and the axon converts these processed signal into outputs that are passed to the next neuron via the synapses. Neural networks are advantageous in their ability to model a process as a 'black box' with inputs and outputs but the processing time required can be long.

1.2. Aims and objectives

The aim of this project is to produce a membrane with increased mechanical properties (since membranes are generally very thin and fragile) and the ability to remove synthetic oil from water at reasonable filtration fluxes. The membrane will be modelled using artificial neural networks (ANN) and an attempt to decrease concentration

polarisation by inducing turbulent flow in a tube. These aims will be achieved by meeting the following objectives:

a) Production of carbon nanotubes (CNTs) using ferrocene
b) Production of a CNT infused polysulfone (PSF)/polyvinyl alcohol (PVA) bi-layer membrane
c) Analysis of the membrane by mechanical testing and flux and rejection testing
d) Reducing CP by inducing rotational flow in a tube housing a membrane
e) Developing an ANN model to describe the performance of the membrane

1.3. Research questions

Some questions will be answered while achieving the final goal of this project and these questions are:

a) What is the effect of CNT production temperature on the CNT structure?
b) Can the addition of CNTs to PSF increase the polymer's strength and not have a negative effect on the membrane forming characteristics of the polymer?
c) Can using twisted tapes to induce rotational flow in a tube housing a membrane decrease CP?
d) Is ANN an effective method for describing the performance of the membrane?

1.4. Overview of the thesis

Chapter 1:

This chapter discusses the motivation of this research, the aims, the research questions and the outline of the study.

Chapter 2:

The second chapter gives an introduction to CNTs including the structure and the properties of the tubes. The different production methods of CNTs are described including the chemical vapour deposition method which is used in this thesis. The literature then moves on to describe the types of membranes that can be made and the production methods used. The pore formation methods and the filtration models are discussed and the interactions between CNTs and polymers investigated. The chapter then goes on to describe the ANN modelling process which is used to model the membrane filtration process in this work. The chapter concludes by introducing the different membrane modules that are used in industry.

Chapter 3:

In this chapter CNTs are produced from ferrocene using argon as a carrier gas. Different temperatures are tested for the production of CNTs and the CNTs are characterised using TEM and Raman spectroscopy.

Chapter 4:

In chapter 4 a thin film composite membrane with CNT reinforcement in the bottom layer is prepared. Different CNT concentrations in the membrane are tested in order to determine the optimal concentration for maximum mechanical strength transfer from the CNTs to the polymer and this mechanical strength is tested using a nanotensile tester. The membrane is characterised by SEM and BET to determine the pore sizes. A synthetic oil in water emulsion is filtered using the composite membrane in order to test its filtration properties.

Chapter 5:

Chapter 5 introduces the concept of concentration polarisation by presenting several models that have attempted to model this phenomenon. A brief explanation of the solution to CP in the form of turbulence promoters is given. The proposed design of a tubular housing for the membrane with a twisted tape insert is given and tested to see whether CP can be decreased by using the tape.

Chapter 6:

This chapter deals with the use of an artificial neural network to model the flux through the composite membrane created in chapter 4. The .Net framework based version of Encog is used in order to get the neural network and its weights. Matlab is also used to create a neural network based on the results given by Encog and this network is used to find the parameters that yield the highest cumulative flux.

Chapter 7:

This chapter will summarise the findings of this thesis and present any recommendations for further investigation.

References

Abadi, S. R., Sebzari, M. R., Rekabdar, M. H. & Mohammadi, T., 2011, 'Ceramic membrane performance in microfiltration of oily wastewater', Desalination 265, 222–228.

Bagchi, A. & Nomura, S., 2006, 'On the effective thermal conductivity of carbon nanotube reinforced polymer composites', Composites Science and Technology 66, 1703-1712.

Bertram, C.D., Hoogland, M.R., Li, H., Odell, R.A. & Fane, A.G., 1993, 'Flux enhancement in crossflow microfiltration using a collapsibletube pulsation generator', Journal of Membrane Science 84, 279–292.

Bevis, A., 1992, 'The treatment of oily water by coalescing', Filtration & Separation 29, 295-301.

Bowen, W.R. & Jenner, F., 1995, 'Theoretical descriptions of membrane filtration of colloids and fine particles: an assessment and review', Advances Colloid Interface Science 56, 141–200.

Chakrabarty, B., Ghoshal, A. K. & Purkait, M. K., 2008, 'Ultrafiltration of stable oil-in-water emulsion by polysulfone membrane', Journal of Membrane Science 325, 427–437.

Chakrabarty, B., Ghoshal, A. K. & Purkait, M. K., 2010, 'Cross-flow ultrafiltration of stable oil-in-water emulsion', Chemical Engineering Journal 165, 447-456.

Chen, H. & Kim, A. S., 2006, 'Prediction of permeate flux decline in crossflow membrane filtration of colloidal suspension: a radial basis function neural network approach', Desalination 192, 415–428.

Coleman, J. N., Khan, U. & Gunko, Y. K., 2006a, 'Mechanical reinforcement of polymers using carbon nanotubes', Advanced Materials 18, 689-706.

Dennis, S., 1997, 'Introduction to Neural Networks'. Available from http://itee.uq.edu.au/~cogs2010/cmc/chapters/Introduction. [September 2013].

Finnigan, S.M. & Howell, J.A., 1989, 'The effect of pulsatile flow on ultrafiltration fluxes in a baffled tubular membrane system', Chemical Engineering Research and Design 67, 278–282.

Goloka, B. S. & Chittaranjan, R., 2006, 'Predicting flux decline in crossflow membranes using artificial neural networks and genetic algorithms', Journal of Membrane Science 283, 147–157.

Hilal, N., Al-Zoub, H., Darwish, N.A., Mohammad, A.W. & Abu Arabi, M., 2004, 'A comprehensive review of nanofiltration membranes: Treatment, pretreatment, modelling, and atomic force microscopy', Desalination 170, 281-308.

Hirai, T., Asada, Y., Suzuki, T. & Hayashi, S., 1989, 'Studies on elastic hydrogel membrane. I. effect of preparation conditions on the membrane performance', Journal of Applied Polymer Science 38, 491–502.

Ibrahim, N. A. & Abo-Shosha, M. H., 1993, 'Preparation and characterization of carboxylic cation exchange resins from the reaction of poly(vinyl alcohol) with

melamine-formaldehyde and some hydroxy acids', Angewandte Makromolekulare Chemie 210, 7–20.

Kroner, K.H. & Nissinen, V., 1988, 'Dynamic filtration of microbial suspensions using an axially rotating filter', Journal of Membrane Science 36, 85–100.

Millward, H.R., Bellhouse, B.J. & Walker, G., 1995, 'Screw-thread flow promoters: an experimental study of ultrafiltration and microfiltration performance', Journal of Membrane Science 106, 269–279.

Mondal, S. & Wickramasinghe, S. R., 2008, 'Produced water treatment by nanofiltration and reverse osmosis membranes', Journal of Membrane Science 322, 162–170.

Sablani, S. S., Goosen, M. F. A., Al-Belushi & R., Wilf, M., 2001, 'Concentration polarization in ultrafiltration and reverse osmosis: a critical review', Desalination 141, 269-289.

Shetty, G. R. & Chellam, S., 2003, 'Predicting membrane fouling during municipal drinking water nanofiltration using artificial neural networks', Journal of Membrane Science 217, 69–86.

Siriverdin, T. & Dallbauman, L., 2004, 'Organic matrix in produced water from the osage-skiatook petroleum environmental research site', Chemosphere 57, 463-469.

United Nations Development Programme, 2009, 'Resource Guide on Gender and Climate Change'. Available from http://www.undp.org/climatechange/library_gender.shtml. [May 2014].

Valentini, L., Armentano, I., Santilli, P., Kenny, J. M., Lozzi, L. & Santucci, S., 2003, 'Electrical transport properties of conjugated polymer onto self-assembled aligned carbon nanotubes', Diamond and Related Materials 12, 1524-1531.

Van der Bruggen, B., Manttari, M. & Nystromb, M., 2008, 'Drawbacks of applying nanofiltration and how to avoid them: a review', Seperation and Purification Technologies 63, 251–263.

WHO/UNICEF Joint Monitoring Programme for Water Supply and Sanitation, 2010, 'Progress on Sanitation and Drinking Water 2010'. Available from www.wssinfo.org/. [May 2014].

WHO/UNICEF, 2009, 'Diarrhoea: Why children are still dying and what can be done'. Available from http://www.unicef.org/health/index_51412.html. [May 2014].

World Health Organization, 2004, 'Costs and benefits of water and sanitation improvements at the global level'. Available from http://www.who.int/water_sanitation_health/wsh0404/en/. [May 2014].

Zhao, N., Cui, Q., He, C., Shi, C., Li, J., Li, H. & Du, X., 2007, 'Synthesis of carbon nanostructure with different morphologies by CVD of methane', Materials Science and Engineering A 460 – 461, 255 -260.

Zhou, Z., Lee, J. Y., Chung, T., 2014, 'Thin film composite forward- osmosis membranes with enhanced internal osmotic pressure for internal concentration polarization reduction', Chemical Engineering Journal 249, 236–245.

CHAPTER 2

2. Literature Review

2.1. Carbon nanotube theory

2.1.1. Structure of Carbon nanotubes

Carbon nanotubes were first discovered by Iijima, (1991) although he called them "helical microtubules." They are considered to be a one dimensional form of fullerenes because their length to diameter ratio is very high. Daenen et al. (2003) state that a carbon nanotube can be considered to have two separate regions with differing chemical and physical properties (Figure 2-1).

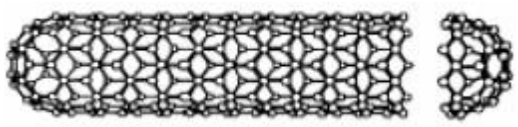

Figure 2-1: The different regions of a nanotube (Daenen et al., 2003).

The "cap" region has a similar structure to half a C_{60} fullerene. The other region is the single wall carbon nanotubes (SWCNTs) and it can be considered to be a single, one atom thick, sheet of graphite that has been rolled into a tube (Figure 2-2) (Thomsen, 2005). A MWCNT can be likened to a number of SWCNTs of different diameters together.

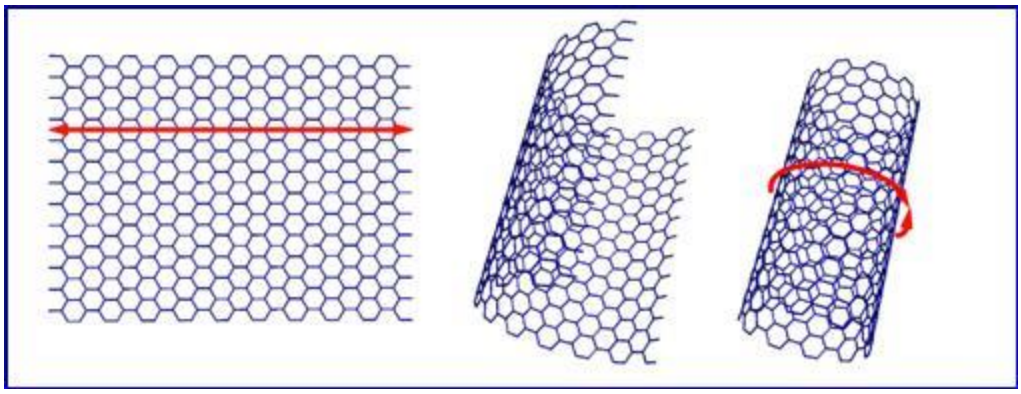

Figure 2-2: Graphene sheet being rolled into a nanotube (Thomsen, 2005).

A single wall nanotube can be completely described, excepting the length, by a chiral vector, $\vec{C}$. If two atoms on the graphene sheet are chosen and one is taken to be the origin, then $\vec{C}$ is the vector pointing from the first atom to the second (Figure 2-3). The equation describing $\vec{C}$ as per Belin and Epron (2005),

$$\vec{C} = n\vec{a}_1 + m\vec{a}_2 \tag{2.1}$$

where *n* and *m* are integers and $\vec{a}_1$ and $\vec{a}_2$ the unit cell vectors of the two-dimensional lattice formed by the graphene sheets.

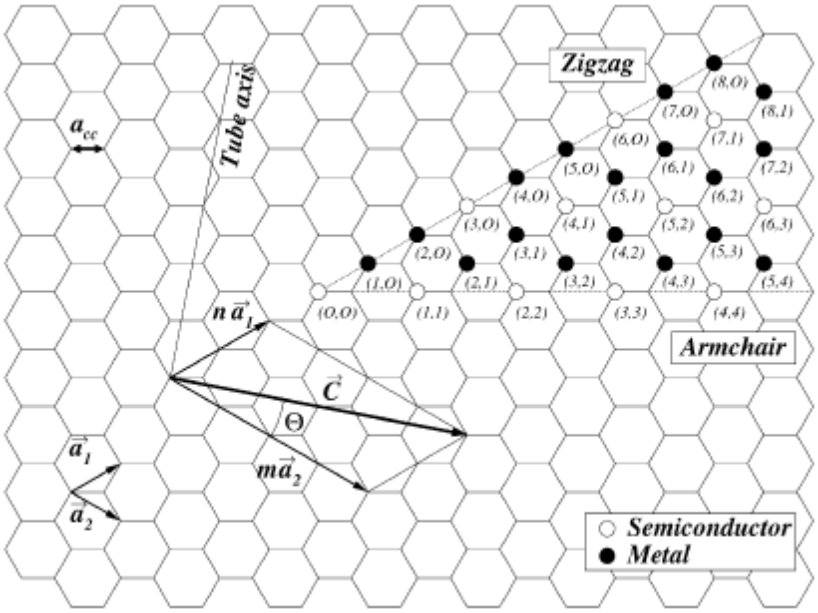

Figure 2-3: Chiral vector for a (2, 4) nanotube (Belin and Epron, 2005).

The direction of the nanotube axis is perpendicular to the chiral vector. There are three models that describe the formation of CNTs namely, coaxial cylindrically curved, coaxial polygonized and scolls graphene sheets (Figure 2-4).

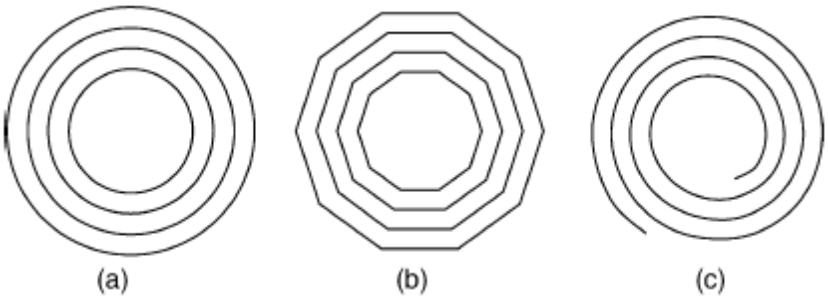

Figure 2-4: The different models describing nanotubes: a) coaxial cylindrically curved, b) coaxial polygonized and c) scroll (Belin and Epron, 2005).

The cylindrically curved model is the most widely accepted of the three models. The length of the chiral vector is equal to the circumference of the nanotube and is described by the equation below,

$$c = \left|\vec{C}\right| = a\sqrt{n^2 + nm + m^2} \tag{2.2}$$

where a is the length of the unit cell vector. This a is related to the carbon-carbon bond length by,

$$a = |\overrightarrow{a_1}| = |\overrightarrow{a_2}| = a_{cc}\sqrt{3} \tag{2.3}$$

where a_{cc} is the carbon-carbon bond length and is equal to 0.1421 nm (Wildoer et al., 1998). If the curvature of the nanotube is taken into account then a slightly larger value of 0.144 nm should be used (Murakami et al., 2003, Saito et al., 2000). The diameter of the nanotube is described by,

$$D = \frac{c}{\pi} \tag{2.4}$$

where c is the circumferential length and the angle between the chiral vector and the "zigzag" nanotube axis is described by Belin and Epron, 2005 as,

$$\theta = tan^{-1}\left(\frac{m\sqrt{3}}{m + 2n}\right) \tag{2.5}$$

Nanotubes are described by the integers (n, m) which are related to the chiral vector. When *n* = *m*, the nanotube is called "armchair" type (θ= 0^o); when *m* = 0, then it is of the "zigzag" type (θ= 30^o) and when $n \neq m$, it is a "chiral" tube and θ takes a value between 0^o and 30^o (Figure 2-5) (Jorio et al., 2001). The value of (*n, m*) determines the chirality of the nanotube and affects the optical, mechanical and electronic properties.

Nanotubes with $|n-m| = 3q$ are metallic and those with $|n-m| = 3q \pm 1$ are semiconducting (q is an interger) (Belin and Epron, 2005).

a) 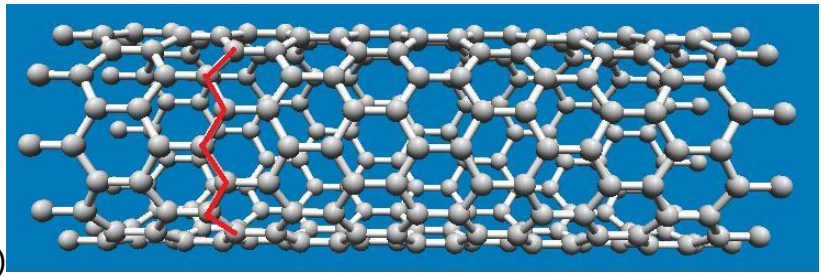

b) 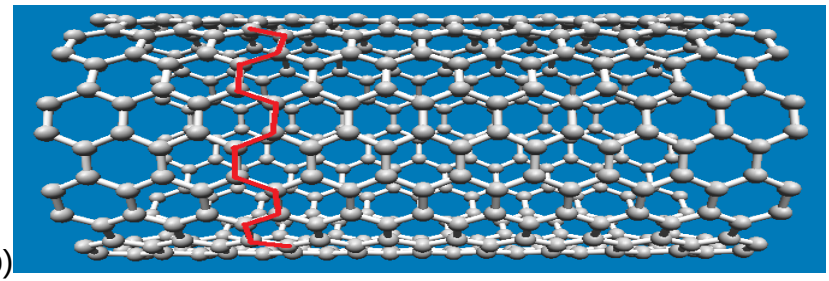

c) 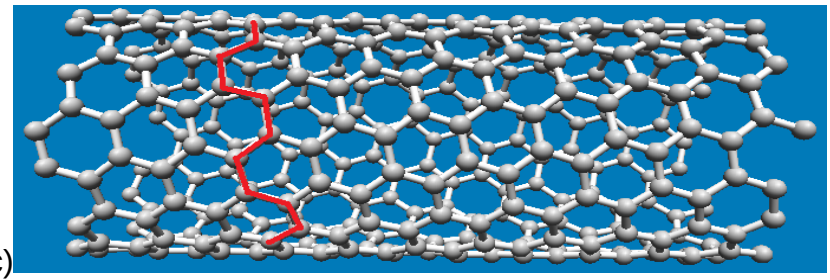

Figure 2-5: The different types of CNTs a) zigzag, b) armchair and c) chiral (these images were generated from the Nanotube Modeler, 2014 software).

2.1.2. Properties of Carbon nanotubes

Carbon nanotubes are the stiffest and strongest fibre known with a Young's modulus of approximately 1500 GPa (Saito et al., 1998) and a tensile strength of approximately 45 billion Pascals (Teng, 2010). This strength occurs because of the sp^2 bonds between the carbon atoms. The conductivity of a CNT along the tube is very good and the insulating capabilities of the tube axially are also high. The thermal conductivity along the tube is between 1750 and 5800 W/mK (Hone et al., 1999). The conductance of a CNT is predicted to be $2G_0$ independent of the diameter and length, where $G_0 = \frac{2e^2}{h} = \frac{1}{12.9} K\Omega$, which is one unit of the conductance quantum, e is the charge on one electron and h Plank's constant (Frank et al., 1998). CNTs have been found to conduct current ballistically without dissipating heat. They can also carry the highest current density known of any material, which has been measured as high as 109 A/cm^2.

2.1.3. Production Methods

Arc discharge

It is found, according to Keidar (2007), that arc discharge is the most practical method for synthesizing SWCNTs. It produces SWCNTs with fewer defects than those methods which operate at low temperature such as CVD. This is believed to be true due to the fast growth rate of the SWCNTs in arc discharge. It is believed to be of a general consensus that the key parameter of nanotube growth in arc discharge is the anode erosion rate. Although the arc discharge and laser-ablation methods both produce high yields of SWCNTs (>70%), the arc discharge method is the much cheaper option

(Popov, 2004) and has been shown to be able to produce large scale SWCNTs (Journet et al., 1997). Figure 2-6 shows a simplified schematic drawing of arc discharge apparatus.

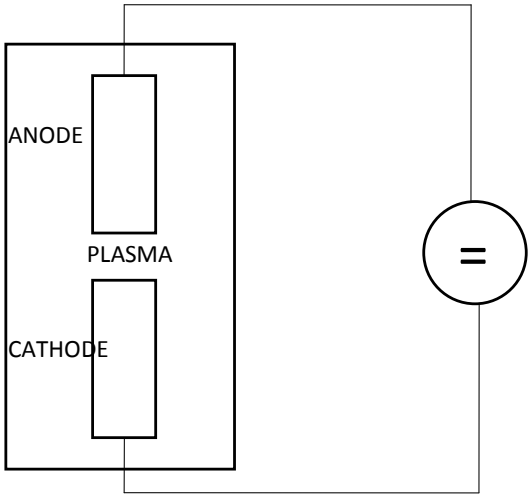

Figure 2-6: Arc discharge setup showing 2 graphite electrodes which are used to produce an electric arc discharge in an inert gas atmosphere (Popov, 2004).

Laser Ablation

Laser ablation is a process in which laser pulses heat a carbon target, for example graphite with cobalt and nickel catalyst present, and vaporises them. This high energy vapour expands rapidly and then condenses to form clusters of carbon nanotubes (Rafique and Iqbal, 2011). High yields of SWCNTs are produced (>70%). Figure 2-7 shows the apparatus used for laser ablation. The disadvantages of arc discharge and laser-ablation are that 1) they are both uneconomically energy intensive for large scale production (Rafique and Iqbal, 2011), 2) they require solid carbon to be vaporised at

very high temperatures (>3000^{o}C) (Popov, 2004) and 3) they produce highly entangled nanotubes which require extensive purification methods (Rafique and Iqbal, 2011).

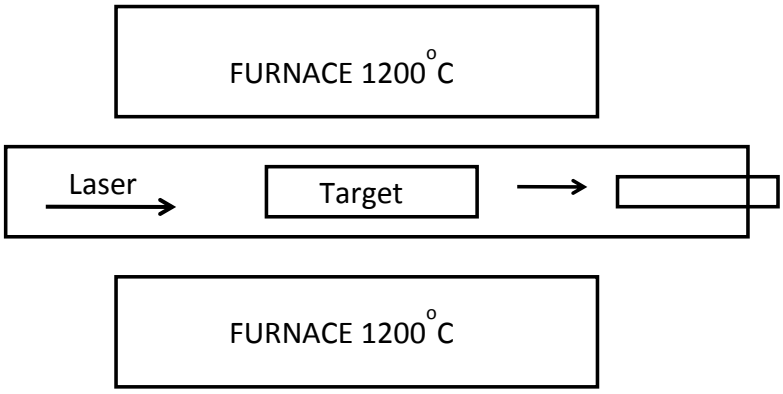

Figure 2-7: Laser ablation schematic depicting a laser beam which vapourises a target consisting of a mixture of graphite and a metal catalyst (Popov, 2004).

Chemical vapour deposition

In this process hydrocarbons are made to react with a heated catalyst (which may be on a substrate) at temperatures between 700^{o}C and 900^{o}C. The CNTs are formed by the decomposition of the hydrocarbon and its deposition and growth on the metal catalyst particle (Rafique and Iqbal, 2011). There are horizontal CVDs (Figure 2-8) and vertical CVDs (Figure 2-9) and the vertical CVDs allow for the production of CNTs under fluidized bed conditions. There are also two CVD processes which are the homogenous and the heterogeneous processes. The homogeneous CVD processes are based on a homogeneous phase decomposition of two precursors, one for the metallic catalyst and the other one for the carbon precursor and the CNTs can be collected either in or at the exit of the reactor (Figure 2-8a) (Philippe, 2007) but the disadvantages of this method include reactor plugging and the inability to control catalyst particle size. Heterogeneous

processes consist of the decomposition of certain hydrocarbons on small metal particles (in the form of powders) or thin films deposited on a substrate (Figure 2-8b) which is commonly silicon with metallic particles deposited on it by electron beam evaporation, sputtering or solution diffusion (Rafique and Iqbal, 2011). The advantage of this method is that by choosing the correct substrate/catalyst formation process, it is possible to produce aligned CNTs that have the required properties.

In this work CNTs are produced using a vertical CVD for the purpose of increasing the mechanical strength of the bottom layer of a thin film composite membrane by addition of the CNTs to the casting solution of the membrane.

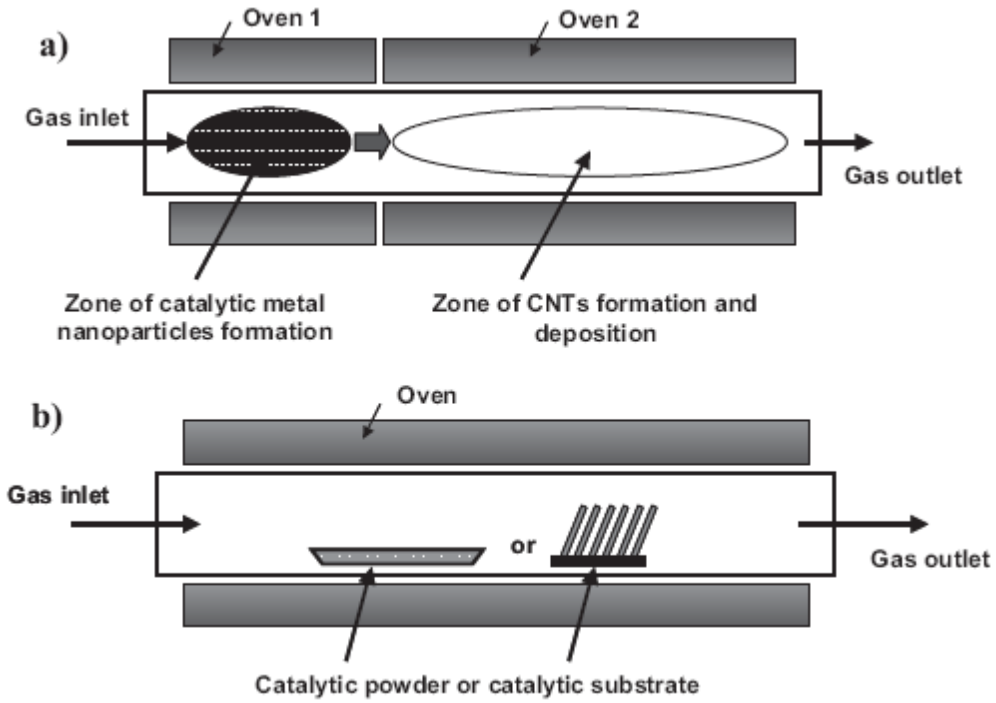

Figure 2-8: a) Homogenous horizontal CVD b) Heterogeneous horizontal CVD (Philippe, 2007).

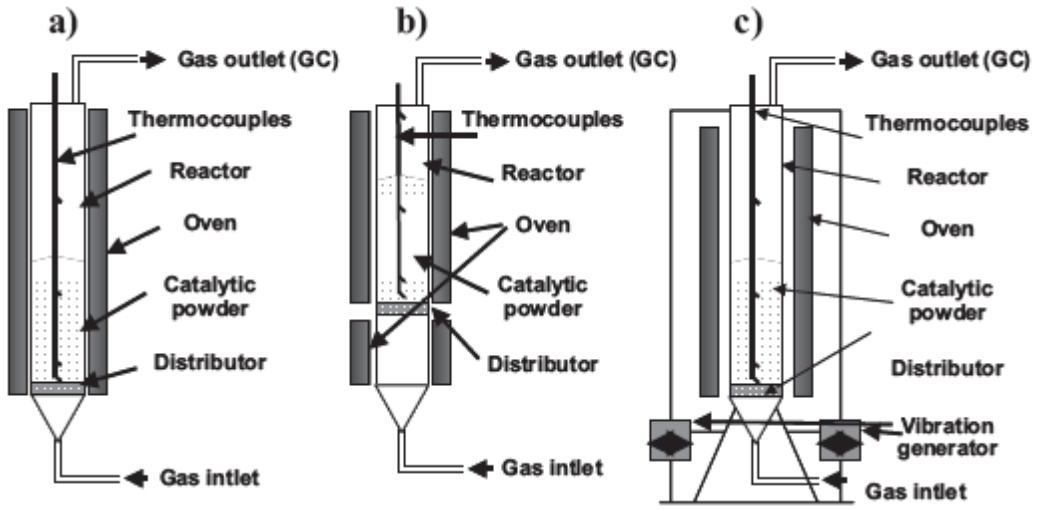

Figure 2-9: a) Standard fluidised bed CVD reactor, b) fluidised bed CVD reactor with gas pre-heating, c) vibro-fluidised-bed reactor (Philippe, 2007).

2.2. Membrane theory

2.2.1. Types of membranes

A membrane is simply a thin interface which regulates the permeation of the chemical species in contact with it. This interface can be homogenous, which means it is completely uniform in composition and structure, or heterogenous, meaning it could contain pores or have a layered structure. Figure 2-10 schematically shows the different types of membranes.

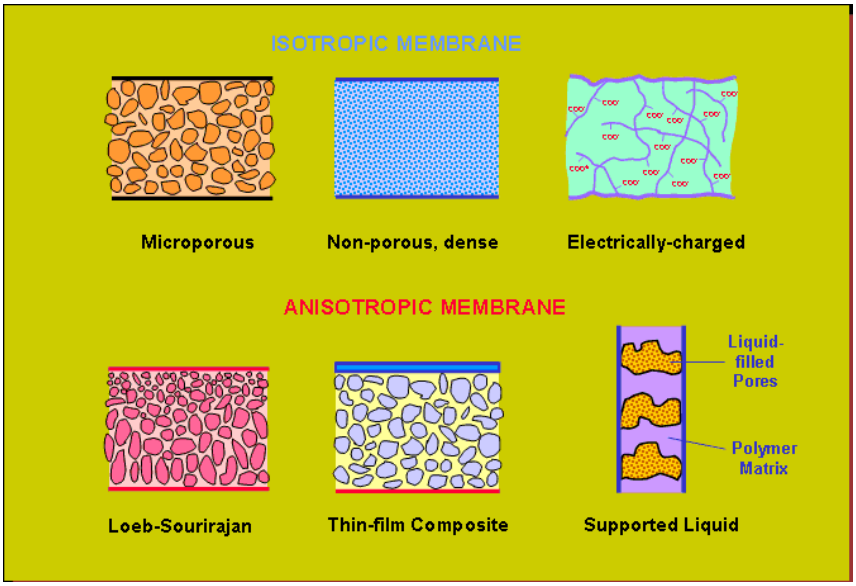

Figure 2-10: Schematic diagram of types of membranes (Cheah, 2014).

Symmetrical (Isotropic) membranes

Isotropic membranes have a uniform structure throughout and they can be porous or dense. The permeation rate is determined by the thickness of the membrane. A decrease in the thickness results in an increase in the permeation rate. Isotropic membranes are not frequently used in oil/water separations except for the microporous membrane. The reason that nonporous membranes are not used is probably because the flow rates through this membrane would be very low. Isotropic membranes also perform separations based on the difference in solubilities of the materials in the membrane but this is not necessary when dealing with oil and water. Oil and water can be separated by size exclusion which is a simpler separation method than solubility differences and therefore it is unnecessary to use an isotropic membrane for the separation. Electrically charged membranes would also be ineffective as there is no

clear charge difference between the oil and water and charge difference is the basis for electrically charged membrane separation.

Microporous membranes

A microporous membrane is similar in structure to a conventional filter. The difference between the two is the size of the pores. The membrane has extremely small pores in the range of 0.01 to 10 micrometers in diameter. The separation function is mainly dependent on the particle size and the membrane pore size distribution. Zhou et al. (2010) used a microporous membrane to reduce the oil in water emulsion concentration of 1g/L by 97.8%.

Nonporous (Dense) membranes

This membrane consists of a dense film through which the permeate is transported by diffusion under a driving force of pressure, concentration or electrical potential. The separation of components in a mixture is related to the transport rates of each component within the membrane, which are determined by the diffusivity and solubility of the components in the membrane material. Therefore this type of membrane can separate particles of similar size as long as their solubility within the membrane differs significantly.

Electrically charged (ion-exchange) membranes

They are finely microporous membranes (although they could also be dense) with a positively or negatively charged ions within the wall of the pores. Separation happens by exclusion of the ions with the same charge as the pore charge and it is affected by the charge and concentration of ions in the solution.

Anisotropic membranes

This membrane consists of a number of layers with differing structures and permeability. The membrane has a thin relatively dense layer on top of a thicker more porous bottom layer. Separation properties and permeate flux is determined exclusively by the thin top layer and the bottom layer acts as a mechanical support and does not participate in the separation. The thin film layer is always on the high pressure side so as to make maximum use of the mechanical strength of the bottom layer. Both the phase separation and the thin film composite membrane can be used for oil/water separation. In this work the choice was made to use a thin film membrane instead of a phase separation membrane because of the flexibility of the thin film design. The phase separation membrane is made from a single material and thus the material would have to possess both good mechanical properties and good separation properties. On the other hand the thin film membrane allows for the use two different materials for the membrane and therefore the bottom layer material can be chosen and modified (such as in the addition of CNTs in this work) for mechanical stability and the top layer can be chosen and modified for separation.

Phase separation membrane (Loeb-Sourirajan membrane)

These membranes are made when a single phase (the casting solution) is precipitated into a two phases where one phase is the solid polymer rich (this forms the polymer matrix of the membrane) phase and the other is a liquid (this forms the pores of the membrane) (Loeb and Sourirajan, 1964). The Loeb-Sourirajan method is a special case of membrane precipitation where the casting solution is immersed within a non-solvent bath (usually water). The other methods are water vapour absorption where the casting

solution is placed in a humid atmosphere and the absorption of the water causes the membrane to precipitate. Thermal gelation is when the membrane is cast while hot and the precipitation takes place as the membrane cools down. Solvent evaporation is when one of the solvents that are used to create the membrane solution is evaporated off thus causing the membrane to precipitate.

Interfacial (Thin-film) composite membrane

This membrane consists of a thin, highly cross-linked, dense membrane formed on a thicker more porous support (for example an ultrafiltration membrane) (Zhou et al., 2014). It is found that under this thin layer there is a gel layer that fills the top pores of the support membrane. Because the thin layer is highly cross-linked the membrane selectivity is high. It is because of this high selectivity that interfacial composite membranes are used in reverse osmosis and nanofiltration.

2.2.2. Production of membranes

Isotropic Membranes

The solution casting method is usually only used for laboratory scale membrane preparation. A thin film of the polymer solution is spread on the surface of a flat plate by using a casting knife. A typical casting knife is shown in Figure 2-11 and it consists of a casting blade and two screws that give a precise gap between the blade and the plate. The viscosity of the casting solution is important when using a casting knife as low viscosity solutions will “run” on the plate and therefore the typical solution concentrations are 15 – 20% (Baker, 2000). Once the solution is cast the solvent (which

would ideally be a moderately volatile solvent such as acetone and ethyl acetate) is allowed to evaporate off leaving the polymer membrane behind.

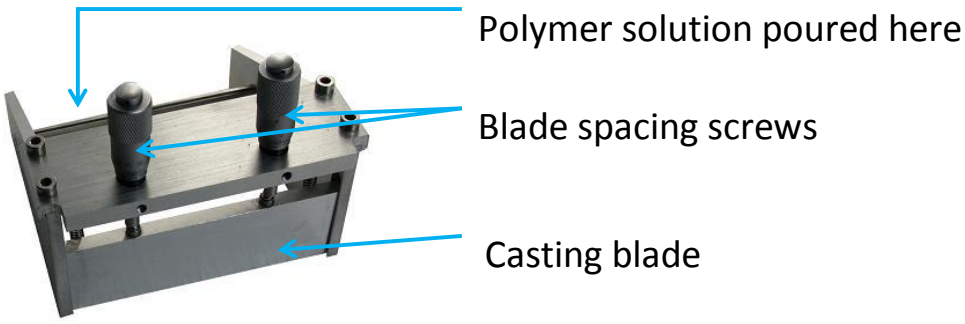

Figure 2-11: Typical handheld membrane solution casting knife by the MTI Corporation.

Other methods for the production of isotropic membranes are:

- Melt extruded film
- Track etching
- Expanded film

Anisotropic Membranes

Phase Separation Membrane

The phase separation method also called the non-solvent induced phase separation (NIPS) (Wang and Lai, 2013) technique creates a membrane by introducing a polymer non-solvent into a polymer solution. This demixes the solution into 2 phases: the solid polymer rich phase that becomes the membrane matrix and the liquid polymer poor phase that creates the membrane pores. There are different methods that can be used

to achieve phase separation and Wang and Lai (2013) describe them thusly: the solution can be immersed in a bath filled with non-solvent and the precipitation of the polymer is caused by the non-solvent absorbtion; the solution can be placed in a humid atmosphere and the precipitation takes place by water vapour absorbtion; the solvent evaporation method works by creating a polymer solution with different solvents that differing volatilities and by evaporating one, the composition of the solution changes and precipitation takes place; and the final method is a combination of the bath immersion and the solvent evaporation method where the cast solution is allowed to stand for some time while the solvent evaporates before being immersed in the non-solvent bath.

The Loeb-Sourirajan (Loeb and Sourirajan, 1964) method is a case of the solvent evaporation and the bath immersion methods, with the condition that the non-solvent is water and the membrane is then annealed in a bath of hot water. The greatest achievement of the Loeb-Sourirajan method is that it allowed the creation of commercially viable reverse osmosis membranes by the membranes having the ability to reject salts at an acceptable flux (Wang and Lai, 2013).

A popular method for describing the membrane formation mechanism is using a phase ternary diagram to describe the mixture of polymer, solvent and non-solvent. The pure components are represented by the corners of the triangle (Figure 2-12).

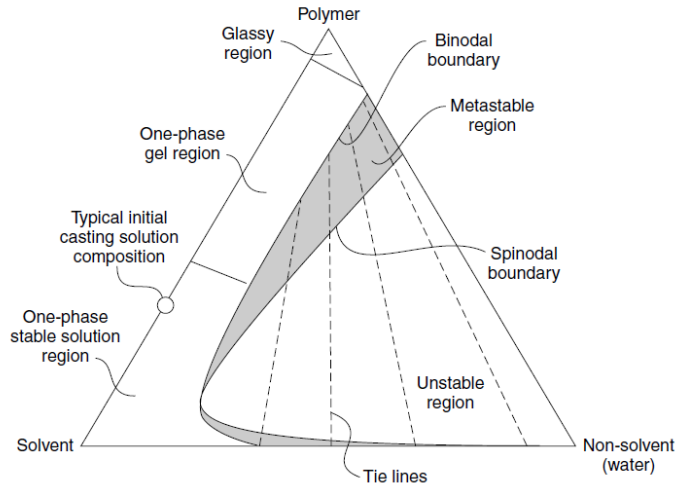

Figure 2-12: Ternary phase diagram depicting the different one phase regions and the unstable two phase region (Baker, 2000).

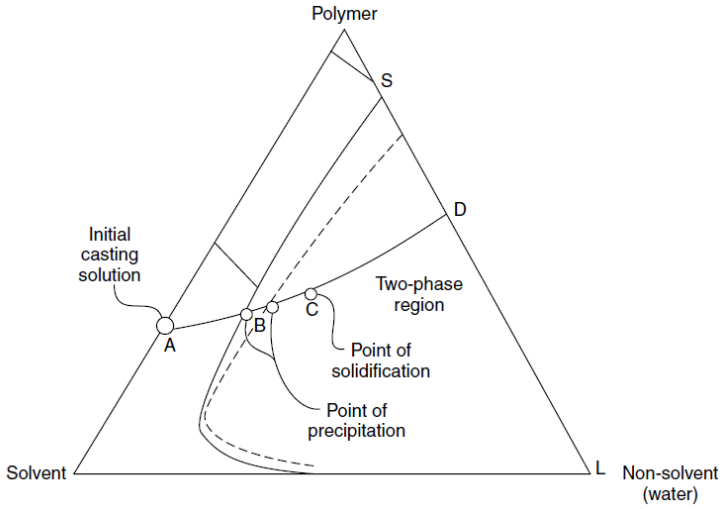

Figure 2-13: A theoretical depiction of the movement of a one phase polymer solution to a two phase membrane through the ternary diagram (Baker, 2000).

From Figure 2-12 if a typical polymer solution is prepared it would lie in the stable one phase solution area on the left of the bimodal curve. If the concentration of polymer to solvent increases, the single phase would shift from solution through the gel region to

the glassy region, where the polymer would appear to be a single solid phase (Baker, 2000). Figure 2-13 shows how the polymer solution moves from a single phase solution to a two phase membrane. A is the initial solution composition and D is the final membrane composition. The line AD is the path of precipitation of the membrane while the position of D on the SL line in Figure 2-13 determines the porosity. Anisotropic membranes have dense top layers and a more porous bottom structure. This means that the top layer has a differing precipitation rate to the bottom layer and thus the path of the top layer on the ternary diagram will differ from the path of the bottom layer. This leads to having two different paths with differing porosities on the ternary diagram for the same anisotropic membrane as shown in Figure 2-14.

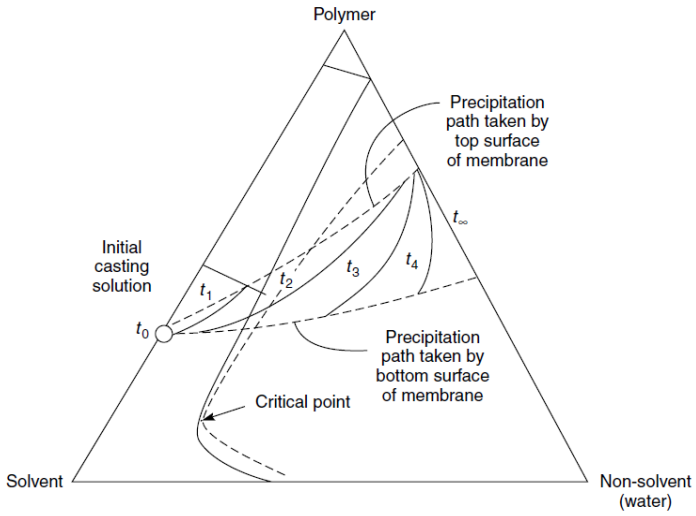

Figure 2-14: A theoretical depiction of the movement of a one phase polymer solution to a two phase anisotropic membrane through two differing precipitation pathways for the top dense layer and the bottom porous support layer on a ternary diagram (Baker, 2000).

The Loeb-Sourirajan membranes can be cast on a glass plate using a casting knife for lab scale quantities. For commercial purposes a casting machine will be required. As shown in Figure 2-15 the polymer solution is cast onto a belt and a little solvent evaporation takes place before the solution is immersed in a bath.

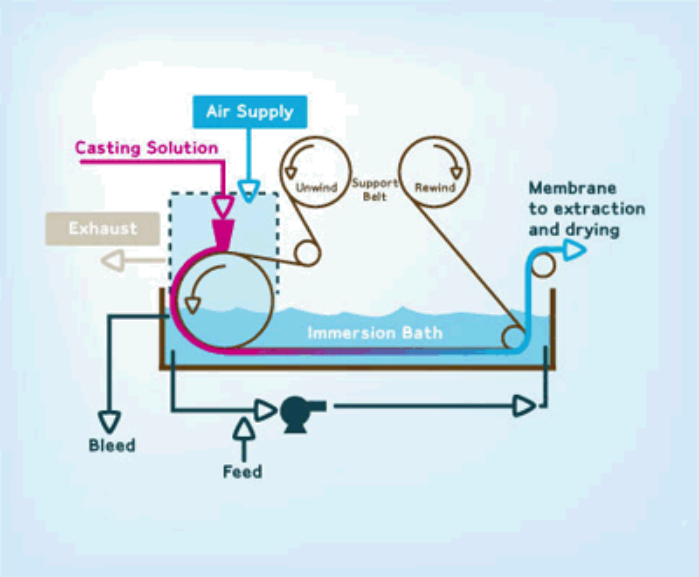

Figure 2-15: Schematic of a commercial immersion casting method by Millipore Corporation, 2014.

Thin Film Composite (Interfacial Polymerization) Membranes

Considered as big a breakthrough as the introduction of the Loeb-Sourirajan membranes the thin film composite membranes were discovered by Morgan (1965) and they produced superior salt rejections and fluxes than the Loeb-Sourirajan type membranes. The membrane created by Morgan (1965) did not make an impact in industrial applications until John Cadotte created a series of thin film membranes by interfacial crosslinking of piperazine with trimesoyl chloride\isophthaloyl chloride mixture (Cadotte et al., 1976 and Cadotte et al., 1978). Figure 2-16 shows the formation of a

thin film membrane where a monomer (which is the amine) is first deposited on the surface of the support layer (which is the polysulfone). The support with the amine layer is then immersed into a water immiscible solvent such as diacid chloride in hexane which reacts with the amine on the support surface creating a densely crosslinked very thin membrane layer.

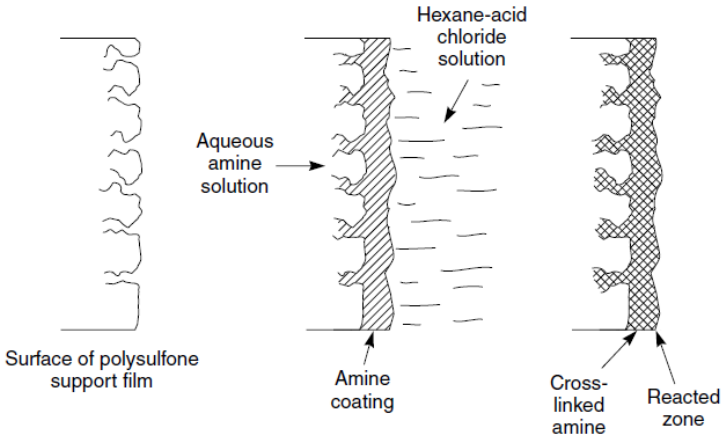

Figure 2-16: Schematic of the formation of a thin film membrane using an amine and hexane-acid chloride solution (Cadotte and Petersen, 1981).

The most commonly used monomers for the thin film layer formation are piperazine (PPD), m-phenylenediamine (MPD) and p-phenylenediamine (PPD) and the acid chloride monomers are trimesoyl chloride (TMC), isophthaloyl chloride (IPC) and 5-isocyanato-isophthaloyl chloride (ICIC) (Lau et al., 2012).

2.2.3. Pore formation mechanisms

The mechanisms of the formation of pores and macrovoids (elongated pores) during membrane synthesis have been studied (Matz, 1972, Strathmann et al., 1975, Strathmann, 1985, Altena, 1982 and Young and Chen, 1995) but there is no unifying theory. Strathmann et al. (1975) and Strathmann (1985) describes the formation of

pores and macrovoids as due to solvent syneresis (which is the withdrawal of a liquid from a gel) which causes shrinkage stress in the skin layer. If precipitation is rapid, the polymer molecules don't have time to 'relax' and this causes fractures to develop (Figure 2-17).

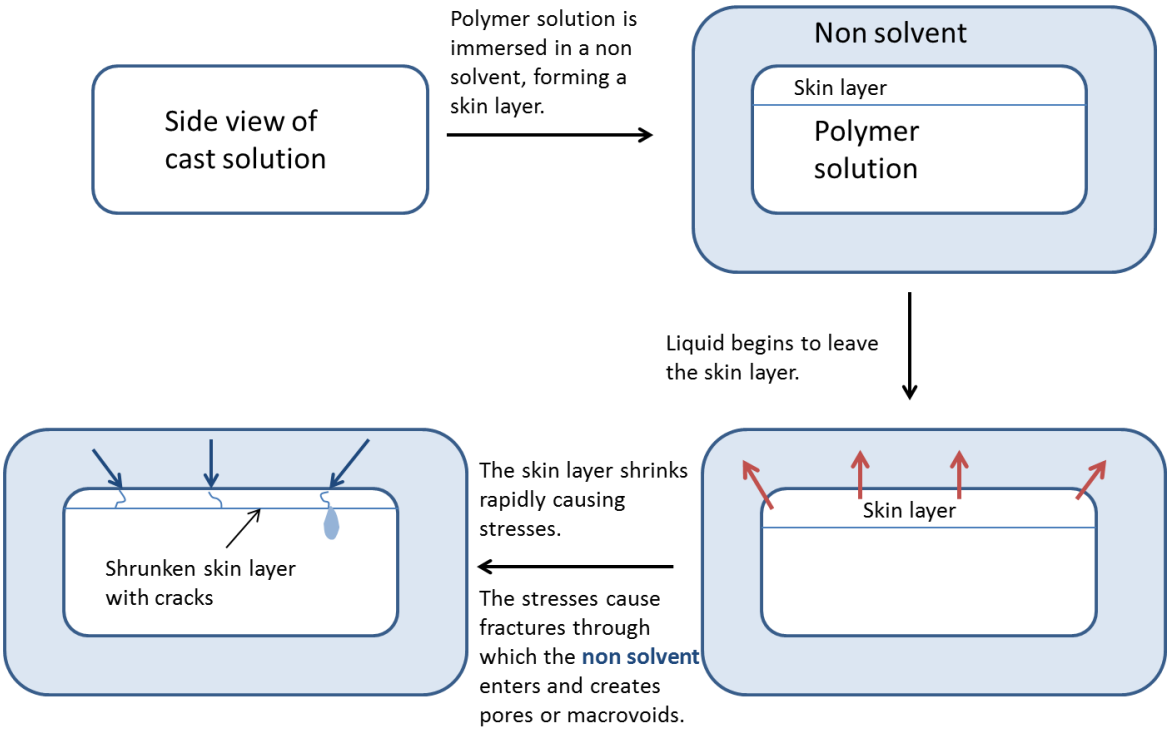

Figure 2-17: Diagram displaying the pore formation mechanism proposed by Strathmann et al. (1975) and Strathmann (1985).

These fractures are then the starting points of pores or macrovoids. Altena (1982) states that after the formation of a 'skin' layer (first layer of membrane created at the moment the membrane solution comes into contact with the non-solvent) of the membrane, the non-solvent penetrates the skin at weak spots and thus the macrovoid is initiated. Void growth is caused by solvent non-solvent diffusion (Figure 2-18).

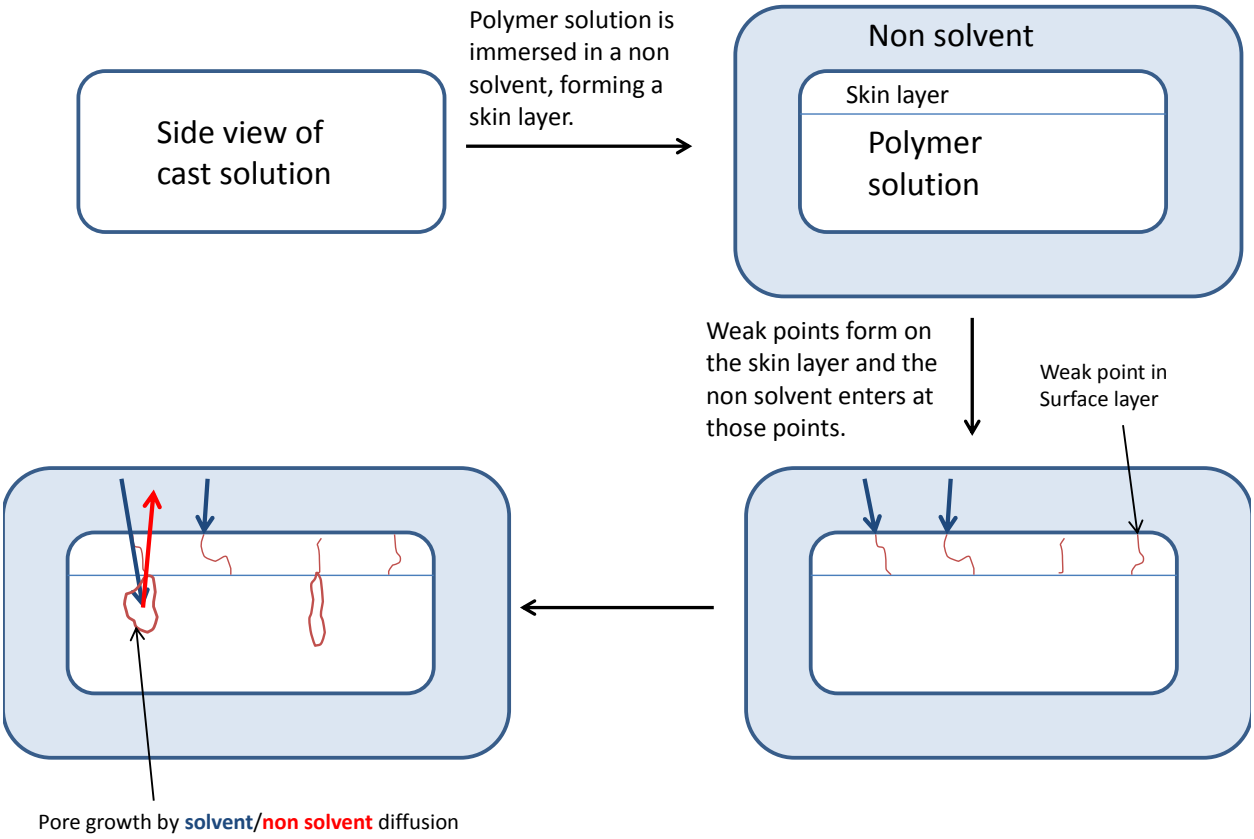

Figure 2-18: Diagram displaying the pore formation mechanism proposed by Altena (1982).

Young and Chen (1995) state that a dense layer is formed when the membrane solution comes into contact with the non-solvent and this is because the solution desolvates rapidly into the coagulation bath while the non-solvent dissolves slowly into the solution. The non-solvent then begins to diffuse through the dense top layer and a nucleus is formed in the polymer poor phase (Figure 2-19) which becomes a pore with the continued addition of non-solvent. The pore will continue to grow with the continued addition of non-solvent which causes the solvent around the pore to diffuse into it (Figure 2-20). The diffusion of the solvent into the pore increases the concentration of

the polymer until the polymer enters a solidification region and the pore stops growing. If the top layer is too dense, nuclei formation in the sub-layer is hindered. If the top layer is porous then more non-solvent makes its way to the sub-layer and more nuclei/pores are created. The structure of the membrane is determined by the diffusion rate of the solvent and non-solvent.

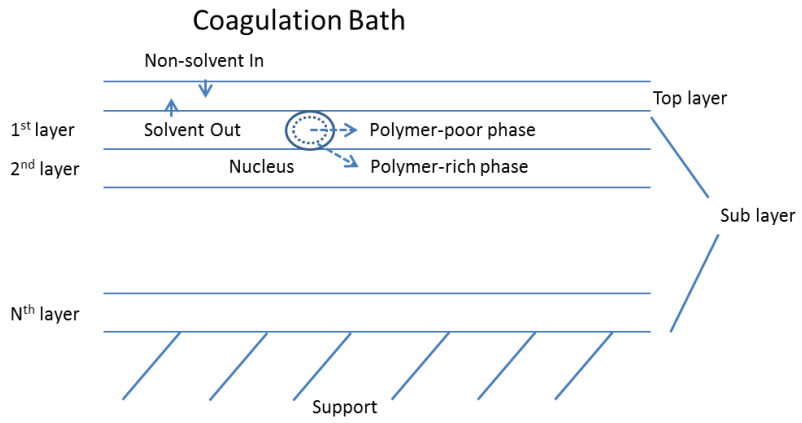

Figure 2-19: Diagram displaying the nucleus formation (Young and Chen, 1995).

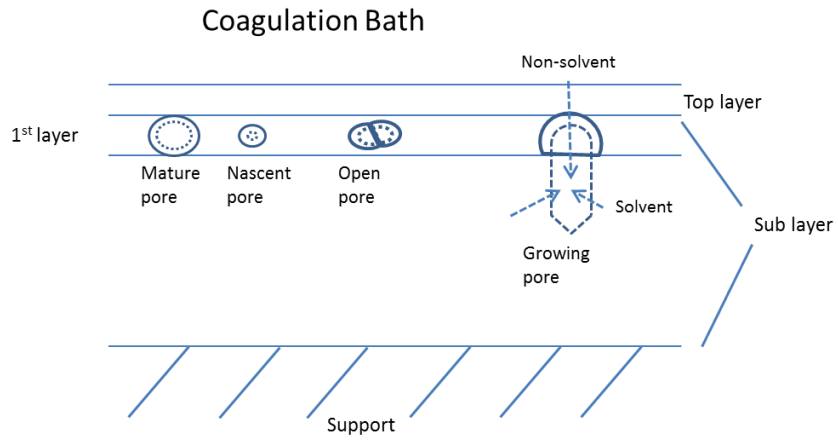

Figure 2-20: Diagram showing the growth of a pore (Young and Chen, 1995).

2.2.4. Membrane filtration processes

Membrane filtration processes include microfiltration, ultrafiltration, nanofiltration and reverse osmosis. Microfiltration refers to processes that separate suspended particles in the range of 0.1 and 10 µm. The membrane materials that are being used for microfiltration include polyacrylonitrile-polyvinyl chloride copolymer, polyvinylidene fluoride, polysulfone, cellulose triacetate and various nylons. More recently polyethersulfone (Susanto et al., 2009) and ceramic (Jana et al., 2010) membranes have been developed for their properties. The polyethersulfone membranes have high flux and a stable hydrophilic nature and the ceramic membranes are resistant to corrosion and can be used in high temperature and pressure atmospheres and have a generally longer life span. Microfiltration is used in waste water treatment (Nelson et al., 2007), the food industry (Saboya and Maobois, 2000) and bioprocesses (van Reis and Zydney, 2007). Ultrafiltration uses a finely porous membrane to separate water and microsolutes from macromolecules and colloids. The range of separation of the membranes is between 10 and 1000 Å. The membrane materials used for ultrafiltration are similar to those of microfiltration and also include some aromatic polyamides and cellulose acetate. Ultrafiltration applications can be summarised as concentration and fractionation, separation of two media in one step and waste water treatment (Jonsson and Tragbirdh, 1990). Nanofiltration membranes have pore sizes in the order of nanometers. They are similar to reverse osmosis membranes but they offer a higher flux. Some nanofiltration membrane materials include polyimide and polyamideimide, polydimethylsiloxane, polyoctenamer, poly (ethylene-co-propylene-co-diene), and polyacrylonitrile (Sereewatthanawut et al., 2008). The main use of nanofiltration is in

drinking water production (where it is usually pre-treatment to reverse osmosis) and wastewater treatment (Hilal et al., 2004). Reverse osmosis is a process of desalting water using membranes permeable to water but impermeable to salt. Pressurized water is contacted with the membrane and low-pressure water is obtained on the other side as permeate. Reverse osmosis membrane materials include cellulose acetate, polyamide membranes and m-phenylenediamine crosslinked with trimesoyl chloride (FT-30) and more recently zeolite (Li et al., 2007). The main application of reverse osmosis is production of high quality drinking water. Figure 2-21 shows a schematic of the different membrane filtration processes and their general rejections.

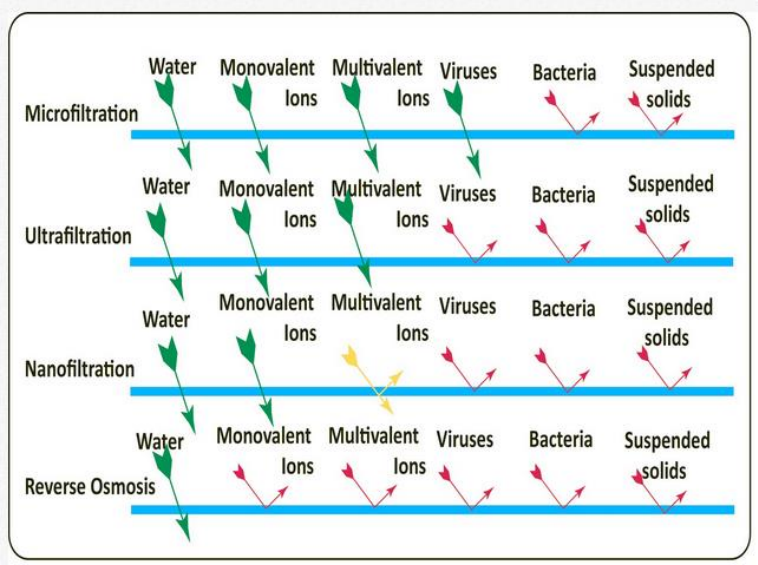

Figure 2-21: Spectrum of membrane process rejections (Aquafield Technologies, 2014).

The above membrane filtration processes have been used in the treatment of oil and water solutions and have been demonstrated in literature, with examples of the membrane processes used given in Table 2-1. It is clear from Table 2-1 that though

microfiltration can separate oil from water to some extent it cannot be used as the sole separating device to achieve the required oil concentrations in water. The ultrafiltration membranes can achieve oil/water separations that are acceptable and they would seem to be well suited to being used as oil/water separators accept that the nanofiltration membrane by Rahimpour et al. (2011) delivers good separation with high flux values. But, the nanofiltration membrane only treats water that has already been treated by a microfiltration membrane. It would be interesting to see whether a nanofiltration membrane can achieve the strict oil in water concentrations while delivering high flux and having no pre-treatment process ahead of it.

Membrane Filtration Models

The primary function of a membrane is to control the permeation of different substances. There are 2 models that have been used to describe the permeation of substances through a membrane. Those models are the solution-diffusion model and the pore-flow model. The solution-diffusion model states that permeants dissolve in the membrane material and then diffuse through the membrane down a concentration gradient. The different substances are separated based on the difference in their solubilities in the membrane material and their different diffusion rates through the membrane. The pore-flow model states that permeants are transported by a pressure driven convective flow through the pores of the membrane. Separation occurs because one of the permeants is excluded from some of the pores of the membrane (permeant size is larger than the pore size) through which the other permeants (whose size is less than the pore size) can move through.

Solution-Diffusion Model

The solution-diffusion model is rooted in thermodynamics where pressure, temperature, concentration and electrical potential are interrelated. The overall driving force for the movement of permeate is found to be the gradient in its chemical potential. The flux of component i (J_i(g/cm^{2}s)) is described by

$$J_i = -\mathrm{L_i}\frac{\mathrm{d}\mu_\mathrm{i}}{\mathrm{dx}} \tag{2.6}$$

where $d\mu_i/dx$ is the chemical potential gradient of component i and L_i is the coefficient of proportionality linking the gradient to the flux. According to Baker (2000) the chemical potential is expressed as

$$d\mu_i = \mathrm{RTd}\ln(\gamma_\mathrm{i}\mathrm{n_i}) + \upsilon_\mathrm{i}\mathrm{dP} \tag{2.7}$$

where n_i is the mole fraction of component i, γ_i is the activity coefficient linking the mole ratio to activity, P is the pressure and υ_i is the molar volume of i. Integrating equation 2.7 with respect to volume and pressure, since for incompressible phases such as liquids and solids the volume does not change with pressure, gives

$$\mu_i = \mu_\mathrm{i}^0 + \mathrm{RT}\ln(\gamma_\mathrm{i}\mathrm{n_i}) + \upsilon_\mathrm{i}(\mathrm{P} - \mathrm{P_i^0}) \tag{2.8}$$

where μ_i^0 is the chemical potential of pure i at the reference pressure P_i^0.

According to Baker (2000) for compressible fluids (gasses) the molar volume changes with a change in pressure thus integrating equation 2.7 gives

$$\mu_i = \mu_\mathrm{i}^0 + \mathrm{RT}\ln(\gamma_\mathrm{i}\mathrm{n_i}) + \mathrm{RT}\ln\left(\frac{\mathrm{P}}{\mathrm{P_i^0}}\right) \tag{2.9}$$

Table 2-1: Examples of membrane process used in the treatment of oily wastewater.

Filtration Process	Description	Efficiencies	Reference
Microfiltration	Tubular ceramic (α-Al_2O_3) microfiltration membrane system used for treatment of industrial oily waste water effluent.	Reduction of oil and grease content to 4mg/L and TOC removal higher than 95%.	Abadi et al., 2011.
Microfiltration	Kaolin, quartz and calcium carbonate membranes created by compaction method and sintered. Feed oil of 250 mg/L is filtered.	85% rejection of the oil.	Vasanth et al., 2011.
Microfiltration	A tubular coal based membrane is used for oily wastewater treatment. Uniform pore structure and narrow pore size distribution was achieved.	Oil rejections were found to exceed 98%. Flow rates of 25 L/h were achieved at 0.1MPa.	Pan et al., 2007.
Microfiltration	Al_2O_3 membrane is modified by $ZrCl_4$ nano particles to make the membrane	The steady flux that is achieved was found to be 88% of the original flux	Zhou et al., 2010.

	more hydrophilic. 1g/L engine oil emulsion is used as the feed into the system.	and oil rejection was found to be above 97%.	
Ultrafiltration	A polysulfone membrane is modified by polyvinypirrolidone and polyethylene glycol to increase its porosity and hydrophilicity in order to treat oily wastewater.	The membranes showed an oil retention of 90% and a permeate of 10mg/L oil. The membranes have also proved to be resilient against fouling.	Chakrabarty et al., 2008.
Utrafiltration	This system was designed to filter highly concentrated and unstable oil in water emulsions.	99.5% rejection of oil were achieved at flow rates of 10 to 60 L/m^2h.	Falahati and Tremblay, 2011.
Ultrafiltration	A composite membrane prepared by the interfacial polymerization of polyvinyl alcohol, piperazine and terephthalyl chloride on polyether sulfone (PES) is used in oil/water	An oil rejection of 90% was achieved with a flux of 60 L/m^2h.	Shang and Peng, 2007.

	separation. A thin polyamide-PVA layer is formed on top of the (PES) support.		
Nanofiltration	A commercial NF-2 and a self-made NF-5 membrane are used to treat oily wastewater. The wastewater was pre-treated by microfiltration prior to the nanofiltration process which took place at pressures from 5 to 20 bar at 5 bar increments and temperatures of 20, 30 and 40^{o}C.	The flux obtained from the membranes was between 20 and 265 kg/m^{2}h, with the increase in flux relating to the increase in pressure and temperature. The chemical oxygen demand (COD) and the electrical conductivity (EC) were both decreased by an order of magnitude of 10.	Rahimpour et al., 2011.

where P_i^0 is the saturation vapour pressure of component I ($P_{i,\,sat}$), therefore equations 2.8 and 2.9 become

$$\mu_i = \mu_i^0 + RT\ln(\gamma_i n_i) + \upsilon_i\left(P - P_{i,sat}^0\right) \tag{2.10}$$

and

$$\mu_i = \mu_i^0 + RT\ln(\gamma_i n_i) + RT\ln\left(\frac{P}{P_{i,sat}^0}\right) \tag{2.11}$$

respectively (Wijmans and Baker, 1995).

Several assumptions made by Baker (2000) for the solution-diffusion model:

- Fluids on either side of the membrane are in equilibrium with the membrane material at the interface.
  - The gradient of chemical potential is continuous from one side of the membrane to the other.
  - The rates of adsorption and desorption at the membrane interface are higher than the diffusion rates through the membrane.
- When pressure is applied on a dense membrane the pressure across the entire membrane is constant at its highest value
  - In the solution-diffusion model pressure is transmitted in the same way as liquids.
  - The pressure within the membrane is uniform.
  - The chemical potential gradient of component i across the membrane is expressed only as a function of concentration gradient.

If it is assumed that γ_i is constant and that there is no pressure gradient through the membrane then

$$J_i = \frac{\mathrm{RTL_i}}{\mathrm{n_i}} \times \frac{\mathrm{dn_i}}{\mathrm{dx}} \tag{2.12}$$

Figure 2-22 shows the diffusion of a single component through a dense membrane using the solution-diffusion model with the previously mentioned assumptions.

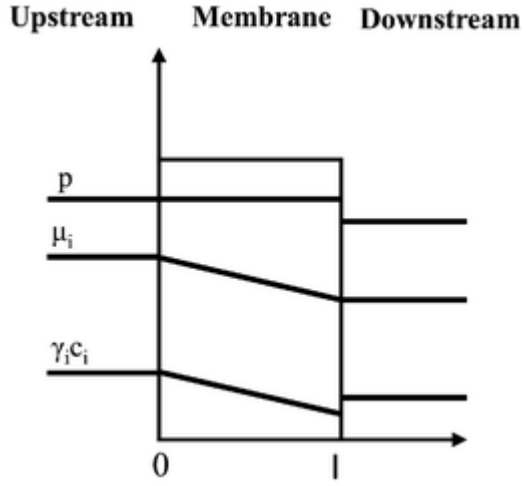

Figure 2-22: Depiction of the solution-diffusion model for a single component diffusing through a membrane (Vandezande et al., 2008).

From equation 2.12 the gradient of component i is expressed in terms of the mole fraction of i. If the concentration of i, c_i (g/cm^3) is expressed as

$$c_i = \mathrm{m_i \rho n_i} \tag{2.13}$$

where m_i is the molecular weight (g/mol) of component i and ρ is the molar density (mol/cm^3), then equation 2.12 can be written as

$$J_i = \frac{\mathrm{RTL_i}}{\mathrm{c_i}} \times \frac{\mathrm{dc_i}}{\mathrm{dx}} \tag{2.14}$$

Since equation 2.14 has the same form as Fick's law, RTL_i/c_i can be replaced by the diffusion coefficient D_i to give

$$J_i = -D_i \frac{dc_i}{dx} \tag{2.15}$$

and after intergration

$$J_i = -D_i \frac{\left(c_{i,o,(m)} - c_{i,l,(m)}\right)}{l} \tag{2.16}$$

where (m) is the phase of the membrane, o is the feed side of the membrane and l is the permeate side of the membrane.

Figure 2-23 describes the solution-diffusion model using osmosis as an example. In Figure 2-23(a) shows a semipermeable membrane separating a salt solution from water. In the example only water and not the salt is considered for simplicity. The membrane is assumed to be very selective therefore the concentration of salt within the membrane is very small. The pressure on both sides of the membrane is equal and constant ($P_o = P_m = P_l$) and the chemical potential of the water across the membrane is a smooth gradient from the water side ($\mu_{i,l}$) to the solution side ($\mu_{i,o}$). The solvent activity ($\gamma_{i,(m)}n_{i,(m)}$) falls from the water side to the solution side indicating that the water passes from the right side to the left. Figure 2-23(b) shows the situation of osmotic equilibrium when a pressure is exerted on the solution side that brings the flow across the membrane to zero. As can be seen from the figure the solvent activity is constant throughout the membrane and therefore there is no longer a driving force for the movement of water. Figure 2-23(c) is a situation where the salt solution pressure is increased to a point above the osmotic pressure then the solvent activity forms a

gradient from the solution side to the water side thus promoting flow from left to right. The process that is depicted in Figure 2-23(c) is called reverse osmosis.

According to Wijmans and Baker (1995) the solution-diffusion model predicts membrane performance very well when describing dialysis, gas separation, reverse osmosis and pervaporation systems but does not describe ultrafiltration membranes well even when the ultrafiltration membrane is able to separate small solutes (such as sucrose and raffinose. The ultrafiltration process is best described by the pore-flow model. Nanofiltration membranes lie between reverse osmosis and ultrafiltration and thus possess properties of both filtration systems. There is a 'transition region' as stated by Wijmans and Baker (1995) that is not well described by either the solution-diffusion model or by the pore-flow model. This short coming of the conventional models for membranes needs to be addressed by a modelling system that is not based on empirical equations but on the experimental data of the process itself.

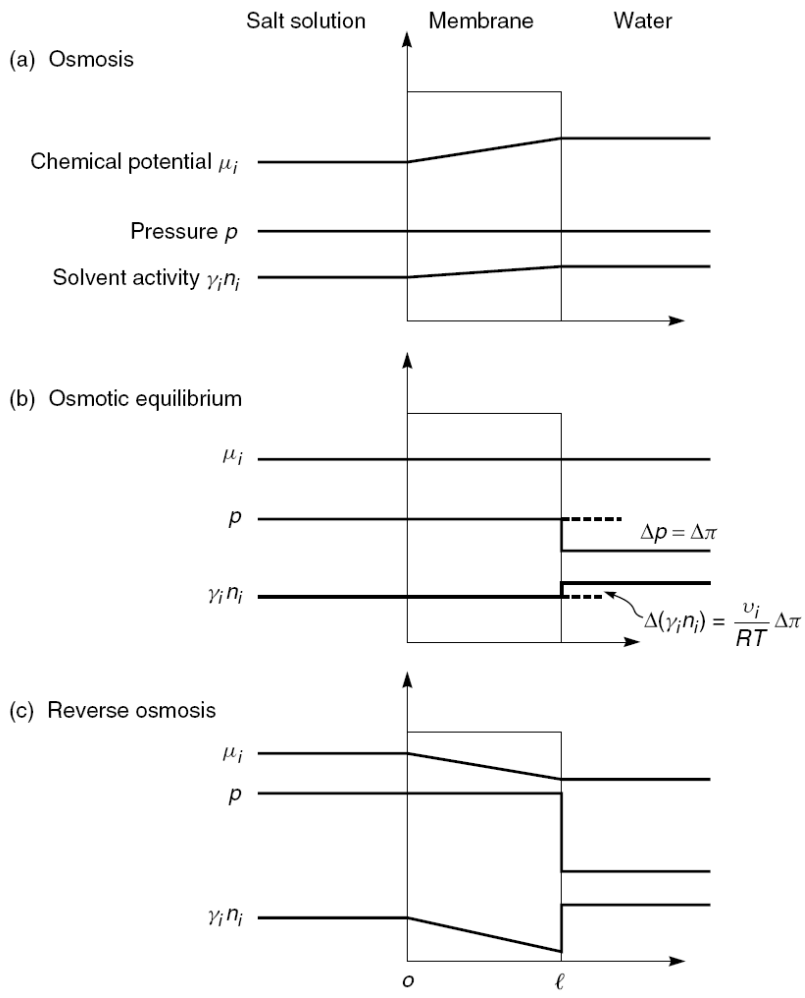

Figure 2-23: Depiction of the solution-diffusion model for a single component using osmosis as an example (Baker, 2000).

Pore-flow model

Baker (2000) determines three properties of pore-flow membranes that govern the flux through the membrane and the separation effectiveness of the membranes. The first is porosity which is the fraction of total membrane volume that is porous. The second factor is tortuosity which is the average length of a membrane pore compared with the thickness of the membrane. If a pore is a perfect vertical bore through the membrane

then the tortuosity will be one. If the pore is at an angle through the membrane or it forms a winding route through the membrane then the tortuosity will be higher than one. The last factor is the pore diameter which is the most important factor as it dictates the size of the particles that will be able to enter the membrane. The pore-flow mechanism takes place in ultrafiltration and microfiltration processes and it operates on the surface where it is called screen.

Screen Filtration

Screen filtration is simply that the pores on the surface are smaller than the particles that need to be removed. These particles are then captured on the surface of the membrane and accumulate there. Screen filters are usually anisotropic membranes with a fine surface layer and a more microporous support. The equation used to describe this type of filtration is

$$\frac{A}{A_o} = \frac{(\mathrm{r}-\mathrm{a})^2}{\mathrm{r}^2} \tag{2.17}$$

where A is the area of the pore that is available for solute transport ($\pi(r\text{-}a)^2$), r is the radius of the circular capillary, a is the radius of the solute molecule and A_o is the area of the pore that is available for solvent transport (πr^2) (Baker, 2000). Equation 2.17 can be adjusted for the parabolic velocity profile of liquid flowing through a pore to take the form of (Baker, 2000)

$$\left(\frac{A}{A_o}\right)' = 2\left(1-\frac{\mathrm{a}}{\mathrm{r}}\right)^2 - \left(1-\frac{\mathrm{a}}{\mathrm{r}}\right)^4 \tag{2.18}$$

where $\left(\frac{A}{A_o}\right)' \sim \frac{c_l}{c_o}$ and c_l is the solute concentration in the filtrate and c_o is the solute concentration in the feed. Solute rejection is described as (Baker, 2000)

$$R = \left[1 - 2\left(1 - \frac{a}{r}\right)^2 - \left(1 - \frac{a}{r}\right)^4\right] \times 100\% \quad (2.19)$$

Globular proteins can be used to find the pore sizes of the membrane by finding the retention measurements because the protein sizes can be calculated very accurately.

2.2.5. Polymer-Carbon nanotube interactions

Soon after the discovery of the extraordinary properties of CNTs scientific focus shifted to the creation of composite materials that can be improved by the properties of CNTs (Ajayan et al., 1994). The modification of a polymer by CNTs can be divided into two categories depending on whether the bonding between the polymer and the nanotube is non-covalent or covalent. Non-covalent modification is when the polymer physically covers the CNT surface and by the π-bond interactions with the polymer matrix, forces that act on the polymer matrix can be transferred to the CNTs. The benefit of the non-covalent bonding is that the CNT structure is not altered and thus retains its original properties. The covalent bonding (also called grafting) method creates a strong bond between the CNT and the polymer and there are two approaches to this method, “grafting to” and “grafting from”. “Grafting to” involves the creation of a polymer chain which terminates with a reactive group which is then reacted with the nanotubes by the addition reaction (Liu, 2005; Homenick et al., 2007). The “grafting from” technique involves the immobilisation of chemical initiators (monomers) of a polymerisation reaction on the nanotube wall. The monomer is introduced and a polymerisation reaction begins at the surface of the nanotube (Liu, 2005; Homenick et al., 2007).

CNT-Polymer composite processing methods

Solution processing

This process is the simplest method of creating CNT-polymer composites. The CNTs are added to a solvent and dispersed using sonication and then the polymer is mixed into this solution and the solvent is then vaporised leaving behind the composite. The composite mixture can be cured after the evaporation stage (Ajayan et al., 1994). Jin et al. (1998) caused the CNTs in the composite to align by stretching thin strips of the composite at 100^{o}C. The CNTs aligned in the direction of the mechanical tension. Geng et al. (2002) used fluorinated CNTs and poly(ethylene oxide) as a suspension that is used in a roll-casting system. The system consists of two rollers that have an adjustable gap between them and the CNT-polymer solution is dropped onto one of the rollers forming a film after evaporation of the solvent. This method has rendered composites that transfer mechanical loads from the polymer matrix to the CNTs very well. Because of the tendency of CNTs to agglomerate in the polymer solution during solvent evaporation, Du et al. (2003) proposed a coagulation method whereby the CNT-polymer solution is placed in a “bad” solvent (usually water) which causes rapid precipitation of the polymer and entrapping the CNTs in place.

Bulk Mixing

Bulk mixing is a process whereby the CNTs and polymer are pulverised by mechanical means to produce a composite powder. Xia et al. (2004) used pan milling to create a CNT-polypropylene powder which was melt-mixed with the aid of a twin-roll masticator to get a homogeneous composite. High energy ball milling has also been used to create CNT-polymer composites and was also found to give a good dispersion of CNTs in the polymer matrix (Ghose et al., 2006).

Melt mixing

Melt mixing is usually applied to polymers that cannot be processed using the solution techniques because of their insolubilities in common solvents. Therefore the ability of the polymer to soften when exposed to heat is used in conjunction with the application of extreme shear forces which leads to the blending of the CNTs with the polymer. An example of this process is by Haggenmueller et al. (2000) the CNT-polymer mixture is repeatedly hot pressed into a film and then broken up into pieces again which improved the CNT dispersion with each consecutive step. The composite film that is found after this process is spun into a fibre using a melt spinning apparatus which produced draw ratios of between 20 and 3600. Because of the alignment of the CNTs during this spinning process the mechanical properties of the composite increased with an increase in the draw ratio and CNT load.

2.2.6. Conventional Membrane Modules

For membranes to be used at industrial scale, large volume areas will be required. Membrane modules package membranes in a space saving and economically viable manner. The most common modules are the Plate-and-frame, tubular, spiral-wound and hollow fibre modules. Plate-and-frame modules (Figure 2-24) are one of the earliest membrane systems. Membrane, feed spacers and the product spacers are layered together between two ends and the feed is forced across the surface of the membrane. Some of the feed passes through the membrane and enters the permeate channel which ends up at the central permeate collection manifold. These modules are used for small scale applications such as electrodialysis and pervaporation (Stern, 1965). They are expensive units compared to the other modules and require high maintenance.

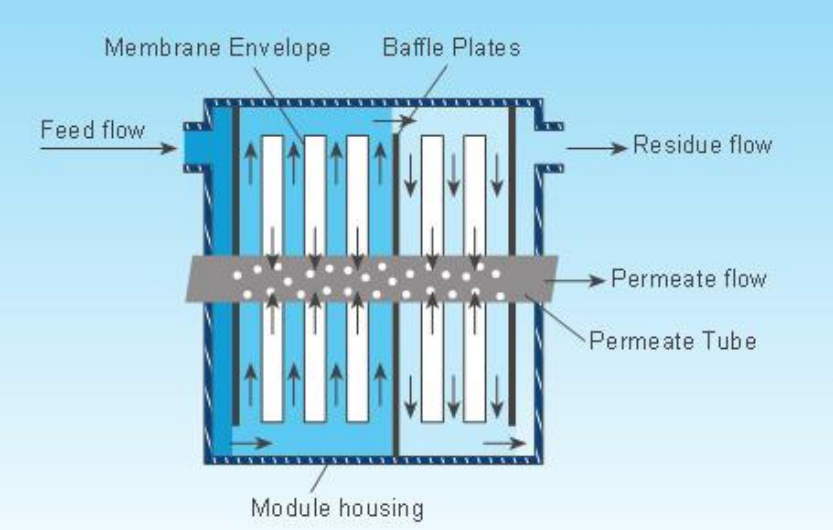

Figure 2-24: Schematic of Plate-and-frame module (Eurofilm, 2014).

Tubular modules (Figure 2-25) are simply tubes with porous paper or fibreglass support and the membrane on the inside of the tube. Smaller tubes of 0.5 and 1 cm are usually packed into a larger tube. In a typical system the tubes are manifolded in series and the permeate is collected from each tube. Tubular modules are generally only used for ultrafiltration applications (Baker, 2000).

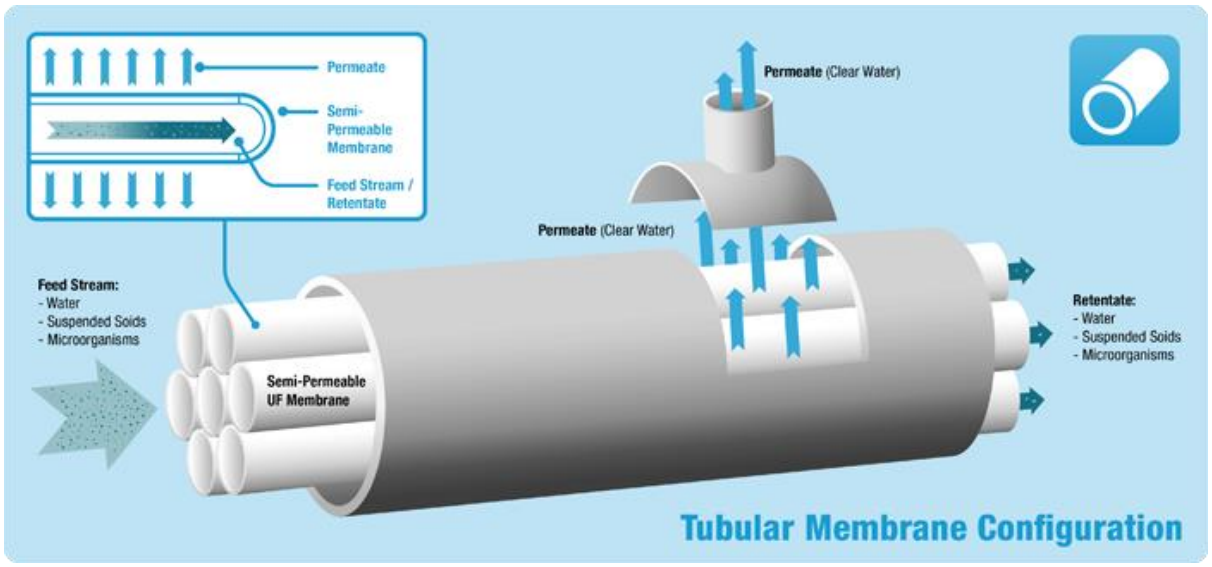

Figure 2-25: Representation of a tubular membrane configuration (Koch Membrane Systems, 2014).

Spiral-wound modules (Figure 2-26) consist of a membrane envelope of spacers and membrane wound around a perforated collection tube. The feed passes axially down the module and across the membrane envelope and a portion of the feed permeates through the membrane and into the collection tube. These modules were originally developed for use with artificial kidney designs but can now be used for reverse osmosis (Wagner, 2001).

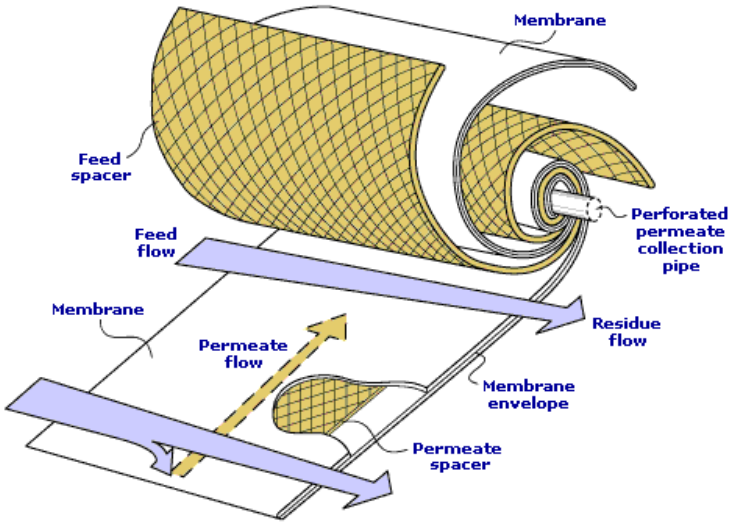

Figure 2-26: Schematic of a spiral-wound module (MTR, 2014).

Figure 2-27 is a schematic of a shell side feed where there is a closed (on one side) bundle of fibres in a pressure vessel and the system is pressurised from the shell side. The permeate passes through the fibre walls and exits at the open ends. This design is easy to make and gives large membrane areas. Because of high hydrostatic pressures the fibres have small diameters and thick walls (Baker, 2000)

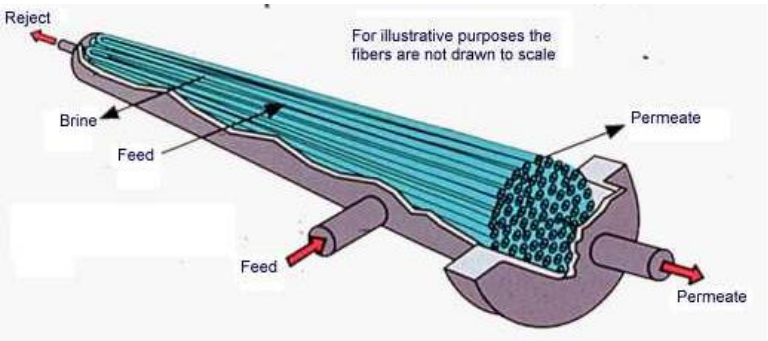

Figure 2-27: Schematic of a hollow fibre module (GE Power & Water, 2014).

In all the modules that have been presented the velocity of the fluid pumped across the membrane surface is high. It has been stated that a rapid fluid flow on the membrane surface decreases concentration polarisation (Sablani et al., 2001). The increase of turbulence on a membrane surface by using a rotating disk membrane module (RDMM) was found to break the concentration polarisation layer (Sen et al., 2010). Liu et. al (2010) found that the turbulence caused by their helical module was enough to increase flux by 48 – 69% without the need for extra energy input into the system as in the RDMM.

2.3. Artificial Neural Networks

Due to the nature of the nanofiltration membranes, it is difficult to model the membrane flux using conventional models such as the solution-diffusion and the pore flow models. It is therefore necessary to use empirical models that can predict results using experimental data. Artificial neural networks offer this ability and the basic requirements for an ANN are (McClelland and Rumelhart, 1986):

- A set of processing units (artificial neurons)
- An output for every unit, y_j

- A connection between the units denoted by weights w_{nj}, which is the effect unit n has on unit j
- A propagation rule, which is the effective input s_n from external inputs
- An activation function σ which determines the new level of activation dependent on the $s_j(t)$ and the current activation y_j
- A bias for each unit b_j
- A learning rule
- A system that provides inputs and error signals

An artificial neuron (processing unit) has a simple task, it receives input and computes an output. Figure 2-28 shows a processing unit which consists of inputs, weights, a bias, a summation function, an activation function and an output.

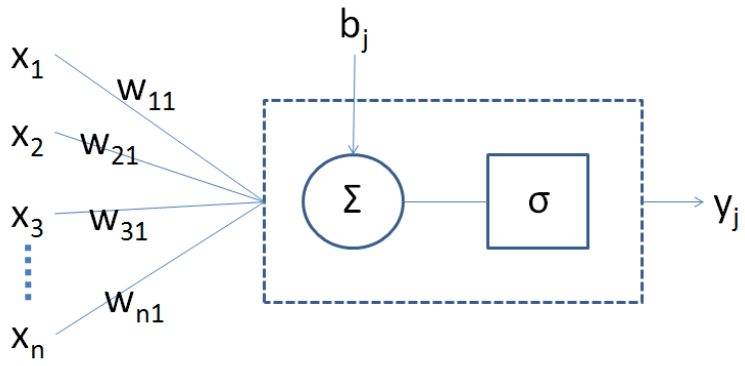

Figure 2-28: A single processing unit (artificial neuron) (TUM, 2014).

The input to unit j is the weighted sum of the separate outputs from the connected units plus the bias (b_j). The summation function can be expressed as (Krose and van der Smagt, 1996):

$$s_j(t) = \sum_j w_{nj}(t)x_n(t) + b_j(t) \tag{2.20}$$

The rule that gives the effect of the total input on the activation of unit j is:

$$y_j(\mathrm{t}+1) = \sigma_j\left(\mathrm{s_j(t)}\right) = \sigma_\mathrm{j}(\sum_\mathrm{n} \mathrm{w_{nj}(t)x_n(t)} + \mathrm{b_j(t)}) \tag{2.21}$$

where σ_j is the function that takes $s_k(t)$ and $y_k(t)$ and produces a new value y_j. There are several activation functions σ_j that can be used and some are in Figure 2-29.

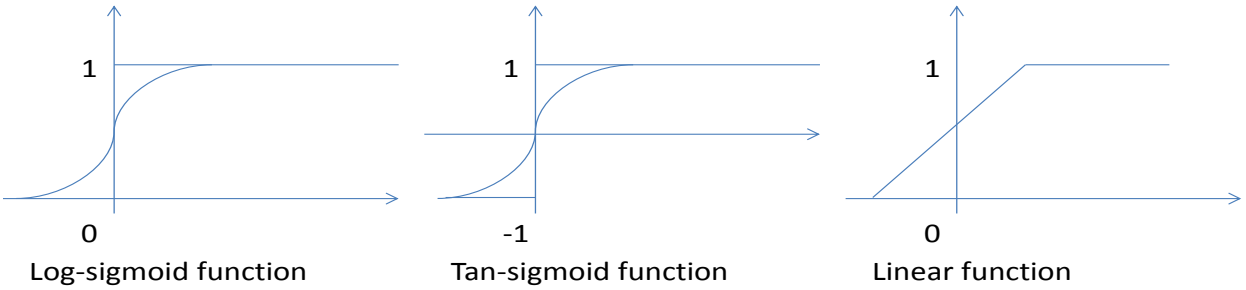

Figure 2-29: Some of the common activation functions that can be used in a neural network (TUM, 2014).

The most commonly used activation function is the sigmoid function such that:

$$y_j = \sigma(\mathrm{s_j}) = \frac{1}{1+\mathrm{e}^{\mathrm{s_j}}} \tag{2.22}$$

There are two main types of ANN which are the feedforward network and the recurrent network. Feedfoward networks have data flowing in a single direction (from the input to the output) (Figure 2-30a) while recurrent networks contains connections that go in the opposite direction (Figure 2-30b).

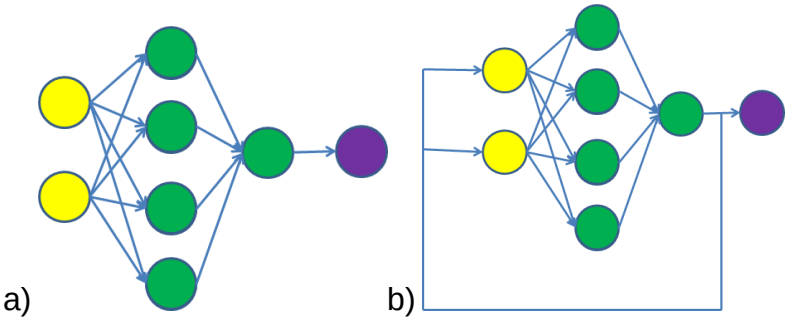

Figure 2-30: A graphical example of a) feedfoward network and b) recurrent network (Dennis, 1997).

Since a given network has to provide the required outputs for a given set of inputs, it has to be configured (trained). There are two training directions a network can take. The first is supervised learning where the network is given inputs with their corresponding outputs. The network "learns" by adjusting the weights of the network so that the given inputs produce the given outputs. Unsupervised learning the system is only given the inputs and it must statistically discover a pattern in the inputs within its own framework. Both learning methods require that the weights between units be adjusted. One of the oldest learning rules is by Hebb (1949) and it states that if two units (n and j) are activated simultaneously then their connection must be strengthened. If unit j receives input from unit n then:

$$w_{jn} = \gamma y_j x_n \tag{2.23}$$

where γ is a positive constant representing the learning rate. Another commonly used learning rule, also called the Widrow-Hoff rule, is the delta rule:

$$w_{jn} = \gamma x_n (d_j - y_j) \tag{2.24}$$

where d_j is the activation provided by the "teacher".

A single layer network with a linear activation function is described by Krose and van der Smagt (1996) as:

$$y = \sum_n w_n x_n + b \tag{2.25}$$

The network would need to be trained such that for all the input values x^p the network output approaches the target values d^p as closely as possible. For every input the output differs from the target output by (d^p – y^p) where y^p is the output for the pattern. The error function (E) is given by the least mean square (LMS):

$$E = \sum_p E^p = \frac{1}{2}\sum_{\mathrm{p}} (\mathrm{d^p} - \mathrm{y^p})^2 \tag{2.26}$$

where p ranges over the input patterns and E^p is the error on pattern p. LMS attempts to minimize the error by gradient descent. The change of the weight is then proportional to the derivative of the error of the current pattern with respect to each weight (Krose and van der Smagt, 1996):

$$\Delta_p \mathrm{w_n} = \gamma \frac{\partial \mathrm{E^p}}{\partial \mathrm{w_n}} \tag{2.27}$$

where γ is a constant of proportionality. The derivative is

$$\frac{\partial E^p}{\partial w_n} = \frac{\partial \mathrm{E^p}}{\partial \mathrm{y^p}} \frac{\partial \mathrm{y^p}}{\partial \mathrm{w_n}} \tag{2.28}$$

Since

$$\frac{\partial y^p}{\partial w_n} = \mathrm{x_n} \tag{2.29}$$

and

$$\frac{\partial E^p}{\partial y^p} = (\mathrm{d^p} - \mathrm{y^p}) \tag{2.30}$$

then

$$\Delta_p \mathrm{w_n} = \gamma \delta^{\mathrm{p}} \mathrm{x_n} \tag{2.31}$$

where $\delta^p = (d^p - y^p)$ is difference between the target output and the output for pattern p.

2.3.1. Backpropagation

Backpropagation is described as a generalisation of the delta rule for multi-layer networks and nonlinear activation functions. A feedfoward network consists of multiple layers with connections between units in the direction from inputs to outputs (there are no connections between units in the same layer. The layers between the input and output layer are called hidden layers and are designated with, $N_{h,l}$ where h is for "hidden" and the l is the number of the hidden layer. The input and output layers are designated with N_i and N_o respectively. Figure 2-31 shows a backpropagation network.

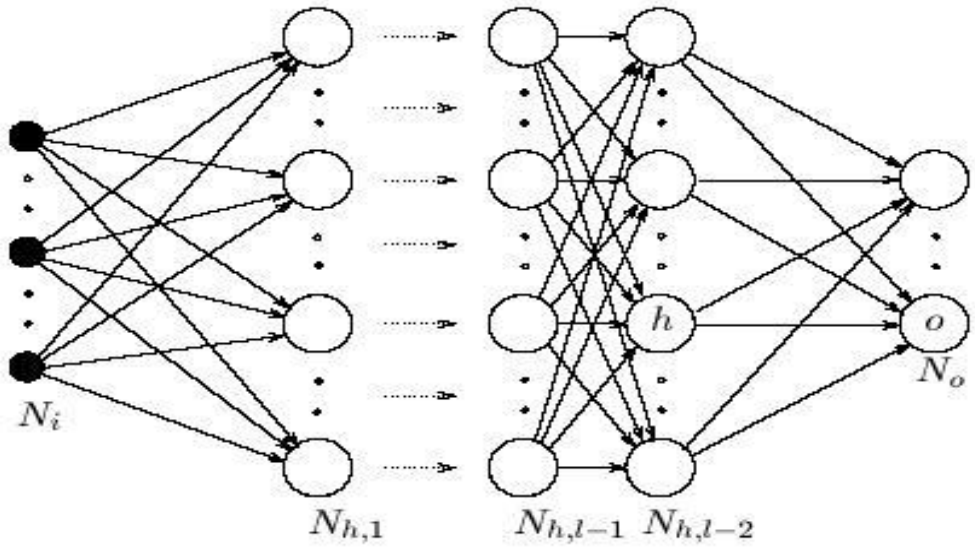

Figure 2-31: Feedfoward backpropagation network with l hidden layers (Neuro AI, 2013).

The activation function is given by

$$y_j^p = \sigma\left(\mathrm{s_j^p}\right) \tag{2.32}$$

where

$$s_j^p = \sum_{\mathrm{n}} \mathrm{w_{nj} x_n^p} + \mathrm{b_j} \tag{2.33}$$

To get to the correct generalization rule (Neuro AI, 2013) set

$$\Delta_p \mathrm{w_{nj}} = \gamma \frac{\partial \mathrm{E^p}}{\partial \mathrm{w_{nj}}} \tag{2.34}$$

E^p is defined as the total quadratic error for pattern p at the output units (Krose and van der Smagt, 1996):

$$E^p = \frac{1}{2} \sum_{\mathrm{o}=1}^{\mathrm{N_o}} \left(\mathrm{d_o^p} - \mathrm{y_o^p}\right) \tag{2.35}$$

where d^p_o is the target output for unit o when pattern p is clamped. E is set as $E = \sum_p E^p$ (Neuro AI, 2013) which is the sum of squared errors, then

$$\frac{\partial E^p}{\partial w_{nj}} = \frac{\partial \mathrm{E^p}}{\partial \mathrm{s_j^p}} \frac{\partial \mathrm{s_j^p}}{\partial \mathrm{w_{nj}}} \tag{2.36}$$

where (by equation 2.33)

$$\frac{\partial s_j^p}{\partial w_{nj}} = \mathrm{x_n^p} \tag{2.37}$$

It is defined as

$$\delta_j^p = \frac{\partial \mathrm{E^p}}{\partial \mathrm{s_j^p}} \tag{2.38}$$

The delta rule which will provide a gradient descent with weight changes of

$$\Delta_p \mathrm{w_{nj}} = \gamma \delta_\mathrm{j}^\mathrm{p} \mathrm{x_n^p} \tag{2.39}$$

To calculate δ_j^p the chain rule is used to write the partial derivative (equation 2.38) as two factors (Krose and van der Smagt, 1996). One factor is the change in error as a function of the output unit and the other factor is the change in output as a function of the input:

$$\delta_j^p = \frac{\partial \mathrm{E^p}}{\partial \mathrm{y_j^p}} \frac{\partial \mathrm{y_j^p}}{\partial \mathrm{s_j^p}} \tag{2.40}$$

From equation 2.32

$$\frac{\partial y_j^p}{\partial s_j^p} = \sigma'\left(\mathrm{s_j^p}\right) \tag{2.41}$$

Assuming that unit j is an output unit j = o of the network

$$\frac{\partial E^p}{\partial y_o^p} = \left(d_o^p - y_o^p\right) \tag{2.42}$$

Substituting equations 2.41 and 2.42 into equation 2.40 the result is

$$\delta_o^p = \left(\mathrm{d_o^p} - \mathrm{y_o^p}\right)\sigma'\left(\mathrm{s_o^p}\right) \tag{2.43}$$

for any output unit o (Neuro AI, 2013).

If j is not an output unit but a hidden unit j = h instead, the contribution of the unit to the output of the network is not readily known. According to Krose and van der Smagt

(1996) the error can be written as a function of the net inputs from the hidden layer to the output, $E^p = E^p\left(s_1^p, s_2^p, \dots, s_n^p, \dots\right)$ and the chain rule is used to get

$$\frac{\partial E^p}{\partial y_h^p} = \sum_{o=1}^{N_o} \frac{\partial E^p}{\partial s_o^p}\frac{\partial s_o^p}{\partial y_h^p} = \sum_{o=1}^{N_o} \frac{\partial E^p}{\partial s_o^p}\frac{\partial}{\partial y_h^p}\sum_{n=1}^{N_h} w_{jo}x_n^p = \sum_{o=1}^{N_o} \frac{\partial E^p}{\partial s_o^p} w_{ho}$$
$$= \sum_{o=1}^{N_o} \delta_o^p w_{ho} \tag{2.44}$$

Substituting equation 2.44 into equation 2.40

$$\delta_h^p = \sigma'\left(s_h^p\right)\sum_{o=1}^{N_o} \delta_o^p w_{ho} \tag{2.45}$$

A simpler explanation of backpropagation than the equations above is that when a learning pattern is given the activation functions are propagated to the output units and the network output is compared to the target output there is an error. The objective is to make this error zero and this is done by changing the connections in the neural network in such a way that the next time the error will be zero. To reduce the error, the incoming weights have to be adjusted according to (Krose and van der Smagt, 1996)

$$w_{ho} = (d_o - y_o)y_h \tag{2.46}$$

The weights coming from the input layer to the hidden layer need to be adjusted. To do this, the delta rule is applied again but the hidden layer does not have an explicit δ value and thus equation 2.45 (derived from equation 2.44) is used. Therefore the delta of a hidden unit h is derived from the delta of each output unit o.

2.3.2. Resilient Backpropagation (Rprop)

The backpropagation training rule is a good method for training ANN but the training takes time and the iterations done are quite numerous. The resilient backpropagation rule is a modification of the backpropagation rule and it gives the required error minimisation in a shorter time. The advantages of Rprop are that it is very fast and robust (Riedmiller, 1994; Riedmiller and Braun, 1993) compared to other supervised learning methods. Rprop is a general method and it is not dependent on certain network topologies. The rule is dependent on the sign of the derivative and not the amount (Igel and Husken, 2003). The Rprop algorithm is explained by (Riedmiller and Braun, 1993) that the partial derivative on the weight step (equation 2.34) is eliminated and only the sign of the derivative is used to determine the direction of the weight update. The size of the change is determined by an update value, $\Delta_{nj}^{(t)}$:

$$\Delta w_{nj}^{(t)} = \begin{cases} -\Delta_{nj}^{(t)} \ , \ if \ \dfrac{\partial E^{(t)}}{\partial w_{nj}} > 0 \\ +\Delta_{nj}^{(t)} \ , \ if \ \dfrac{\partial E^{(t)}}{\partial w_{nj}} < 0 \\ 0 \quad , \quad else \end{cases} \tag{2.47}$$

Now to determine the new update values:

$$\Delta_{nj}^{(t)} = \begin{cases} \eta^{+} * \Delta_{nj}^{(t-1)} \ , \ if \ \dfrac{\partial E^{(t-1)}}{\partial w_{nj}} * \dfrac{\partial E^{(t)}}{\partial w_{nj}} > 0 \\ \eta^{-} * \Delta_{nj}^{(t-1)} \ , \ if \ \dfrac{\partial E^{(t-1)}}{\partial w_{nj}} * \dfrac{\partial E^{(t)}}{\partial w_{nj}} < 0 \\ \Delta_{nj}^{(t-1)} \quad , \quad else \end{cases} \tag{2.48}$$

where $0 < \eta^- < 1 < \eta^+$. To explain the equations, if the partial derivative changes its sign, then the last update was too large and the algorithm passed the local minimum and thus the update value needs to be changed accordingly (by multiplying with η^-). If the derivative does not change sign then the update value is increased only slightly to promote convergence. If there is a change in sign then the next learning step should have no adaptation (set $\frac{\partial E^{(t-1)}}{\partial w_{nj}} := 0$). The Algorithm for the Rprop learning rule as provided by Riedmiller (1994) is given below:

$\forall i,j(For\ all\ i,j) :\ \Delta_{nj}(t) =\ \Delta_o$

$\forall i,j :\ \frac{\partial E}{\partial w_{nj}}(t-1) = 0$

Repeat

Compute Gradient $\frac{\partial E}{\partial w}(t)$

For all weights

{

If $(\frac{\partial E}{\partial w_{nj}}(t-1) * \frac{\partial E}{\partial w_{nj}}(t) > 0)$

then

{

$\Delta_{nj}(t) = minimum\ (\Delta_{nj}(t-1) * \eta^+, \Delta_{max})$

$\Delta w_{nj}(t) = -sign\ \left(\frac{\partial E}{\partial w_{nj}}(t)\right) * \Delta_{nj}(t)$

$w_{nj}(t+1) = w_{nj}(t) + \Delta w_{nj}(t)$

$\frac{\partial E}{\partial w_{nj}}(t-1) = \frac{\partial E}{\partial w_{nj}}(t)$

}

Else if $\left(\frac{\partial E}{\partial w_{nj}}(t-1) * \frac{\partial E}{\partial w_{nj}}(t) < 0\right)$

then

{

$\Delta_{nj}(t) = maximum\ (\Delta_{nj}(t-1) * \eta^{+}, \Delta_{min})$

$\frac{\partial E}{\partial w_{nj}}(t-1) = 0$

}

Else if $\left(\frac{\partial E}{\partial w_{nj}}(t-1) * \frac{\partial E}{\partial w_{nj}}(t) = 0\right)$

then

{

$\Delta w_{nj}(t) = -sign\left(\frac{\partial E}{\partial w_{nj}}(t)\right) * \Delta_{nj}(t)$

$w_{nj}(t+1) = w_{nj}(t) + \Delta w_{nj}(t)$

$\frac{\partial E}{\partial w_{nj}}(t-1) = \frac{\partial E}{\partial w_{nj}}(t)$

}

}

Until (convergence)

The Rprop algorithm takes in the initial update value Δ_o and a limit for the maximum step size Δ_{max}. Δ_o is usually set as 0.1 but the value of Δ_o is not critical as it changes as learning continues. The maximum weight-step is determined by the size of the update value but it is limited in order to prevent the weights being too large. The upper bound is set by Δ_{max} and is usually 50 (Riedmiller and Braun, 1993). Again the convergence is not sensitive to this parameter but it may be needed if the problem requires small steps to be taken. The minimum step size is always set to $\Delta_{min} = 1e^{-6}$.

In this work a neural network will be used to model the membrane produced in chapter 4 using Encog and the Matlab neural network toolbox.

References

Abadi, S. R. H., Sebzari, M. R., Hemati, M., Rekabdar, F. & Mohammadi, T., 2011, 'Ceramic membrane performance in microfiltration of oily wastewater', Desalination 265, 222–228.

Ajayan, P.M., Stephan, O., Colliex, C. & Trauth, D., 1994, 'Aligned carbon nanotube arrays formed by cutting a polymer resin–nanotube composite', Science 265, 1212–1214.

Altena, F., 1982, 'Phase Separation Phenomena in Cellulose Acetate Solutions in Relation to Asymmetric Membrane Formation', PhD Dissertation, Twente University of Technology, Enschede, Netherlands.

Aquafield Water Services, 2014, 'Aquafield – Technologies'. Available from http://www.aquafieldservices.com/index.php/technologies/membrane-filtration. [May 2014].

Baker, R.W., 2000, 'Membrane Technology and Applications', West Sussex, John Wiley & Sons.

Belin, T. & Epron, F., 2005, 'Characterization methods of carbon nanotubes: a review', Materials Science and Engineering B 119, 105–118.

Cadotte, J. E. & Petersen, R. J., 1981, 'Thin-film composite reverse osmosis membranes: origin, development and recent advances', ACS Symposium Series 153, 305 – 326.

Cadotte, J.E., Cobian, K.E., Forester, R.H. & Petersen, R.J., 1976, 'Continued evaluation of in situ-formed Condensation Polymers for Reverse Osmosis Membranes: Final Report', NTIS Report No. PB 253193, US Department of Interior.

Cadotte, J.E., Steuck, M.J. & Petersen, R.J., 1978, 'Research on in-situ-formed condensation polymers for reverse osmosis membranes', NTIS Report No. PB 288387, US Department of Interior.

Chakrabarty, B., Ghoshal, A.K. & Purkait, M.K., 2008, 'Ultrafiltration of stable oil-in-water emulsion by polysulfone membrane', Journal of Membrane Science 325, 427–437.

Cheah, S. M., 2014, 'Membrane Classification'. Available from http://separationprocesses.com/Membrane/MainSet6.htm. [May 2014].

Daenen, M., de Fouw, R.D., Hamers, B., Janssen, P.G.A., Schouteden, K. & Veld, M.A.J., 2003, 'The Wondrous World of Carbon Nanotubes 'a review of current carbon nanotube technologies'', Eindhoven University of Technology.

Dennis, S., 1997, 'Introduction to Neural Networks'. Available from http://staff.itee.uq.edu.au/janetw/cmc/chapters/Introduction/. [October, 2014].

Du, F., Fischer, J.E. & Winey, K.I., 2003, 'Coagulation method for preparing singlewalled carbon nanotube/poly(methyl methacrylate) composites and their modulus, electrical conductivity, and thermal stability', Journal of Polymer Science B 41, 3333–3338.

Eurofilm, 2014, 'Membrane Module'. Available from http://www.eurofilm.com.cn/research.asp?small_sort=12&pro_id=50. [May 2014].

Falahati, H. & Tremblay, A.Y., 2011, 'Flux dependent oil permeation in the ultrafiltration of highly concentrated and unstable oil-in-water emulsions', Journal of Membrane Science 371, 239–247.

Frank, S., Poncharal, P., Wang, Z.L. & Heer, W.A., 1998, 'Carbon nanotube quantum resistors', Science 280, 1744–1746.

GE Power & Water, 2014, 'Hollow fiber reverse osmosis modules'. Available from http://www.gewater.com/handbook/ext_treatment/fig9-5.jsp. [May 2014].

Geng, H., Rosen, R., Zheng, B., Shimoda, H., Fleming, L., Liu, J. & Zhou, O., 2002, 'Fabrication and properties of composites of poly(ethylene oxide) and functionalized carbon nanotubes', Advanced Materials 14, 1387–1390.

Ghose, S., Watson, K.A., Sun, K.J., Criss, J.M., Siochi, E.J. & Connell, J.W., 2006, 'High temperature resin carbon nanotube composite fabrication', Composites Science and Technology 66, 1995–2002.

Haggenmueller, R., Gommans, H.H., Rinzler, A.G., Fischer, J.E. & Winey, I., 2000, 'Aligned single-wall carbon nanotubes in composites by melt processing methods', Chemical Physics Letters 330, 219–225.

Hebb, D. O., 1949, 'The Organization Of Behaviour', New York: John Wiley and Sons.

Hilal, N., Al-Zoubi, H., Darwish, N.A., Mohammad, A.W. & Abu Arabi, M., 2004, 'A comprehensive review of nanofiltration membranes: Treatment, pretreatment, modelling, and atomic force microscopy', Desalination 170, 281-308.

Homenick, C.M., Lawson, G. & Adronov, A., 2007, 'Polymer grafting of carbon nanotubes using living free radical polymerization', Polymer Reviews 47, 265‑290.

Hone, J., Whitney, M., Piskoti, C. & Zettl, A., 1999, 'Thermal conductivity of singlewalled carbon nanotubes', Physical Review B 59, 2514-2516.

Igel, C. & Husken, M., 2003, 'Empirical evaluation of the improved Rprop learning algorithms', Neurocomputing 50, 105-123.

Iijima, S., 1991, 'Helical microtubules of graphitic carbon', Letters to Nature.

Jana, S., Purkait, M.K. & Mohanty, K., 2010, 'Preparation and characterization of low-cost ceramic microfiltration membranes for the removal of chromate from aqueous solutions', Applied Clay Science 47, 317–324.

Jin, L., Bower, C. & Zhou, O., 1998, 'Alignment of carbon nanotubes in a polymer matrix by mechanical stretching', Applied Physics Letters 73, 1197–1199.

Jonsson, A. & Tragbirdh, G., 1990, 'Ultrafiltration Applications', Desalination 77, 135-179.

Jorio, A., Saito, R., Hafner, J., Lieber, C., Hunter, M., McClure, T., Dresselhaus, G. & Dresselhaus, M., 2001, 'Structural (n, m) Determination of Isolated Single-Wall Carbon Nanotubes by Resonant Raman Scattering', Physical Review Letters 86, 1118-1121.

Journet, C., Maser, W.K., Bernier, P., Loiseau, A., Lamy de la Chapelle, M., Lefrant, S., Deniard, P., Lee, R. & Fischer, J.E., 1997, 'Large-scale production of single-walled carbon nanotubes by the electric-arc technique', Nature 388, 756-758.

Keidar, M., 2007, 'Factors affecting synthesis of single wall carbon nanotubes in arc discharge', Department of Aerospace Engineering, University of Michigan.

Koch Membrane Systems, 2014, 'About Tubular Membranes'. Available from http://www.kochmembrane.com/Learning-Center/Configurations/What-are-Tubular-Membranes.aspx. [May 2014].

Krose, B. & van der Smagt, P., 1996, 'An introduction to Neural Networks', The University of Amsterdam, 16-37.

Lau, W.J., Ismail, A.F., Misdan, N. & Kassim, N., 2012, ' A recent progress in thin film composite membrane: A review', Desalination 287, 190–199.

Li, L., Donga, J. & Nenoff, T.M., 2007, 'Transport of water and alkali metal ions through MFI zeolite membranes during reverse osmosis', Separation and Purification Technology 53, 42–48.

Liu, L., Xu, X., Zhao, C. & Yang, F., 2010, 'A new helical membrane module for increasing permeate flux', Journal of Membrane Science 360, 142-148.

Liu, P., 2005, 'Modifications of carbon nanotubes with polymers', European Polymer Journal 41, 2693–2703.

Loeb, S. & Sourirajan, S., 1964, 'High flow porous membranes for separating water from saline solutions', US Patent 3133132.

Matz, R., 1972, 'The structure of cellulose acetate membranes. II. The physical and transport characteristics of the porous layer of anisotropic membranes', Desalination 11, 207-215.

Mc Bride, W. S., 2001, 'Synthesis of Carbon Nanotubes by Chemical Vapor Deposition (CVD)', Williamsburg, Virginia.

McClelland, J. L. & Rumelhart, D. E., 1986, 'Parallel Distribution Processing: Explorations in the Microstructure of Cognition', The MIT Press, 9-15.

Millipore Corporation, 2014, 'Casting Processes'. Available from https://www.millipore.com/membrane/flx4/filter_manufacture_hm&tab1=3#tab1=3. [May 2014].

Morgan, P.W., 1965, 'Condensation polymers: by interfacial and solution methods', Polymer Reviews 10, Wiley, New York, 19–64.

MTR, 2014, 'How are VaporSep membranes packaged'. Available from http://www.mtrinc.com/faq.html. [May 2014].

Murakami, Y., Miyauchi, Y., Chiashi, S. & Maruyama, S., 2003, 'Direct synthesis of high-quality single-walled carbon nanotubes on silicon and quartz substrates', Chemical Physics Letters 377, 49-54.

Nanotube Modeler, computer software 2014. Available from http://www.jcrystal.com/products/wincnt/index.htm. [May 2014].

Nelson, H., Singh, R., Toledo, R. & Singh, N., 2007, 'The use of a submerged microfiltration system for regeneration and reuse of wastewater in a fresh-cut vegetable operation', Seperation Science Technology 42, 2473-2481.

Neuro AI, 2013, 'Backpropagation', Available from http://www.learnartificialneuralnetworks.com/backpropagation.html. [September 2013].

Pan, Y., Wang, W., Wang, T. & Yao, P., 2007, 'Fabrication of carbon membrane and microfiltration of oil-in-water emulsion: An investigation on fouling mechanisms', Separation and Purification Technology 57, 388–393.

Philippe, R., Morançais, A., Corrias, M., Caussat, B., Kihn, Y., Kalck, P., Plee, D., Gaillard, P., Bernard, D. & Serp, P., 2007, 'Catalytic Production of Carbon Nanotubes by Fluidized-Bed CVD', Chemical Vapor Deposition 13, 447–457.

Popov, V.N., 2004, 'Carbon nanotubes: properties and application', Materials Science and Engineering Review 43, 61–102.

Rafique, M. M. A. & Iqbal, J., 'Production of Carbon Nanotubes by Different Routes - A Review', Journal of Encapsulation and Adsorption Sciences 1, 29-34.

Rahimpour, A., Rajaeian, B., Hosienzadeh, A., Madaeni, S. S. & Ghoreishi, F., 2011, 'Treatment of oily wastewater produced by washing of gasoline reserving tanks using self-made and commercial nanofiltration membranes', Desalination 265, 190–198.

Riedmiller, M. & Braun, H., 1993, 'A direct adaptive method for faster backpropagation learning: the RPROP algorithm', E.H. Ruspini (Ed.), Proceedings of the IEEE International Conference on Neural Networks, IEEE Press, New York, 586–591.

Riedmiller, M., 1994, 'Advanced supervised learning in multi-layer perceptrons—from backpropagation to adaptive learning algorithms', Computer Standards & Interfaces 16, 265–278.

Riedmiller, M., 1994, 'Rprop – Description and Implementation Details', Technical report, University of Karlsruhe.

Sablani, S.S., Goosena, M.F.A., Al-Belushi, R. & Wilf, M., 2001, 'Concentration polarization in ultrafiltration and reverse osmosis: a critical review', Desalination 141, 269-289.

Saboya, L.V. & Maobois, J.L., 2000, 'Current developments of microfiltration technology in the dairy industry', Lait 80, 541-553.

Saito, R., Dresselhaus, G. & Dresselhaus, M., 1998, 'Physical properties of carbon nanotubes', Imperial College Press, Imperial College, London.

Saito, R., Dresselhaus, G. & Dresselhaus, M., 2000, 'Trigonal warping effect of carbon nanotubes', Physical Review B 6, 2981.

Sen, D., Sarkar, A., Das, S., Chowdhury, R. & Bhattacharjee, C., 2010, 'Batch hydrolysis and rotating disk membrane bioreactor for the production of galacto-oligosaccharides: A comparative study', Industrial Engineering and Chemistry Research 51, 10671-10681.

Sereewatthanawut, I., Boam, A.T. & Livingston, A.G., 2008, 'Polymeric Membrane Nanofiltration and Its Application to Separations in the Chemical Industries', Macromolecular Symposium 264, 184–188.

Shang, Y. & Peng, Y., 2007, 'Research of a PVA composite ultrafiltration membrane used in oil-in-water', Desalination 204, 322–327.

Stern, S.A., Sinclair, T.F., Gareis, P.J., Vahldieck, N.P. & Mohr, P.E., 1965, 'Helium Recovery by Permeation', Industrial Engineering Chemistry 57, 49-60.

Strathmann, H., 1985, 'Production of microporous media by phase inversion processes', ACS Symposium Series 269, 165-195.

Strathmann, H., Kock, K., Amar, P. & Baker, R.W., 1975, 'The formation mechanism of asymmetric membranes', Desalination 16, 179-203.

Susanto, H., Stahra, N. & Ulbricht, M., 2009, 'High performance polyethersulfone microfiltration membranes having high flux and stable hydrophilic property', Journal of Membrane Science 342, 153–164.

Teng, A., 2010, 'Physical Properties of Carbon Nanotubes', Department of Physics, University of Tennessee.

Thomsen, C., 2005, 'Electronic transition energies and vibrational properties of carbon nanotubes', Physikalisches Kolloquium, Montag.

TUM, 2014, 'Informatics V – Scientific Computing'. Available from http://www5.in.tum.de/wiki/index.php/Pendulum_Project. [October, 2014].

van Reis, R. & Zydney, A., 2007, 'Bioprocess membrane technology', Journal Membrane Science 297, 16-50.

Vandezande, P., Gevers, L. E. M. & Vankelecom, I. F. J., 2008, 'Solvent resistant nanofiltration: separating on a molecular level', Chemical Society Review 37, 365 – 405.

Vasanth, D., Pugazhenthi, G. & Uppaluri, R., 2011, 'Fabrication and properties of low cost ceramic microfiltration membranes for separation of oil and bacteria from its solution', Journal of Membrane Science 379, 154-163.

Wagner, J., 2001, 'Membrane Filtration Handbook Practical Tips and Hints', 2nd edition, Osmonics.

Wang, D. & Lai, J., 2013, 'Recent advances in preparation and morphology control of polymeric membranes formed by non-solvent induced phase separation', Current Opinions in Chemical Engineering 2, 229 – 237.

Wijmans, J. G. & Baker, R. W., 1995, 'The solution-diffusion model: a review', Journal of Membrane Science 107, 1-21.

Wildoer, J., Venema, L., Rinzler, A., Smalley, R. & Dekker, C., 1998, 'Electronic structure of atomically resolved carbon nanotubes', Nature 391, 59-62.

Xia, H., Wang, Q., Li, K. & Hu, G.H., 2004, 'Preparation of CNT/polypropylene composite powder with a solid state mechanochemical pulverization process', Journal of Applied Polymer Science 93, 378–386.

Young, T. & Chen, L., 1995, ‘Pore formation mechanism of membranes from phase inversion process’, Desalination 103, 233–247.

Zhou, J., Changa, Q., Wang, Y., Wang, J. & Meng, G., 2010, ‘Separation of stable oil–water emulsion by the hydrophilic nano-sized ZrO2 modified Al2O3 microfiltration membrane’, Separation and Purification Technology 75, 243–248.

Zhou, Z., Lee, J. Y. & Chung, T., 2014, ‘Thin film composite forward-osmosis membranes with enhanced internal osmotic pressure for internal concentration polarization reduction’, Chemical Engineering Journal 249, 236–245.

CHAPTER 3

3. Synthesis of Carbon Nanotubes from Ferrocene using a Chemical Vapour Deposition Reactor

3.1. Introduction

The work presented in this chapter has been published in the article titled “Synthesis of Large Carbon Nanotubes from Ferrocene: The Chemical Vapour Deposition Technique” in the journal Trends in Applied Sciences Research 6. The contributions of the author were experimental, the analysis of the results and writing of the article. The Ethical Guidelines and Editorial Policy of Science Alert and Trends in Applied Sciences Research state that “Doctoral dissertations that are made available by UMI/ProQuest or institutional repositories are not considered prior publication” (http://scialert.net/guide2.php?issn=1819-3579&id=9) and thus the work in the article can be used in this dissertation.

Ferrocene has already been used as a catalyst to produce CNTs in conjunction with other carbon sources (Iyuke et al, 2009, Endo et al, 2004 and Kuwana et al, 2005). But as ferrocene is relatively easy and cheap to produce (Tanner et al., 1995), it is worthwhile to study ferrocene as both a catalyst and a source of carbon for CNT production. In this chapter the CVD method is used to produce CNTs. The optimization of temperature is important in order to decompose the ferrocene in the presence of argon (which acts as the carrier gas) and provide the correct temperature for CNT formation. The CNTs are characterized by TEM and Raman spectroscopy. The CNTs produced are not purified and are used as made in the reinforcement of the membrane in chapter 4.

3.2. Experimental

The equipment used for the experiment is shown in Figure 3-1. The apparatus consists of a vertical furnace that can be operated up to 1200°C. The flow of gases into the glass furnace reactor is aided by a system of valves and rotameters.

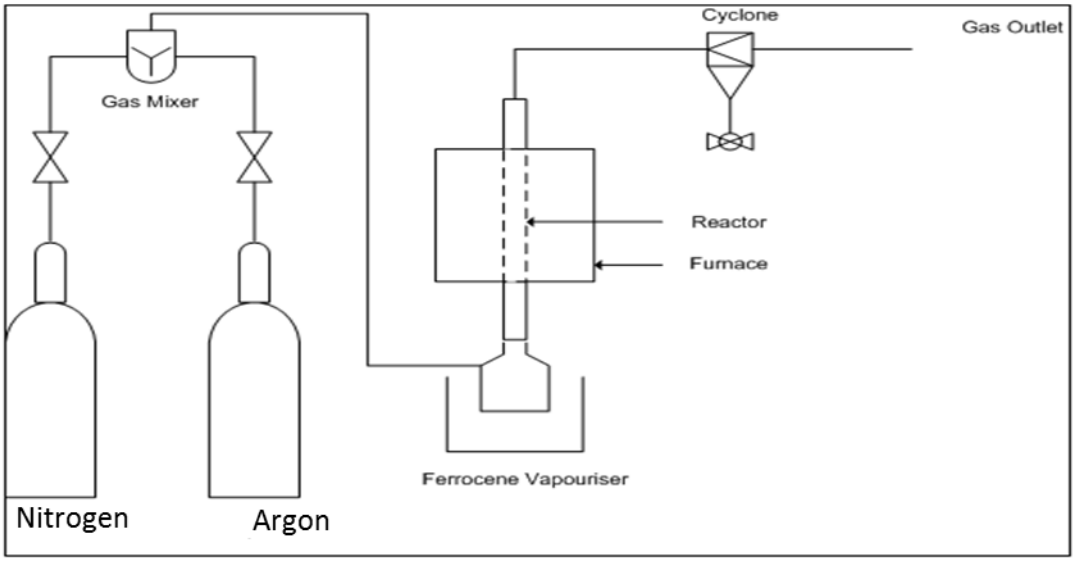

Figure 3-1: Chemical Vapour Deposition Reactor

About 4g of ferrocene was placed in the vapouriser to be used as the carbon source as well as the catalyst precursor. A layer of quartz wool was placed inside the tube for the product to fall on. A heating cord was wrapped around the exposed parts of the vapouriser at the bottom of the reactor. The purpose of this was to maintain a high temperature so that ferrocene does not crystallise. Once the equipment was connected as shown (Figure 3-1), all the connections were sealed with high vacuum grease to ensure that there were no gas leaks. Nitrogen gas was passed through the system for 20 minutes, to flush out contaminants and to ensure that there were no leakages. Argon

was later used to provide an inert atmosphere and to purge unknown gases from the air proof system as well as a carrier gas.

The furnace was turned on and set to the desired reaction temperature (800° C, 850° C, 900° C and 950^{o}C). When the reaction temperature was reached, the vapouriser and heating cord were turned on. The catalyst (ferrocene) was evaporated and transported into the reactor by argon gas. This could be seen since the ferrocene was orange in colour. The reaction was allowed to proceed until all the ferrocene had vapourised. The equipment was then switched off and allowed to cool. The product was collected from the cyclone, quartz wool and also scraped off from the inside of the reactor. The product was analysed with the TEM (model JOEL 100S). The Raman spectroscopy was also carried out using the Jobin-Yvon T6400 Raman Spectrometer with an Argon ion laser. The analysis was conducted in order to determine whether any nanostructures of carbon were formed using ferrocene as the sole carbon source.

3.3. Results and discussion

The TEM images of the reactor product at the different reaction temperatures are shown in Figure 3-2 - Figure 3-4. In Figure 3-2, it can be seen that a CNT of a length around 500 nm was produced. It was possible that other nanostructures of carbon, such as carbon nanofibres (CNFs) or amorphous carbon were also present.

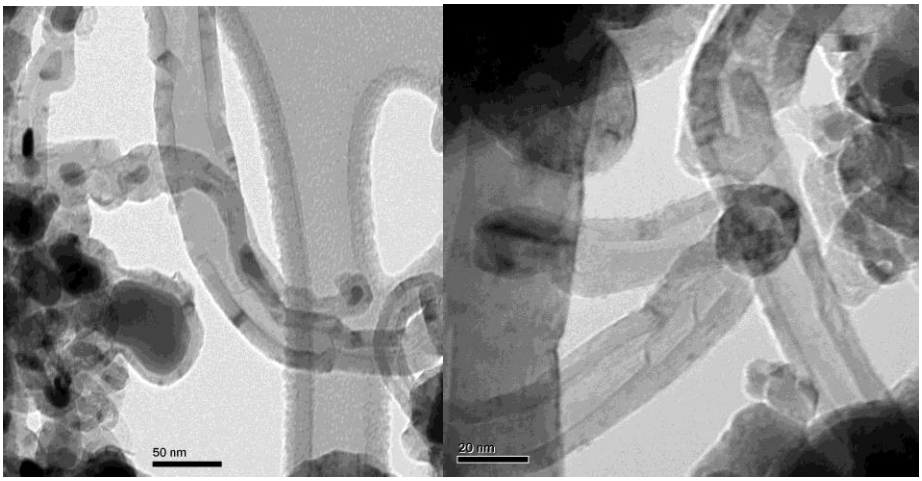

Figure 3-2: TEM image of the reactor product at 800°C (Yah et al., 2011).

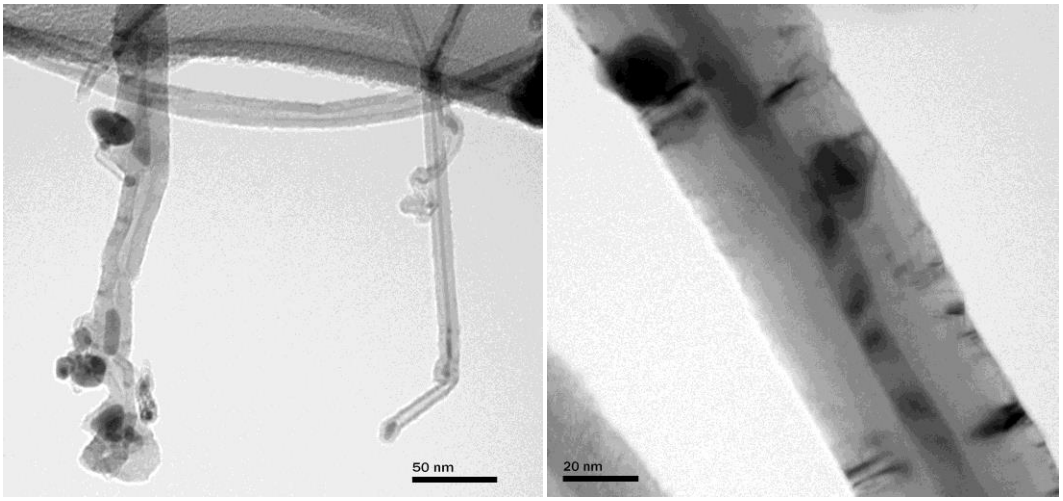

Figure 3-3: TEM image of the reactor product at 850°C (Yah et al., 2011).

Figure 3-3 clearly shows one CNT of about 900 nm long, with a shorter one of around 400 nm and possible CNFs. These CNTs ranged between 400 nm and 1000 nm in length.

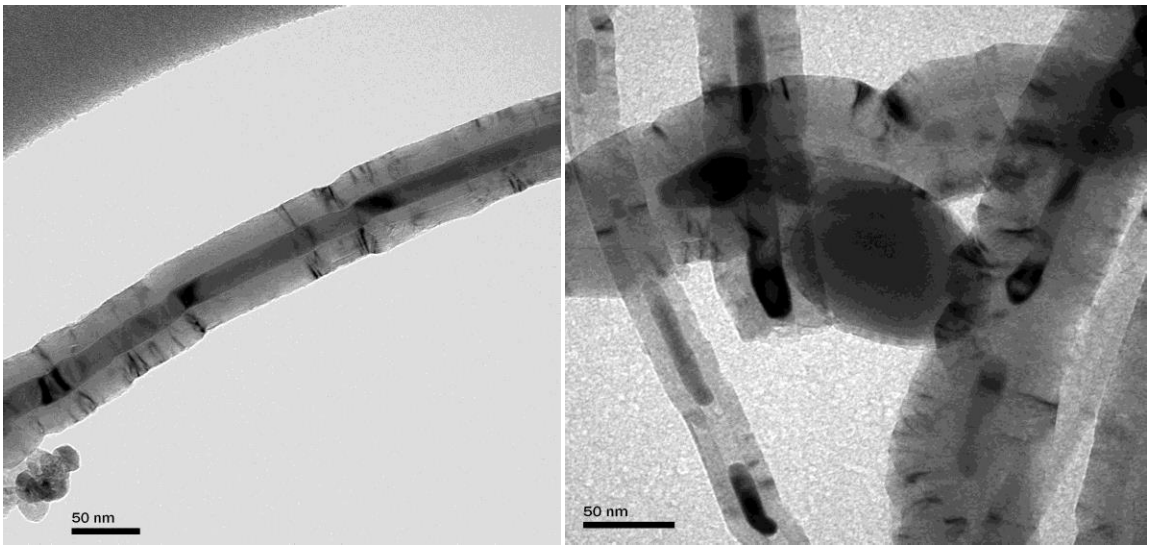

Figure 3-4: TEM image of the reactor product 900°C (Yah et al., 2011).

Figure 3-4 shows CNFs and a few short CNTs, of sizes ranging between 100 nm and 300 nm.

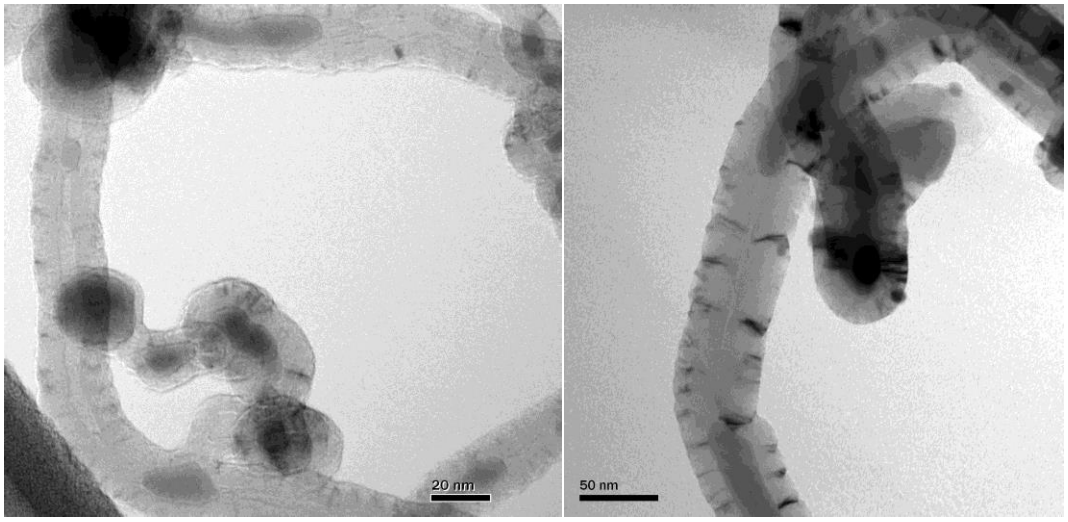

Figure 3-5: TEM image of the reactor sample at 950°C (Yah et al., 2011).

Figure 3-5 shows a CNT having a length of approximately 1.5 μm, with shorter CNTs also present. Catalyst particles can be seen within the hollow tubes of the CNTs.

Figure 3-2 - Figure 3-5 show the synthesis of CNTs at temperatures ranging from 800-950°C. Because ferrocene is a relatively volatile organo-metallic compound with excellent vapourisation above 400^{o}C (Barreiro et al., 2006) it allows for the formation of CNTs at higher temperatures. At 500 to 650°C the ferrocene completely decomposed as shown in equation 3.1 (Barreiro et al., 2006),

$$\mathrm{Fe(C_5H_5)_2} \Rightarrow Fe + H_2 + \mathrm{CH_4} + \mathrm{C_5H_6} + \ldots\ldots\ldots \quad (3.1)$$

Previously, this was supported by the findings of Lewis and Smith (1984) when they found that ferrocene could be consumed through reactions with radicals during the decomposition of ferrocene to unimolecular gas-phase as shown in equation 3.2,

$$\mathrm{Fe(C_5H_5)_2} \Rightarrow Fe + 2C_5H_5 \quad (3.2)$$

Furthermore, Hou et al (2002) reported the pyrolysis of pure ferrocene at 580-700°C resulting in spherical iron nanoparticles with diameters in the order of 10 nm. In addition, Kuwana and Saito (2005) reported the production of iron nanoparticles at 700°C from ferrocene using the CVD technique. Since there is a domination of MWCNTs being produced in this work, it is postulated that there is a higher amount of spherical but aggregated iron particles instead of nanoparticles, which would have led to higher SWCNT production. Hou et al (2002) argued that the inability to produce CNTs in the

process was due to the low carbon/iron ratio in pure ferrocene. In this study, iron to carbon ratio in ferrocene was 30 to 75%. Furthermore, a report by Barreiro et al (2006) has shown that when ferrocene is present at the reaction zone, iron clusters and reactive carbon are produced at the gaseous phase. Barreiro et al (2006) claim that this results in the production of SWCNTs and there is very little production of MWCNTs at temperature ranges of 650 to 900^{o}C. In this work MWCNTs were produced at temperatures ranging from 800 to 900^{o}C. The difference in the results of this work and that of Barreiro et al. (2006) can be attributed to the feeding mechanism of ferrocene into the reactor. The ferrocene is injected into the reactor through a copper nozzle according to Barreiro et al. (2006) which would lead to better dispersion of the ferrocene which in turn would promote nanoparticle formation. The ferrocene is also injected directly into the reaction zone of the reactor which is at high temperatures whereas in this work the ferrocene has to travel to the reaction zone and in this time agglomeration could take place (especially if there is a temperature drop between the vapouriser and the reaction zone of the furnace). The work showed the highest amount of CNTs produced was at 900^{o}C, although there was no significant difference in the amount produced within the temperature range used. In this work, it was noticed that at higher temperatures (800-950^{o}C), there was less adherence of the product to the walls of the reactor such that more of the product could be collected from the cyclone. Therefore, if the process had to be scaled up for industrial production or for continuous production, higher temperatures would be recommended for ease of product collection.

The results of the Raman Spectroscopy for the product formed at the different temperatures are shown in Figure 3-6.

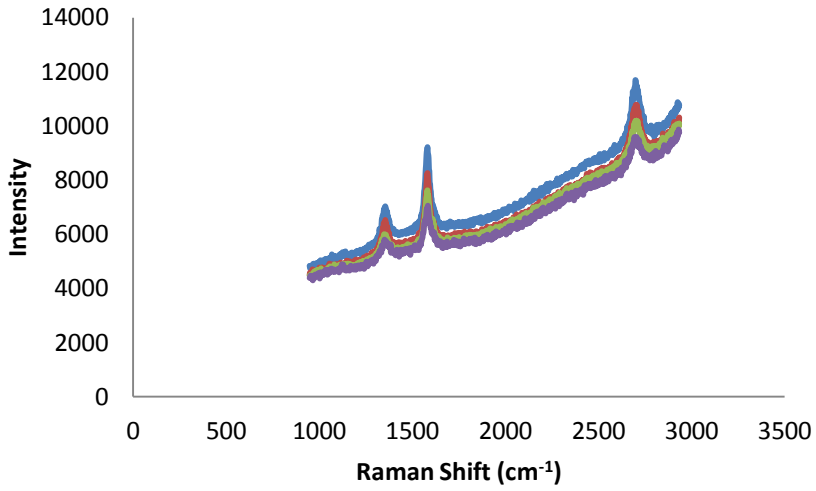

Figure 3-6: Raman Shifts for the Products formed at different temperatures (800-blue, 850-red, 900-green and 950^{o}C-purple) (Yah et al., 2011).

For all the samples, the first peak occurs at 1350 cm^{-1}, known as the D-band, the second peak occurs at 1580 cm^{-1}, called the G-band and the final peak occurs at 2700 cm^{-1}, which is called the G'-band. The ratio of the G-band to D-band intensities provides an indication of the quality of the sample. The calculated I_D/I_G ratios displayed in Table 3.1 show an increasing trend with an increase in temperature which means that as the reactor temperature increases, the carbon nanotubes produced become more graphitic and crystalline. Figure 3-6 revealed the missing radial breathing mode which would support the production of MWCNTs.

The average production of the CNTs varied from 2.0±0.03 to 2.3±0.34 g at 95% confidence interval. The highest production was found at 900°C. Although ferrocene is vapourised at lower temperatures, the maximum yield was found between 850 and 900^{o}C.

Table 3.1: Ratio of D-band to G-band intensities for products formed at different temperatures.

Temperature (°C)	I_D/I_G	Amount of CNT produced (g)
800	0.75	2.0±0.03
850	0.78	2.2±0.12
900	0.78	2.3±0.34
950	0.82	2.1±0.16

3.4. Conclusion

The aim of the study in chapter 3 was to produce CNTs using ferrocene as both a carbon source and catalyst. The temperature range of 800°C to 950°C was investigated and it was found that CNTs could be produced at all the temperatures with no significant difference in the amount of CNTs produced. At higher reaction temperatures, there was less adherence of the product to the walls of the reactor. For industrial processes, higher temperatures would therefore be advisable for CNT production. Raman spectroscopy of the samples showed that MWCNTs were produced.

References

Barreiro, A., S. Hampel, M.H. Rummeli, C. Kramberger & A. Gruneis et al., 2006, 'Thermal Decomposition of Ferrocene as a Method for Production of Single-Walled Carbon Nanotubes without Additional Carbon Sources', Journal of Physical Chemistry B 110, 20973-20977.

Endo, H., Kuwana, K., Saito, K., Qian, D., Andrews, R. & Grulke, E.A., 2004, 'CFD prediction of carbon nanotube production rate in a CVD reactor', Chemical Physics Letters 387, 307 – 311.

Hou, H., Schaper, A.K., Weller, F. & Greiner, A., 2002, 'Carbon Nanotubes and Spheres Produced by Modified Ferrocene Pyrolysis', Chemical Materials 14, 3990-3994.

Iyuke,S.E., Mamvura, T.A., Liu, K., Sibanda, V., Meyyappan, M. & Varadan, V.K., 2009, 'Process synthesis and optimization for the production of carbon nanostructures', Nanotechnology 20, 375602 -375602.

Kuwana, K. & Saito, K., 2005, 'Modeling CVD synthesis of carbon nanotubes: nanoparticle formation from ferrocene', Carbon 43, 2088-2095.

Kuwana, K., Endo, H., Saito, K., Qian, D., Andrews, R. & Grulke, E.A., 2005, 'Catalyst deactivation in CVD synthesis of carbon nanotubes', Carbon 43, 253-260.

Lewis, K.E. & Smith, G.P., 1984, 'Bond dissociation energies in ferrocene', Journal of American Chemical Society 106, 4650–4651.

Tanner, P.S., Jones Jr., W.E., Myers, C.E. & Whittingham, M.S., 1995, 'The Synthesis and Characterization of Ferrocene', Paper Presented at the 210th National Meeting of the American Chemical Society, Chicago,IL, CHED 51.

Yah, C. S., Simate, G. S., Moothi, K., Maphutha K. S. & Iyuke, S. E., 2011, 'Synthesis of Large Carbon Nanotubes from Ferrocene: The Chemical Vapour Deposition Technique', Trends in Applied Sciences Research 6, 1270 – 1279.

CHAPTER 4

4. A Carbon Nanotube-infused Polysulfone Membrane with Polyvinyl Alcohol layer for Treatment of Oil-containing Waste Water

4.1. Introduction

The work presented in this chapter has been published in the journal article titled “A carbon nanotube-infused polysulfone membrane with polyvinyl alcohol layer for treating oil-containing waste water” from the journal Scientific Reports 3 with permission from the journal (Appendix D). The author’s contributions include experimental, data analysis and the writing of the article.

Chapter 4 deals with the addition of CNTs to a polymer membrane and the separation of synthetic oil from water using a composite membrane. Since CNTs have certain desirable mechanical properties, it is equally desirable to be able to transfer those properties to other materials. This chapter studies the mechanical effects of reinforcing polysulfone with CNTs and since the polysulfone is a membrane (with a certain pore structure) there may be other consequences not related to the mechanical properties of the polymer but that are important to the operation of the membrane. The second part to this chapter is the use of PVA as a barrier layer for a composite membrane. PVA has been proven (Gohil and Ray, 2009) to remove NaCl (22.8% rejection) and $MgSO_4$ (83.8% rejection) from solution. In this study the reinforced polysulfone membrane is used as the support layer for the PVA. Commonly, membrane selectivity can be increased through the modification of the chemical structure (Huang and Rhim, 1993; Gimenez et al., 1996) of the polymer by cross-linking, grafting, etc. thus cross-linking of the PVA layer with maleic acid is implemented to improve the separation of oil from

water. The membrane pore structure is characterized by SEM and BET is used to get the average pore size. Nanotensile stress testing is used to test the mechanical strength of the membrane while filtration runs are done to determine the operating efficiency of the membrane.

4.2. Experimental

The phase inversion method (Gohil and Ray, 2009) was used to prepare the membranes in this study. A 10% (w/v) PSF solution was prepared in dimethylformamide (DMF) under constant stirring. The solution was cast on a glass plate with the aid of a casting blade. The cast solution was left in ambient conditions for 10 s and thereafter fully immersed in distilled water for a period of 24 hours. A 1% (w/v) aqueous PVA solution was poured over the PSF membrane (which acts as the support) and kept in contact for 3 minutes after which the excess solution was drained off. A 1% maleic acid (MA), which acts as the cross-linker solution, was poured on the PVA layer and kept in contact for 3 minutes (to allow enough time for cross-linking) after which it was drained off. The membrane was then heated in an oven at 125^{o}C for 15 minutes. The structure of the membranes was characterised using a scanning electron microscope (SEM) (FEI FIB/SEM Nova 600 Nanolab). BET analysis was used to obtain pore size information using the Tristar 3000 V6.05 A. The settings for the analysis can be found in Appendix A.

The CNTs were blended with the polymer solution in varying concentrations (from 0 – 10% w/v) before the solution was cast and immersed in water. The CNTs were dispersed with the aid of ultrasonic agitation in the membrane solution before casting. The mechanical tests on the membranes were carried out on the Hysitron Nanotensile

5000 Tester using thin rectangular (5 mm x 30 mm x 0.05 mm) samples of the membrane. The Young's modulus, toughness, ultimate tensile strength and yield stress were obtained from the mechanical tests (some of the raw data is shown in Appendix A).

- Young's Modulus: A measure of the stiffness of an elastic material.
- Toughness: The ability of a material to absorb energy and plastically deform before fracture.
- Ultimate tensile strength: The maximum stress that a material can withstand while being stretched or pulled before necking.
- Yield stress: The point where the material deforms plastically.

For the demonstration of oil-water separation, a reservoir was filled with distilled water (18 L) and synthetic oil (Figure 4-1). The reservoir was continuously stirred and heated to 35^{o}C to facilitate mixing. The mixture was pumped through the dead-end filtration membrane module (Figure 4-1E) and flow readings were taken using a rotameter. The concentration of oil in water (after ultrasonication and continued stirring) was found to be approximately 287 mg/L. The flux through the membrane is determined using:

$$F = \frac{V}{At} \tag{4.1}$$

where F is the flux, A is the effective membrane area and V is the volume of permeate through the membrane during time t. The rejection of the membrane can be found by:

$$R(\%) = \left[1 - \frac{C_p}{C_f}\right] \times 100 \tag{4.2}$$

where R is the rejection, and C_f and C_p are the feed and permeate concentrations, respectively.

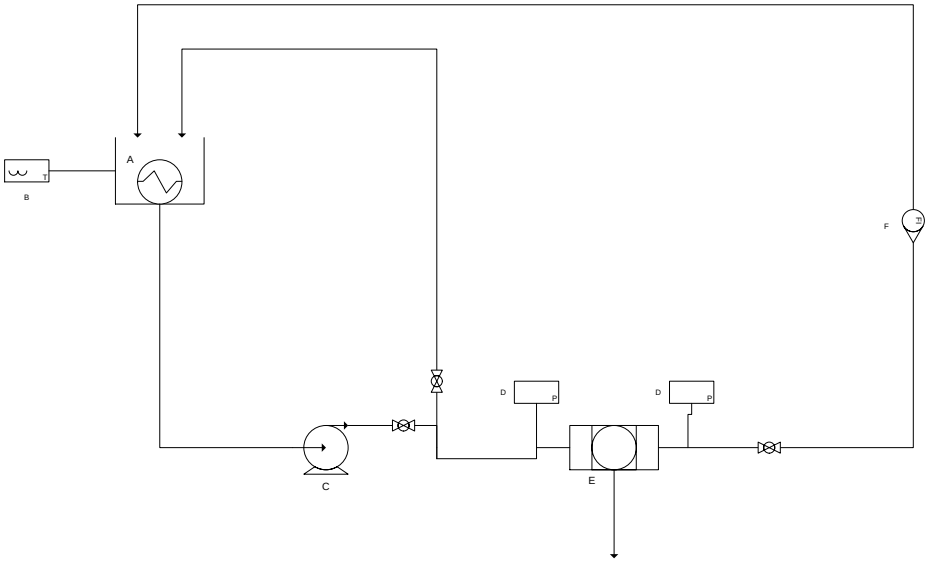

Figure 4-1: Schematic of the filtration rig used for oil/water separation, consisting of A) Reservoir (synthetic oil\water), B) temperature controller, C) pump, D) pressure gauge, E) dead-end filtration membrane module, F) rotameter.

4.3. Results and discussion

Figure 4-2 shows the SEM images of the bottom (PSF) layer of the membrane. This layer is highly porous with the visible pores being less than 10 microns. This particular layer contains no CNTs. Figure 4-3 shows the bottom (PSF) layer of the membrane with 5% and 10% CNTs in the polymer solution. The structure of this layer appears to change with the addition of CNTs. The pores in the membrane for the 10% CNT case appear to be more numerous and more finely dispersed than at lower concentrations. BET analysis gives the average adsorption pore width as 18.91nm at 0% CNT, 27.6nm

at 5% CNT and 31.8nm at 10%. The change in the structure of the membranes is related to the pore formation mechanism of the membranes.

The addition of different CNT concentrations to the polymer solution results in differing membrane structures because of the effect of CNT agglomeration. Since CNTs attach to the polymer structure, when agglomeration occurs the CNTs 'pull' the polymer matrix thereby increasing the rate of syneresis which leads to bigger and larger number of pores being created as per the Strathmann et al. (1975) and Strathmann (1985) mechanism postulation. If there is also a bundle of CNTs near the surface of the PSF membrane then water ingress into the membrane will be at the point of lower polymer concentration. By increasing the CNT concentration the agglomeration effect is increased and thus pore formation frequency is increased. Figure 4-4 shows the PVA layer on top of the bottom (PSF) porous layer indicating no clearly visible pores on the SEM images.

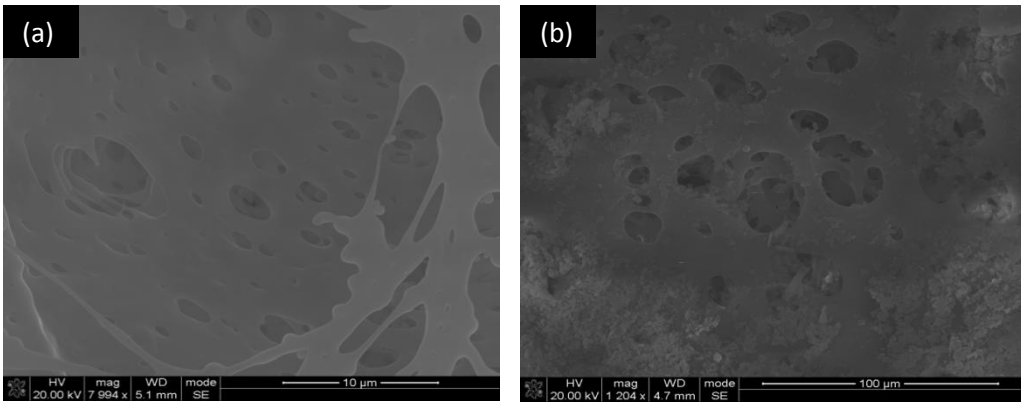

Figure 4-2: SEM image of a polysulfone (PSF) membrane (a) high and (b) low magnification without CNTs. BET analysis gave the average adsorption pore size as 18.9 nm.

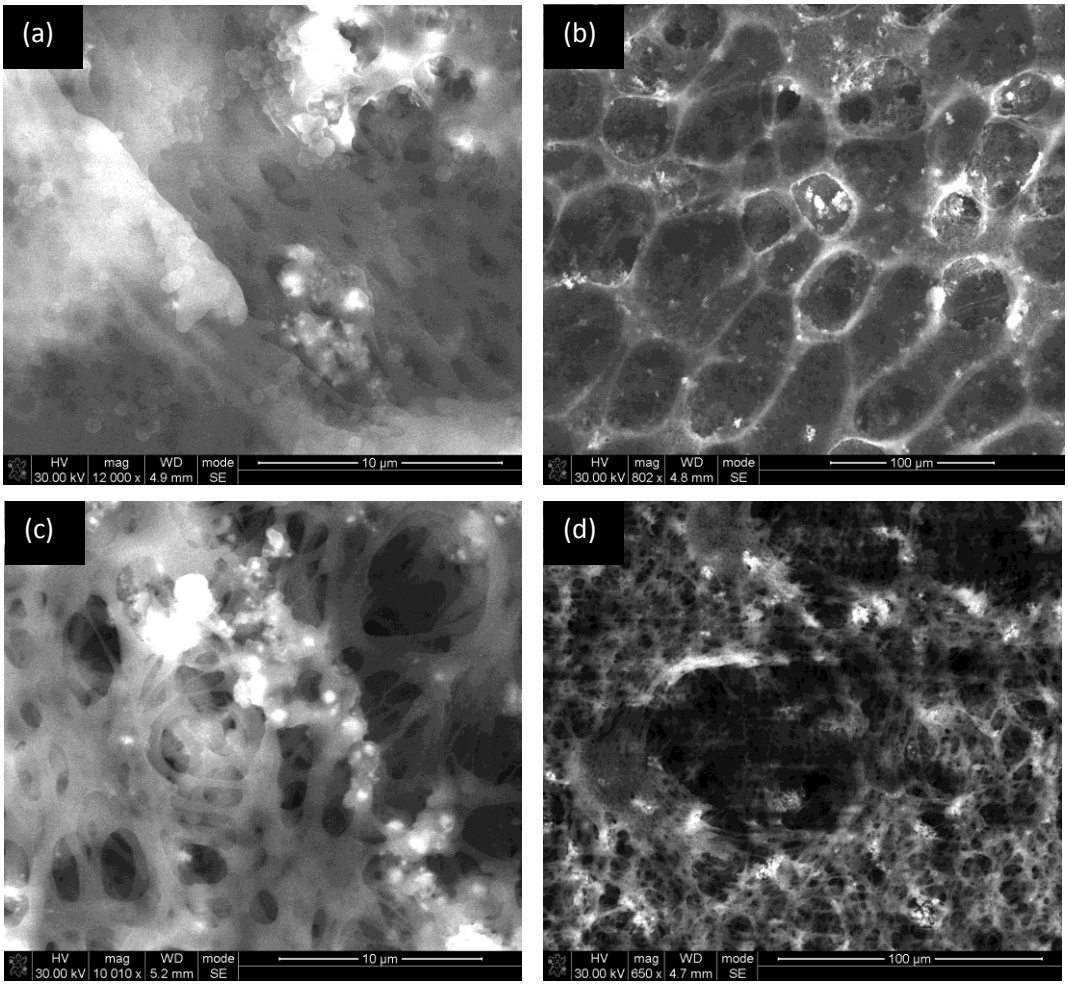

Figure 4-3: PSF membranes with 5% CNT (w/w) loading (a) high and (b) low magnification, PSF membranes with 10 % CNT (w/w) loading (c) high and (d) low magnification. BET analysis gave the average adsorption pore size of 27.6 nm for 5% CNT loading and 31.8 nm for 10% CNT loading.

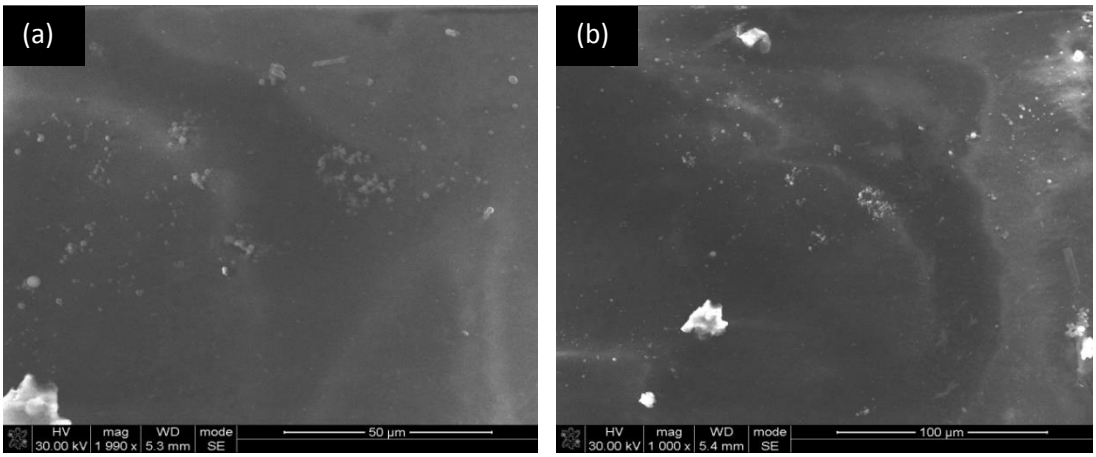

Figure 4-4: SEM image of the polyvinyl alcohol (PVA) thin layer on base (PSF) membrane (a) high and (b) low magnification. Due to the top layer of PVA being present no visible pores can be perceived.

Figure 4-5 shows the results from the nanotensile tests conducted on the fabricated membranes. The Young's modulus and toughness increase with CNT concentration first and then decrease after a threshold concentration (7.5% CNT: PSF) is reached. This drop in mechanical properties is due to the ready agglomeration of CNTs creating bundles at higher concentrations. Studies have shown that CNT bundles display diminished mechanical properties (Coleman et al., 2006b) compared to a single CNT. The effects of CNT fillers on the mechanical properties of polymers have been extensively studied (Tjong, 2006; Moniruzzaman and Winey, 2006; Ma et al., 2010; Spitalsky, 2010). Some of the results of these studies are displayed in Table 4.1. Different processing techniques (which includes the degree of dispersion of the CNTs), CNT concentrations in the polymer and different polymer matrices have been shown to affect the mechanical properties. The mechanical properties obtained in this study are comparable to some of the literature findings (Table 4.1). At 7.5% CNT concentration,

there is a 119% increase in the ultimate tensile strength, 77% increase in the Young's modulus and 258% increase in the membrane toughness (these readings are relative to 0% CNT concentration in the membrane). These values are quite favourable as there was no modification or purification of the CNTs used in the polymer solution. Because of the impurity of the CNT samples used in this study, it is possible to further improve the mechanical properties by using purified CNTs.

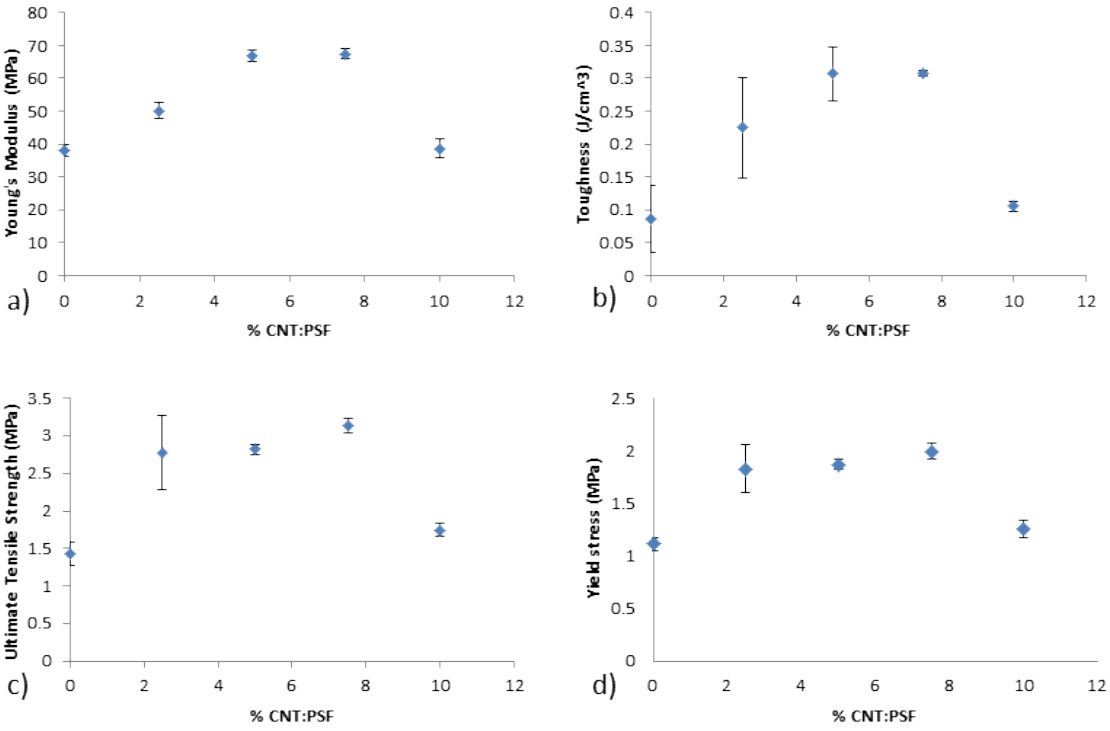

Figure 4-5: Plots of (a) Young's modulus (MPa), (b) Toughness (J/cm3), (c) Ultimate tensile strength (MPa) and (d) Yield Stress (MPa) as a function of CNT loading in PSF. At a concentration of 7.5% CNTs in the polymer composite, there is a 119% increase in the ultimate tensile strength, 77% increase in the Young's modulus, 258% increase in the toughness and a 79% increase in the yield strength. These increases are relative to 0% CNT loading.

Table 4.1: Mechanical properties of CNT-polymer composites (multi-walled CNTs: MWCNTs and single-walled CNTs: SWCNTs).

Polymer matrix	CNT type	CNT weight fraction (%)	Tensile strength (% increase)	Young's modulus (% increase)	Toughness	Reference
Polystyrene	Purified MWCNTs	1	25	42	-	(Qian et al., 2000)
Polystyrene	Purified MWCNTs	5	50	120	-	(Safadi et al., 2002)
Polypropylene	Pristine SWCNTs	1	40	55	-	(Kearns and Shambaugh, 2002)
Polypropylene	Purified MWCNTs	1	20	15	-	(Xia et al., 2004)
Poly(methyl methacrylate)	Pristine MWCNTs	1	0	0	170	(Gorga and Cohen, 2004)
Polycarbonate	Pristine MWCNTs	1	20	20	-	(Fornes et al., 2006)
Polyvinyl alcohol	Purified MWCNTs	1	-	80	60	(Cadek et al., 2002)
Polyacrylonitrile	Pristine MWCNTs	5	75	40	200	(Chae et al., 2005)
Polyimide	Pristine MWCNTs	14.30	-15	40	-	(Ogasawara et al., 2004)
Polyurethane	Pristine SWCNTs	0.50	10	100	-	(Chen and Tao, 2005)
Polyurethane	Amine-modified MWCNTs	2	20	0	75	(Xiong et al., 2006)

The rejection values of the membrane are given in Table 4.2 and are calculated using equation 4.2. Figure 4-6 shows the permeate concentration values. There is an increase if the oil concentration in the permeate and a decrease in the membrane rejection, with an increase in pressure. This may be because as the trans-membrane pressure increases, it rises above the capillary pressure of the membrane, which prevents the oil from entering the pores (Chakrabarty et al., 2008), leading to the oil being forced through the pores. There is also a decrease in the membrane rejection with an increase in the CNT concentration in the membrane. This is expected as the structure of the polysulfone layer is altered, by the membrane pores getting bigger with the addition of CNTs. The structure of the bottom layer in a thin film composite membrane has been shown to have an effect on the flux and the separation efficiency of the membrane by Gohil and Ray (2009). Permeate concentrations below 10 mg/L are achieved at 4 and 5 bar by membranes with 0% and 5% CNT concentrations. Figure 4-7 shows the flux calculated using equation 4.1 for different CNT loading and pressures. The flux through the membrane increases with an increase in pressure and CNT concentration. The flux achieved in this study is comparable to some literature findings (Ebrahimi et al., 2009) and higher than some (Kong et al., 2006; Mondal and Wickramasinghe, 2008). In the same way as membrane separation efficiency was affected, the CNTs altered the pore structure of the PSF layer allowing for greater flux across the membrane. In the SEM images (Figure 4-2 and Figure 4-3), it can be seen that as the CNT concentration increases the pore diameter also increases. The permeate flux can also be attributed to the PVA layer which is hydrophilic. It has been found that hydrophilic membranes are more resistant to fouling and generally have a higher permeate flux (Chunjin et al.,

2008; Srijaroonrat et al., 1999).Cross-linking the PVA layer with dicarboxylic acid (maleic acid) improved stability of the membrane as has been established by studies conducted by Gohil and Ray (2009) and Gohil et al. (2006). The findings of Gebben (1985) showed that the intramolecular crosslinked molecules are smaller in size than the initial polymer molecules with their size being dependent on the degree of crosslinking.

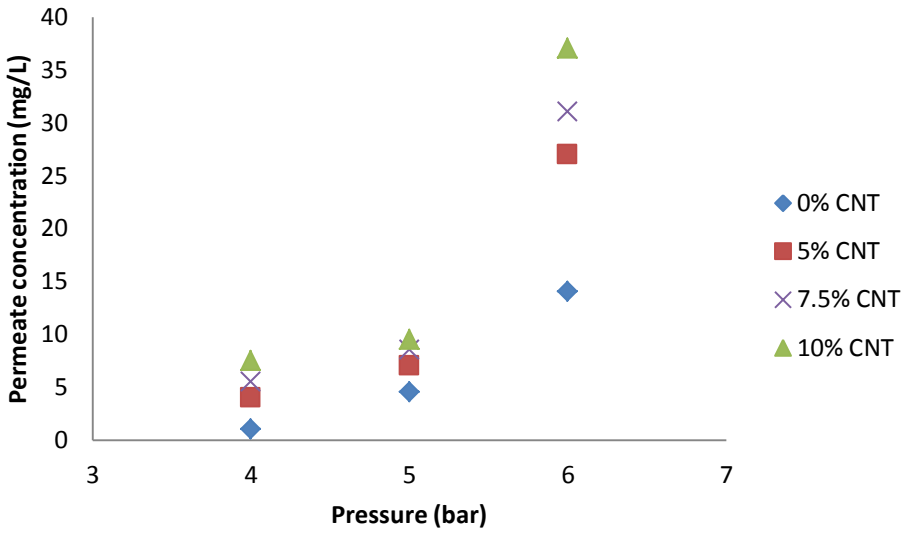

Figure 4-6: The permeate concentration for different % CNT loading. There is an increase in permeate concentration with an increase in pressure and % CNT loading. After 5 bar, the permeate concentration exceeds the lower limit of the allowable discharge concentration which is 10 mg.

Table 4.2: Rejection of oil by thin film membrane.

Pressure (bar)	Feed oil conc. (mg/L)	CNT loading (%)	Rejection (%)
4	287	0.0	99.65
4	287	5.0	98.61
4	287	7.5	98.08
4	287	10.0	97.39
5	287	0.0	98.43
5	287	5.0	97.56
5	287	7.5	97.04
5	287	10.0	96.69
6	287	0.0	95.12
6	287	5.0	90.59
6	287	7.5	89.20
6	287	10.0	87.11

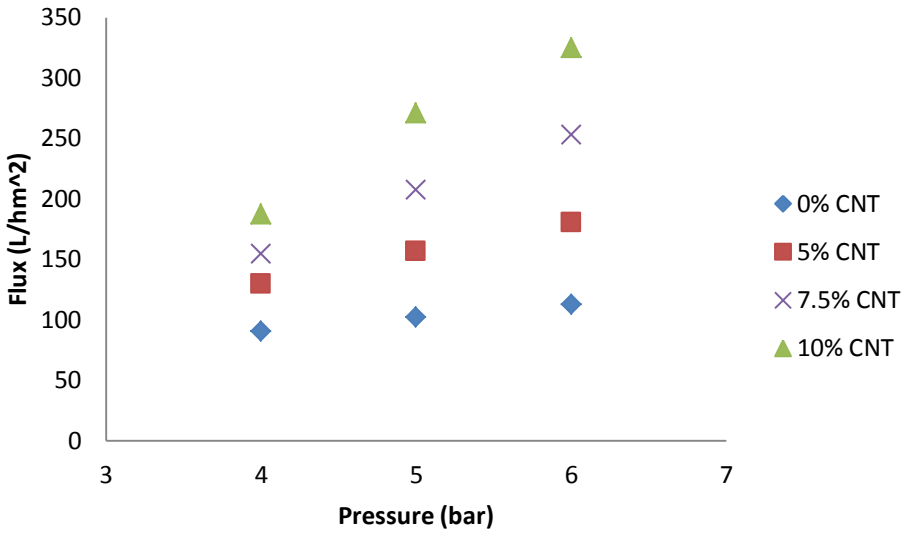

Figure 4-7: The flux through the membrane at different pressures and % CNT loading. The increase in flux is due to the increase in % CNT loading which alters the membrane structure as can be seen in Figure 4-2 and Figure 4-3.

4.4. Conclusion

In chapter 4 a CNT-polymer composite membrane with a polyvinyl alcohol barrier layer was fabricated and tested for the separation of oil from water. At a concentration of 7.5% CNT in the polymer composite, a 119% increase in the ultimate tensile strength, 77% increase in the Young's modulus and 258% increase in the membrane toughness were seen indicating the suitability of the membrane in practical applications. Increasing the trans-membrane pressure decreases the membrane separation but increases flux. In practice, the most important aspect of a membrane is its rejection profile which would have to meet the downstream processes that utilise the permeate. Therefore if the permeate purity requirements are high, then the amount of CNTs that can be added to the membrane decreases because an increase in CNT concentration decreases the

rejection of the membrane. This also means that there will be a limit to the mechanical strength and flux increases that can be achieved. If the downstream permeate purity requirements are lower, then more CNTs can be added to the membrane meaning that mechanical strength benefits and flux increases will be observed.

References

Cadek, M., Coleman, J. N., Barron, V., Hedicke, K. & Blau, W. J., 2002, 'Morphological and mechanical properties of CNT-reinforced semicrystalline and amorphous polymer composites', Applied Physics Letters 81, 5123-5125.

Chae, H. G., Sreekumar, T. V., Uchida, T. & Kumar, S., 2005, 'A comparison of reinforcement efficiency of various types of carbon nanotubes in polyacrylonitrile fiber' Polymer 46, 10925-10935.

Chakrabarty, B., Ghoshal, A. K. & Purkait, M. K., 2008, 'Ultrafiltration of stable oil-in-water emulsion by polysulfone membrane', Journal of Membrane Science 325, 427–437.

Chen, W. & Tao, X., 2005, 'Self-organizing alignment of CNTs in theroplastic polyutherane', Macromolecular Rapid Communications 26, 1763-1767.

Chunjin, W., Aimin, L., Lei, L., Long, Z., Hui, W., Xuehua, Q., et al., 2008, 'Treatment of oily water by a poly(vinyl alcohol) ultrafiltration membrane', Desalination 225, 312-321.

Coleman, J. N., Khan, U., Blau, W. J. & Gunko, Y. K., 2006b, 'Small but strong: A review of the mechanical properties of carbon nanotube-polymer composites', Carbon 44, 1624-1652.

Ebrahimi, M., Shams Ashaghi, K., Engel, L., Willershausen, D., Mund, P., Bolduan, P. & Czermak, P., 2009, 'Characterization and application of different ceramic

membranes for the oil-field produced water treatment', Desalination 245, 533–540.

Fornes, T. D., Baur, J. W., Sabba, Y. & Thomas, E. L., 2006, 'Morphology and properties of melt-spun polycarbonate fibers containing single- and multi-wall carbon nanotubes', Polymer 47, 1704-1714.

Gebben, B., Van den-Berg, H.W.A., Bargeman, D. & Smolders, C.A., 1985, 'Intramolecular crosslinking of poly (vinyl alcohol)', Polymer 26, 1737-1740.

Gimenez, V., Mantecon, A. & Cadiz, V., 1996, 'Crosslinking of poly (viny1 alcohol) using dianhydrides as hardeners', Journal of Applied Polymer Science 59, 425-431.

Gohil, J. M. & Ray, P., 2009, 'Polyvinyl alcohol as the barrier layer in thin film composite nanofiltration membranes: Preparation, characterization, and performance evaluation', Journal of Colloid and Interface Science 338, 121-127.

Gohil, J.M., Bhattacharya, A. & Ray, J., 2006, 'Studies on the cross-linking of poly (vinyl alcohol)', Journal of Polymer Research 13, 161-169.

Gorga, R. E. & Cohen, R. E., 2004, 'Toughness enhancements in PMMA by addition of oriented MWCNTs', Journal of Polymer Science 42, 2690-2702.

Huang, R.Y.M. & Rhim, J.W., 1993, 'Modification of poly (viny1 alcohol) using maleic acid and its application to the separation of acetic acid-water mixtures by the pervaporation technique', Polymer International 30, 129-135.

Kearns, J. C. & Shambaugh, R. L., 2002, 'Polypropylene fibers reinforced with carbon nanotubes', Journal of Applied Polymer Science 86, 2079-2084.

Kong, Y., Shi, D., Yu, H., Wang, Y., Yang, J. & Zhang, Y., 2006, 'Separation performance of polyimide nanofiltration membranes for solvent recovery from dewaxed lube oil filtrates', Desalination 191, 254–261.

Ma, P-C., Siddiqui, N.A., Marom, G. & Kim, J-K., 2010, 'Dispersion and functionalization of carbon nanotubes for polymer-based nanocomposites: a review', Composites: Part A 41, 1345-1367.

Mondal, S. & Wickramasinghe, S. R., 2008, 'Produced water treatment by nanofiltration and reverse osmosis membranes', Journal of Membrane Science 322, 162–170.

Moniruzzaman, M. & Winey, K.I., 2006, 'Polymer nanocomposites containing carbon nanotubes', Macromolecules 39, 5194-5205.

Ogasawara, T., Ishida, Y., Ishikawa, T. & Yokota, R., 2004, 'Characterization of MWNT/phentlethynyl terminated polyimide composites', Composites A 35, 67-74.

Qian, D., Dickey, E. C., Andrews, R. & Rantell, T., 2000, 'Load transfer and deformation mechanisms in carbon nanotube-polystyrene composites', Applied Physics Letters 76, 2868-2870.

Safadi, B., Andrews, R. & Grulke, E. A., 2002, 'Multiwalled carbon nanotube polymer composites: synthesis and characterization of thin films', Journal of Applied Polymer Science 84, 2660-2669.

Spitalsky, Z., Tasis, D., Papagelis, K. & Galiotis, C., 2010, 'Carbon nanotube–polymer composites: chemistry, processing, mechanical and electrical properties', Progress in Polymer Science 35, 357-401.

Srijaroonrat, P., Julien, E. & Aurelle, Y., 1999, 'Unstable secondary oil/water emulsion treatment using ultrafiltration: fouling control by backflushing', Journal of Membrane Science 159, 11-20.

Strathmann, H., 1985, 'Production of microporous media by phase inversion processes', ACS Symposium Series 269, 165.

Strathmann, H., Kock, K., Amar, P. & Baker, R.W., 1975, 'The formation mechanism of asymmetric membranes', Desalination 16, 179.

Tjong, S.C., 2006, 'Structural and mechanical properties of polymer nanocomposites', Materials Science and Engineering 53, 73-197.

Xia, H., Wang, Q., Li, K. & Hu, G. H., 2004, 'Preparation of CNT/polypropylene composite powder with a solid state mechanochemical pulverization process', Journal of Applied Polymer Science 93, 378-386.

Xiong, J., Zheng, Z., Qin, X., Li, M., Li, H. & Wang, X., 2006, 'Thermal and mechanical properties of a polyutherane/MWCNT composite', Carbon 44, 2701-2707.

CHAPTER 5

5. The effect of twisted tape on the concentration polarisation of a tubular module

5.1. Introduction

The purpose of this chapter is to investigate the effects on concentration polarisation and an increase in flux through a membrane by the use of a helical insert in a tube that induces rotational flow and increases turbulence. The phenomenon of concentration polarisation is briefly introduced with the models that attempt to describe the process. The use of turbulence promoters in literature is also briefly looked at before proposing a method of using helical inserts in a tubular membrane module to increase turbulence and thereby decrease the effects of concentration polarisation.

5.1.1. Concentration Polarisation

There are several models that attempt to describe concentration polarisation.

Osmotic pressure model

This model states that during filtration the concentration c_m at the membrane surface is higher than the bulk concentration and thus the osmotic pressure of the solution at the surface can no longer be ignored. Kozinski and Lightfoot (1971) state that if a rejection of 100% is assumed and the osmotic pressure difference is determined by c_m the permeate flux is then described by

$$J = \frac{\Delta P - \Delta \Pi}{R_m} \tag{5.1}$$

where ΔP is the hydraulic pressure difference, $\Delta \Pi$ is the osmotic pressure difference and R_m is the membrane resistance. When the applied pressure increases the flux will

increase. But this leads to an increase in the membrane surface concentration and this in turn leads to an increase in the osmotic pressure difference. Thus the increase in pressure is partially offset by the increase in osmotic pressure (Goldsmith, 1971). Kozinski and Lightfoot (1971) also state that if the osmotic pressure difference increases rapidly with permeate flux, the increase in ΔP may only have a small increase in permeate flux. According to Goldsmith (1971) the osmotic pressure model cannot be used for colloidal suspensions as their osmotic pressure is negligible.

Gel layer model

During filtration the concentration of the solute at the membrane surface, c_m, is much higher than in the bulk solution. If 100% rejection of the membrane is assumed and the influence of the permeate flux and concentration profile on the mass transfer coefficient, k, is neglected, c_m can be described by

$$c_m = c_m \mathrm{e}^{(\frac{\mathrm{J}}{\mathrm{k}})} \tag{5.2}$$

where J is the permeate flux (Bixler et al., 1968; Blatt et al., 1970). The concentration c_m increases rapidly with permeate flux reaching a concentration c_g where the solution at the membrane is no longer fluid. This causes a gel layer to be formed on the membrane and because of this layer when pressure increases the flux increases until it reaches a plateau where no flux increase occurs with pressure increases such that

$$J_\infty = \mathrm{k} \ln\left(c_g / c_b\right) \tag{5.3}$$

where J_∞ is the limiting flux and c_b is the bulk concentration (Bixler et al., 1968; Blatt et al., 1970).

Shear-induced diffusion model

Immediately when the filtration process begins a layer forms on the membrane surface and a steady state is reached where the rate that the rejected particles move towards the membrane because of solvent flow is equalised by diffusion back into the bulk. This is by Brownian diffusion (Blatt et al., 1970) and shear-induced diffusion (Zydney and Colton, 1986).

Novel theory for concentration polarisation

This theory is based on the combination of hydrodynamic and thermodynamic approaches to model concentration polarisation in crossflow filtration of monodisperse, non-interacting, spherical colloidal suspensions (Elimelech and Bhattacharjee, 1998).

5.1.2. Crossflow module with turbulence promoter

Placing turbulence promoters in the membrane system can increase flux. Turbulence promoters added to a membrane reduce the diffusion resistance of concentration polarisation (Balster et al., 2010). These turbulence promoters have been found to be highly efficient from the point of view of energy, capital costs and high flux improvements (Krstić et al., 2003; Krstić et al., 2007). The general trend is that when an insert is placed inside a flow field the velocity increases and the shear rate near the wall also increases. Depending on the geometry of the turbulence promoter and the inlet flow of the fluid, secondary flows can be generated which further increase the migration of particles from the membrane surface (Gupta et al., 1995). Some of the promoters used are smooth rods, cone shaped inserts, disc shaped inserts, spiral wires and twisted tapes. Twisted tapes (Figure 5-1) are favoured as the turbulence promoter to use because of their simple geometry and low pressure drops which mean operating

pressures don't have to be increased (i.e. there will be no need to change pumps in the system) . Popovic and Tekic (2011) have used twisted tapes to increase the turbulence in a ceramic membrane microfiltration system thereby increasing the flux.

Figure 5-1: Picture showing twisted tapes with different twist lengths (Bas and Ozceyhan, 2012).

5.2. Experimental

The membrane module design created for this work is similar to the one by Popovic and Tekic (2011) but the design in this work is modified such that an ultrafiltration membrane can be used instead of a microfiltration membrane. The design, which is taken as a single tube that would be in a tubular module, consists of a tube with multiple bores that has been fitted with a twisted tape. A polymer membrane is secured (wrapped) around the tube so that the feed fluid passes through the bores and through the membrane. Figure 5-2 shows the schematic of the tube.

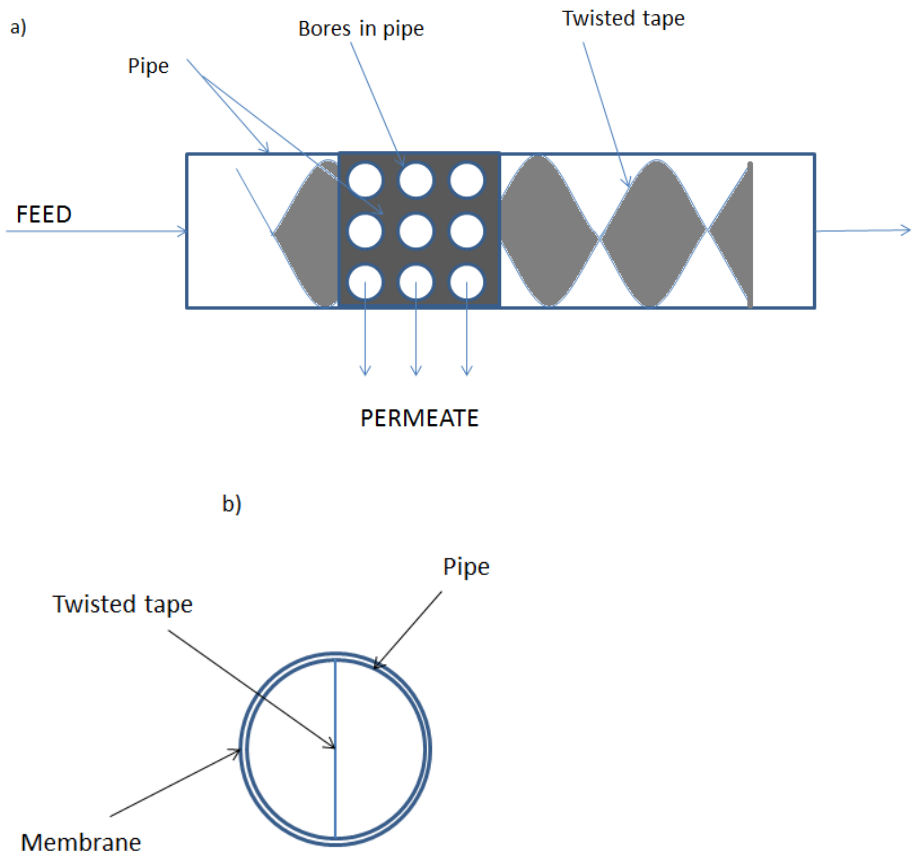

Figure 5-2: a) This is the side view of the schematic of the tube. b) The top view of the tube showing the membrane wound around it.

Calculation of Reynold's number

The Reynold's number (Re) can give an indication of the degree of turbulence in a tube. When Re < 2300 there is laminar flow, when Re > 4000 the flow is turbulent and in between the two numbers is the transition between laminar and turbulent flow. The Re is calculated by

$$Re = \frac{vD_p\rho}{\mu} \tag{5.4}$$

where v is the velocity of the fluid, D_p is the diameter of the tube, ρ is the density of the fluid and μ is the viscosity. Since the concentration of the oil in the water is very small (with the weight fraction of oil being 3.967×10^{-4}), the density and the viscosity of the mixture is assumed to be that of water. The Reynold's number for a tube with twisted tape inserted is calculated in the same way as a normal tube excepting that the velocity is adjusted before calculation. From Popovic and Tekic (2011) if a particle travels along the central axis of the twisted tape the $K_L = 1$. If the particle travels along the edge of the twisted tape K_L is described by:

$$K_L = \left(1 - \frac{\pi^2 r^2}{{L_e}^2}\right)^{1/2} \tag{5.5}$$

where L_e is shown in Figure 5-3 as the length of a single twist in the tape and r is the radial coordinate of a cylindrical coordinate system with an axis that overlaps the tube coordinate system.

Figure 5-3: Diagram of twisted tape showing the diameter (D_{TP}) and twist length (L_e).

The average K_L for the tube with the tape is given by:

$$K_L = 0.5 + 0.5\left(1 + \frac{\pi^2}{4O_{tp}^2}\right)^{1/2} \tag{5.6}$$

where $O_{tp} = diameter\ of\ tape/L_e$ and is the aspect ratio of the tape. The second factor that needs to be accounted for is the finite element of the helical area of the twisted tape and this is given by:

$$K_A = 1 - \frac{4\delta_{tp}}{\pi D_p} \tag{5.7}$$

where δ_{tp} is the thickness of the tape. The actual cross flow velocity is given by:

$$v_{ac} = \mathrm{v}\frac{K_L}{K_A} \tag{5.8}$$

The actual velocity (v_{ac}) is now used in the Re calculations.

The same rig (Figure 4-1) that is used for the dead end filtration experiments in chapter 4 is used for this experiment except the dead end filtration module is replaced by the twisted tape tube (Figure 5-2). Since concentration polarisation is detrimental in ultrafiltration (it is better controlled in reverse osmosis) the membrane used is a polysulfone ultrafiltration membrane with no PVA layer on top (Figure 5-4).

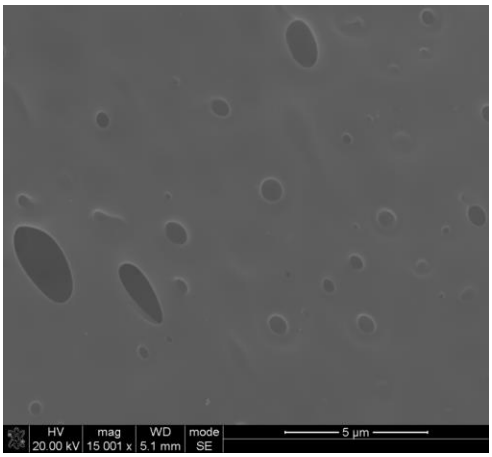

Figure 5-4: Ultrafiltration membrane used for testing the effect of a twisted tape on the flux through a tube.

5.3. Results and Discussion

When comparing the Reynold's numbers of the tubes with and without the twisted tape inserted, it is found that the Re is 4001 without the twisted tape and 5631 with the tape (calculation in Appendix C). Both these Reynold's numbers are above the turbulent range (4000) but since the value with the twisted tape is higher it means that there is an increase in turbulence in the tube. This is expected as the added twisted tape induces a corkscrew vortex to be formed in the tube. Figure 5-5 shows the flux through the membrane in the case of a simple crossflow tube and a crossflow tube with a twisted tape inserted.

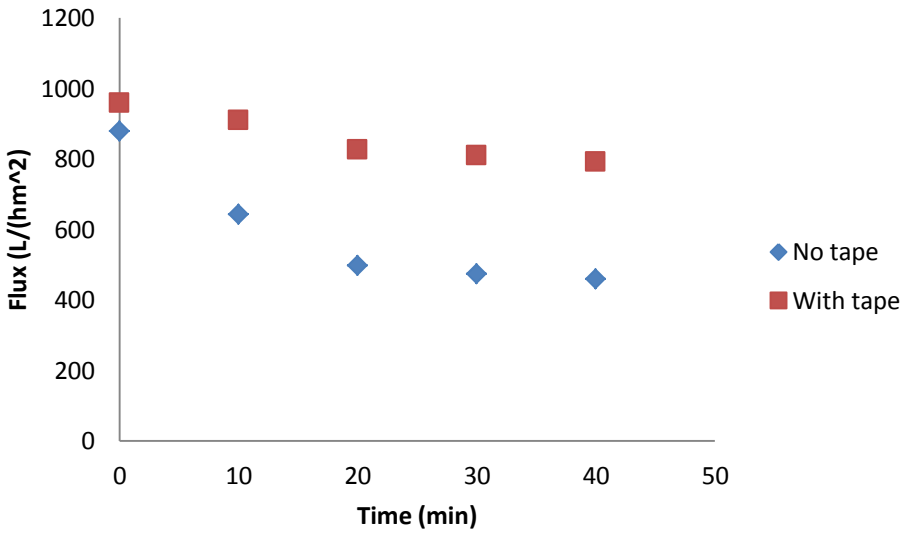

Figure 5-5: Flux results for a tube with a twisted tape and one without. The decrease of Flux with time has been reduced with the addition of the tape.

There is an increase in the flux from normal crossflow tube to the crossflow tube with twisted tape. The difference in the flux between taped and un-taped tubes was pre-empted by the difference in the Re of the two modules. The tape has not only increased

the flux but also decreased the rate at which the membrane fouls (dFlux/dt). For the case of no tape in the tube, $\frac{dFlux}{dt} = -14.99L/(hm^2)/min$ and when the twisted tape is installed, $\frac{dFlux}{dt} = -5.51L/(hm^2)/min$. The flux improvement attributed to the addition of the twisted tape is found to be 72% at the time of 40 minutes for a pitch ratio of 1.2 and a flow rate of 2.8 L/min. This flux improvement is on the high side of the scale as compared to Popovic and Tekic (2011) whose results displayed flux improvements of between 25% and 85% for flow rates between 5.5 and 1 L/min and pitch ratios between 2.5 and 1 respectively.

In order to calculate the membrane resistance the following equation by Popovic and Tekic (2011) is used

$$R_m = \frac{TMP}{\mu_w J_w} \tag{5.9}$$

where R_m is the membrane resistance, TMP is the trans-membrane pressure, μ_w is the water viscosity and J_w is the water flux through the membrane. The membrane resistance is found to be 117665 m^{-1} for when the twisted tape is inserted and when it is not. Fouling resistance is defined by Popovic and Tekic (2011) as

$$R_f = \frac{TMP}{\mu_p J_p} - \mathrm{R}_m \tag{5.10}$$

where R_f is the fouling resistance of the membrane, μ_p is the viscosity of the permeate (which is considered to be that of water in this work because of the low concentrations of oil used in the experiments) and J_p is the permeate flux. The fouling resistance of the case where there is no twisted tape is 128530 m^{-1} and when the tape is added the

fouling resistance drops to 25061 m^{-1}. The addition of the twisted tape to the tube has reduced the fouling resistance by 80% (as calculated using the values in Table C-3).

5.4. Conclusion

In this chapter the use of twisted tapes in the improvement of flux in tubular microfiltration modules has been shown. This work has demonstrated that this technique can also be used in ultrafiltration with a polymer membrane specifically the polysulfone membrane used for the experiments. The addition of a twisted tape to the tube increased the stable flux (which is the flux at 40 minutes) by 72%, reduced the rate at which the flux decreased from -14.99 to -5.51 L/(hm^2)/min and decreased the fouling resistance by 80%.

References

Balster, J., Stamatialis, D.F. & Wessling, M., 2010, 'Membrane with integrated spacer', Journal of Membrane Science 360, 185–189.

Bas, H. & Ozceyhan, V., 2012, 'Heat transfer enhancement in a tube with twisted tape inserts placed separately from the tube wall', Experimental Thermal and Fluid Science 41, 51-58.

Bixler, H.J., Nelsen, L.M. & Bluemle, L.W., 1968, 'The development of a diafiltration system for blood purification', Transactions of American Society, Artificial Internal Organs 14, 99-108.

Blatt, W.F., Dravid, A., Michaels, A.S. & Nelson, L., 1970, 'Solute polarization and cake formation in membrane ultrafiltration: causes, consequences and control techniques', Membrane Science and Technology, Plenum Press, New York, NY, 47-97.

Elimelech, M. & Bhattacharjee, S., 1998, 'A novel approach for modeling concentration polarization in crossflow membrane filtration based on the equivalence of osmotic pressure model and filtration theory', Journal of Membrane Science 145, 223-241.

Goldsmith, R.L., 1971, 'Macromolecular ultrafiltration with microporous membranes', Industrial Engineering & Chemistry Fundamentals 10, 113-120.

Gupta, B.B., Howell, J.A., Wu, D. & Field, R.W., 1995, 'A helical baffle for cross-flow microfiltration', Journal of Membrane Science 99, 31–42.

Kozinski, A.A. & Lightfoo,t E.N., 1971, ‘Ultrafiltration of proteins in stagnation flow’, AIChE Journal 17, 81-85.

Krstić, D., Tekić, M., Carić, M. & Milanović, S., 2003, ‘Kenics static mixer as turbulence promoter in cross-flow microfiltration of skim milk’, Separation Science & Technology 38, 1549–1560.

Krstic, D.M., Höflinger, W., Koris, A.K. & Vatai, G.N., 2007, ‘Energy-saving potential of cross-flow ultrafiltration with inserted static mixer: application to an oil-in-water emulsion’, Separation & Purification Technology 57, 134–139.

Popovic, S. & Tekic, M. N., 2011, ‘Twisted tapes as turbulence promoters in the microfiltration of milk’, Journal of Membrane Science 384, 97 – 106.

Zydney, A.L. & Colton, C.K., 1986, ‘A concentration polarization model for the filtrate flux in crossflow microfiltration of particulate suspensions’, Chemical Engineering Community 47, 1-21.

CHAPTER 6

6. Use of Artificial Neural Network for the prediction of flux decline through nanofiltration membrane used for oil/water separation.

6.1. Introduction

Traditional modelling methods for membrane flux such as mass transfer models, gel-polarisation models and Brownian diffusion models have limitations that include the demand for extensive experimental data that may be difficult to acquire and for the models only being valid for certain special conditions (Razavi et al., 2003). Razavi et al. (2003) also states that modelling methods based on direct analysis of experimental data such as artificial neural networks can be used for membrane modelling and Niemi et al. (1995) conclude that ANNs are easier to use and have approximately the same predictability as mass transfer models. ANNs have been used to model a variety of membrane processes successfully including reverse osmosis for water desalination (Abbas and Al-Bastaki, 2005), nanofiltration (Darwish et al., 2007) and ultrafiltration (Holmqvist et al., 2005). This chapter explores the possibility of using an ANN to model the flux of the membrane from chapter 4 with the limited amount of data gathered. The resilient backpropagation (Rprop) teaching rule is used in this study in order to reduce the network training time. The inputs into the network are pressure, CNT loading and time while the output is membrane flux. The tool used to create the neural network is Encog and it is used here in its .Net iteration. Once a viable neural network was created in Encog, the basic structure of the network was used in Matlab to create a network that was trained using the Levenberg-Marquardt training method and was used to find the

optimum CNT concentration/pressure combinations that yield maximum flux by using a grid search method.

6.2. Generating neural networks

Encog is a framework for java and .Net and it contains several network structures and learning methods that can be used to create a neural network. The program Encog workbench (by Heaton Research) is used, which is a graphic user interface (GUI) for the Encog classes, to create the ANN used in this work. The steps taken to create and train a network are as follows:

- Randomize – Encog is given a file with the input and output information and it shuffles the entries for a more random set.
- Segregate – The random data is separated into a training set and an evaluation set. The training set is used to train the network and the evaluation set is used to test the efficiency of the network.
- Normalize – This is the reduction of the data to a more canonical form. In this case to a value between -1 and 1 although if needed it is possible to normalize between 0 and 1.
- Generate – Encog generates training data into a file that it can process.
- Create – A neural network is generated by Encog. The structure can still be altered if necessary.
- Train – A training method is selectefd and it is used to train the neural network that was created.
- Evaluate – The trained network is evaluated with the evaluation data.

The Encog Analyst was used to create a network that will model the flux through a nanofiltration membrane using data gathered from experiments conducted in chapter 4. The filtration data (Table B-1, Appendix B) is imported into Encog and the Analyst is initiated. From Figure 6-1 it is observed that the Analyst is set to produce a feedfoward Network and do a regression analysis on the data. The target data is explicitly stated, the range of normalization given and the maximum error that can be incurred while training.

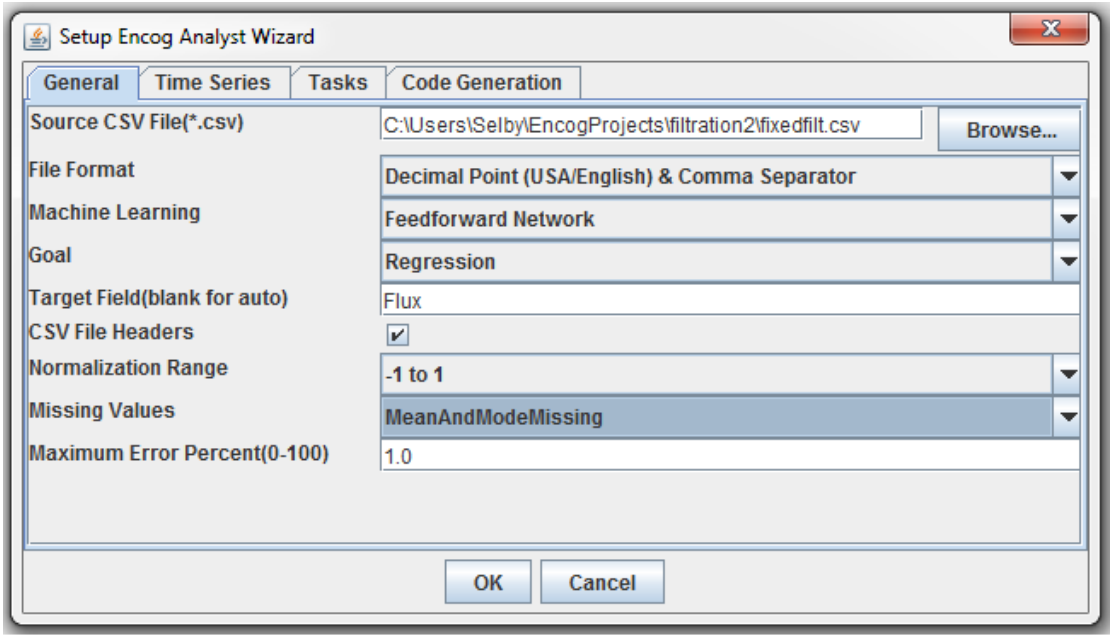

Figure 6-1: Encog Analyst window setting up network generation.

The analyst then generates a script and the only parameters that are changed are the normalization methods. They are changed from “equilateral” to “range” and the script is executed. The data is randomized and normalized into Table B-2 and used to train the network. The neural network that is generated is shown in Figure 6-2 and it has 3 inputs (pressure, CNT loading and time) 13 neurons in the hidden layer and 1 output (flux).

Two bias neurons are attached to the hidden layer and the output layer. The hyperbolic tangent activation function is used in the hidden and output layer. Resilient backpropagation is used to train the network where the maximum step is set to 50 and the initial update is 0.1 (Figure B-1).

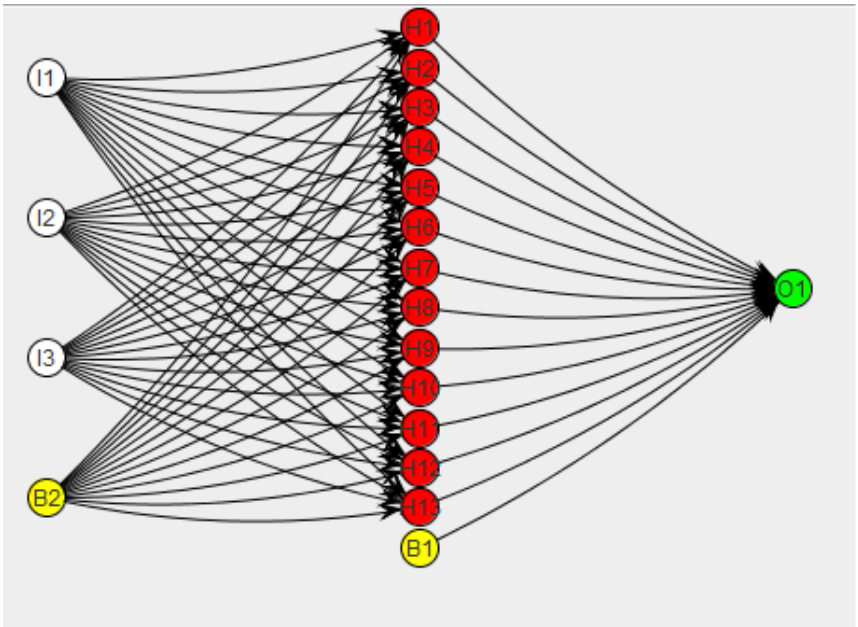

Figure 6-2: The 3 input, 13 neuron hidden layer and single output ANN generated by Encog.

The 3 input, 13 neuron hidden layer and single output neural network generated by Encog is used as the basis for the creation of a neural network in Matlab. Matlab possesses a number of toolboxes that include functions that allow for rapid execution of code and one of these toolboxes is for neural network creation, training, validation, testing and execution. Figure 6-3 displays the neural network used in Matlab. The network has 3 input neurons in the input layer, 13 neurons in the hidden layer and one neuron in the output layer and this setup was chosen because Encog determined this

network as the best for the presented data. The hidden layer uses a sigmoid function and the output layer uses a linear function for calculations. The code used to train, validate and test the neural network is available in Appendix B.

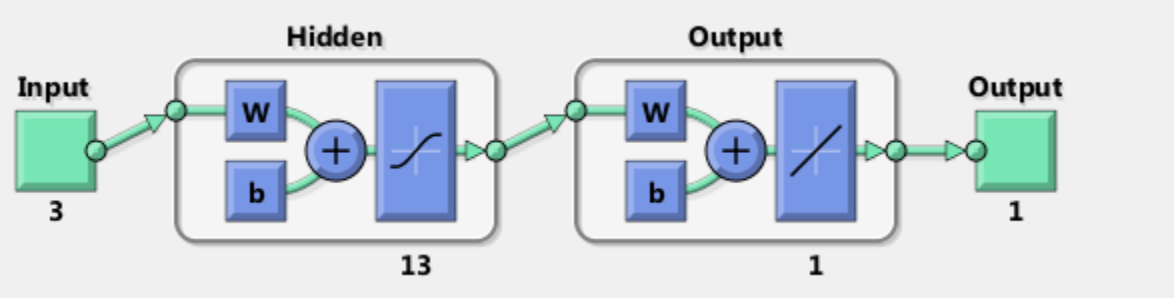

Figure 6-3: The 3 input, 13 neuron hidden layer and single output ANN setup in Matlab based on the neural network generated by Encog.

The training method used to update the weights by Matlab is the Levenberg-Marquardt algorithm as it is the fastest backpropagation algorithm available in the toolbox. Hagan and Menhaj (1994) give a detailed derivation of the Levenberg-Marquardt (which is an approximation of the Newton-Rhapson method) algorithm and how it is implemented in the backpropagation algorithm for training feedfoward neural networks.

6.3. Results and discussion

The Encog network is trained in 21 iterations and has a training error of approximately 0.99% and the mean deviation of approximately 10%. The graph displaying the progression of training (the decrease in error versus the number of iterations) is in Appendix B (Figure B-2). Figure 6-4 gives a graphical account of the ANN results (red) versus the experimental data (blue). Although there is a relatively good correlation between the network flux output and the measured flux the correlations could be better. This is due to the size of the data pool used. Artificial neural networks require a large

amount of experimental data for them to be accurate. But even with the limited amount of data, by using the Rprop learning method it was possible to get accuracy comparable to other studies that used a lot more data and the regular backpropagation method (Chakraborty et al., 2003). The weights that are found to work with the network to give the required output are given in Table 6.1. There are a total of 66 connections and weights.

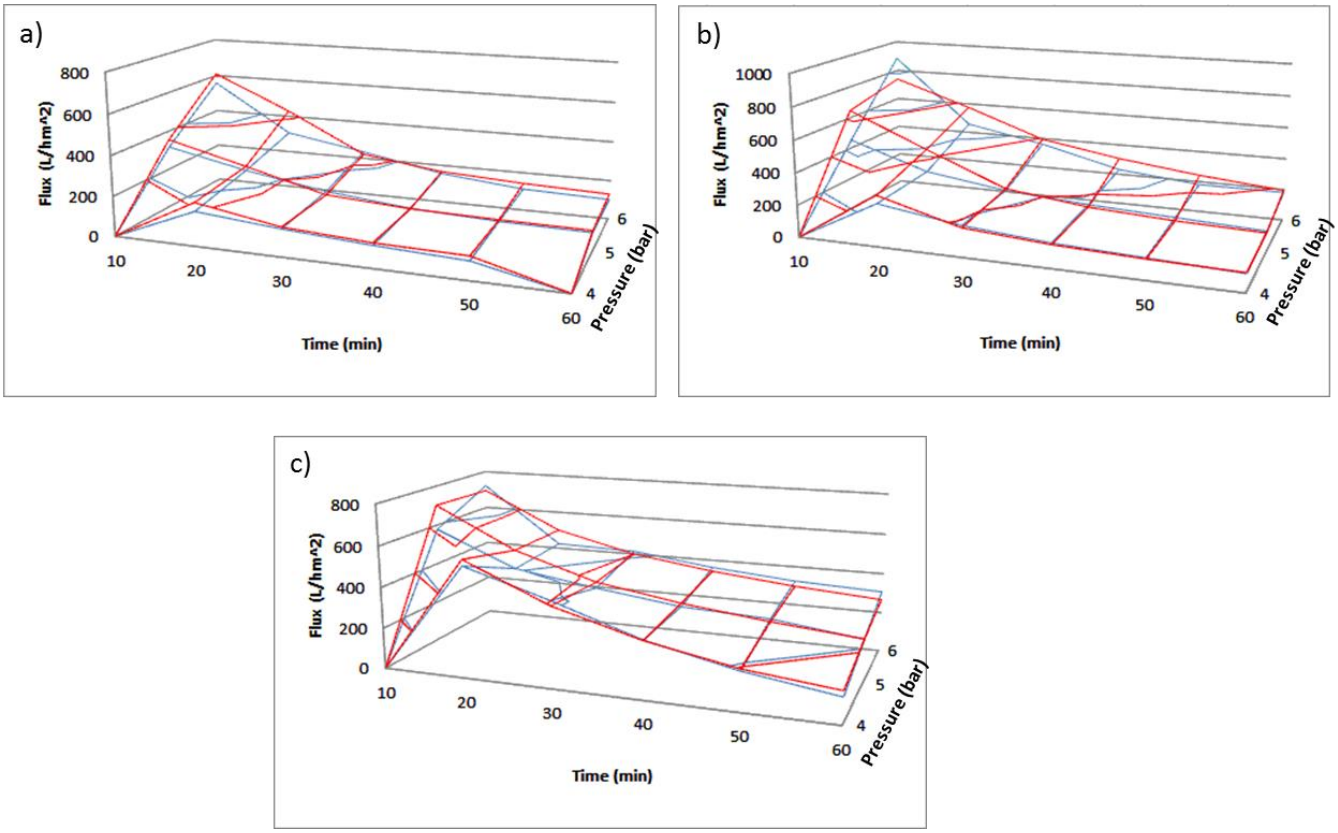

Figure 6-4: Surface plots of the ANN generated data (red) that compares favourably with the experimental data (blue). The plots are done for (a) 0% (b) 5% and (c) 10% CNT loadings.

Table 6.1: Weight values for the generated network (where I is input neuron, H is hidden neuron and O is output neuron). H1->O1 is the connection between hidden neuron H1 and the output O1.

Neuron connection	Weight	Neuron connection	Weight	Neuron connection	Weight
H1->O1	0.185	**I3->H4**	0.321	**I3->H11**	0.819
H2->O1	0.031	**B2->H4**	0.033	**B2->H11**	0.541
H3->O1	0.237	**I1->H5**	1.021	**I1->H12**	0.297
H4->O1	-0.119	**I2->H5**	1.031	**I2->H12**	0.321
H5->O1	-0.217	**I3->H5**	0.402	**I3->H12**	0.380
H6->O1	-0.293	**B2->H5**	0.657	**B2->H12**	-0.300
H7->O1	0.477	**I1->H6**	3.700	**I1->H13**	-0.842
H8->O1	-0.392	**I2->H6**	0.247	**I2->H13**	1.170
H9->O1	0.018	**I3->H6**	0.742	**I3->H13**	1.972
H10->O1	0.154	**B2->H6**	2.098	**B2->H13**	-0.257
H11->O1	0.192	**I1->H7**	-0.292		
H12->O1	-0.081	**I2->H7**	1.082		
H13->O1	0.276	**I3->H7**	-0.399		
B1->O1	-0.342	**B2->H7**	-1.295		
I1->H1	0.494	**I1->H8**	0.713		
I2->H1	0.105	**I2->H8**	0.101		
I3->H1	0.690	**I3->H8**	-0.157		
B2->H1	0.935	**B2->H8**	0.323		
I1->H2	0.135	**I1->H9**	0.063		
I2->H2	-0.368	**I2->H9**	-0.051		
I3->H2	0.937	**I3->H9**	0.215		
B2->H2	-0.287	**B2->H9**	-0.148		
I1->H3	-0.443	**I1->H10**	0.058		
I2->H3	0.818	**I2->H10**	0.212		
I3->H3	1.202	**I3->H10**	0.504		
B2->H3	0.104	**B2->H10**	0.968		
I1->H4	0.207	**I1->H11**	-0.381		
I2->H4	0.672	**I2->H11**	0.839		

In Table 6.1 H represents a hidden neuron, O represents an output neuron and I represents an input neuron. H1 means the first hidden neuron and O1 means the first output neuron and H1->O1 means the connection between hidden neuron 1 and output neuron 1 and the weight associated with this connection is displayed in Table 6.1. This convention of representing neuron connections is used throughout Table 6.1. The code used to generate this neural network can be found in Appendix B. Part of the code can be generated by Encog but the user has to finish it off by adding training instructions.

Since the network generated by Encog displayed good results that approximated the data well, the basic structure of the network was used in Matlab and trained, validated and tested using the neural network toolbox. The training ran for 19 seconds with 14 iterations before the termination criterion (which is the reduction of the mean squared error) was met. From Figure 6-5 the R value (which is the Matlab Neural Network Toolbox equivalent of the coefficient of determination, R^2) achieved for the fit of the output of the network and the target (experimental result) for the training of the network is approximately 95% and for the validation of the network 93%. The trained neural network was tested and the R value was found to be approximately 95% which indicates that the network describes the data well. The data set used for the neural network is randomized and then separated into training data, validation data and testing data in a 70, 15, 15% split respectively. This ensures that the validation and testing data are not repeated data used in training as this would give a false high performance rating.

Once the network was defined in Matlab, code was written in order to determine the best CNT concentration and pressure combination that would yield the highest flux for a

given time period. This code is available in Appendix B. A grid search method is used by selecting a CNT concentration (between 0 and 10%) and a pressure (between 0 and 10 bar) and calculating the accumulated flux for a 100 minute period for the CNT/pressure combination. By performing a grid search the neural network model has to calculate flux values using inputs that are outside the experimental data used to train the network. Figure 6-6 displays the surface plot generated by the grid search. The area of operation for high flux is between 5 and 8% carbon nanotube concentration and pressures between 1 and 4 bars. In chapter 4 it was determined that the concentration of the CNTs in the membrane affects the pore size of the membrane. It was shown that an increase in the CNT concentration led to an increase in the pore size of the membrane. In Figure 6-6 it is shown that the flux decreases with a decrease in the CNT concentration and this corresponds to the findings in chapter 4. Figure 6-6 also shows that at high pressures the cumulative flux is low. This is a surprising find as one would expect that the flux should continue to increase with a continued increase in pressure. But since the neural network and grid search methods are over a period of time it is possible that the results display a situation where prolonged exposure of the membrane to high pressures leads to the oil deforming and entering and blocking the pores of the membrane. This would mean the cumulative flux is lower.

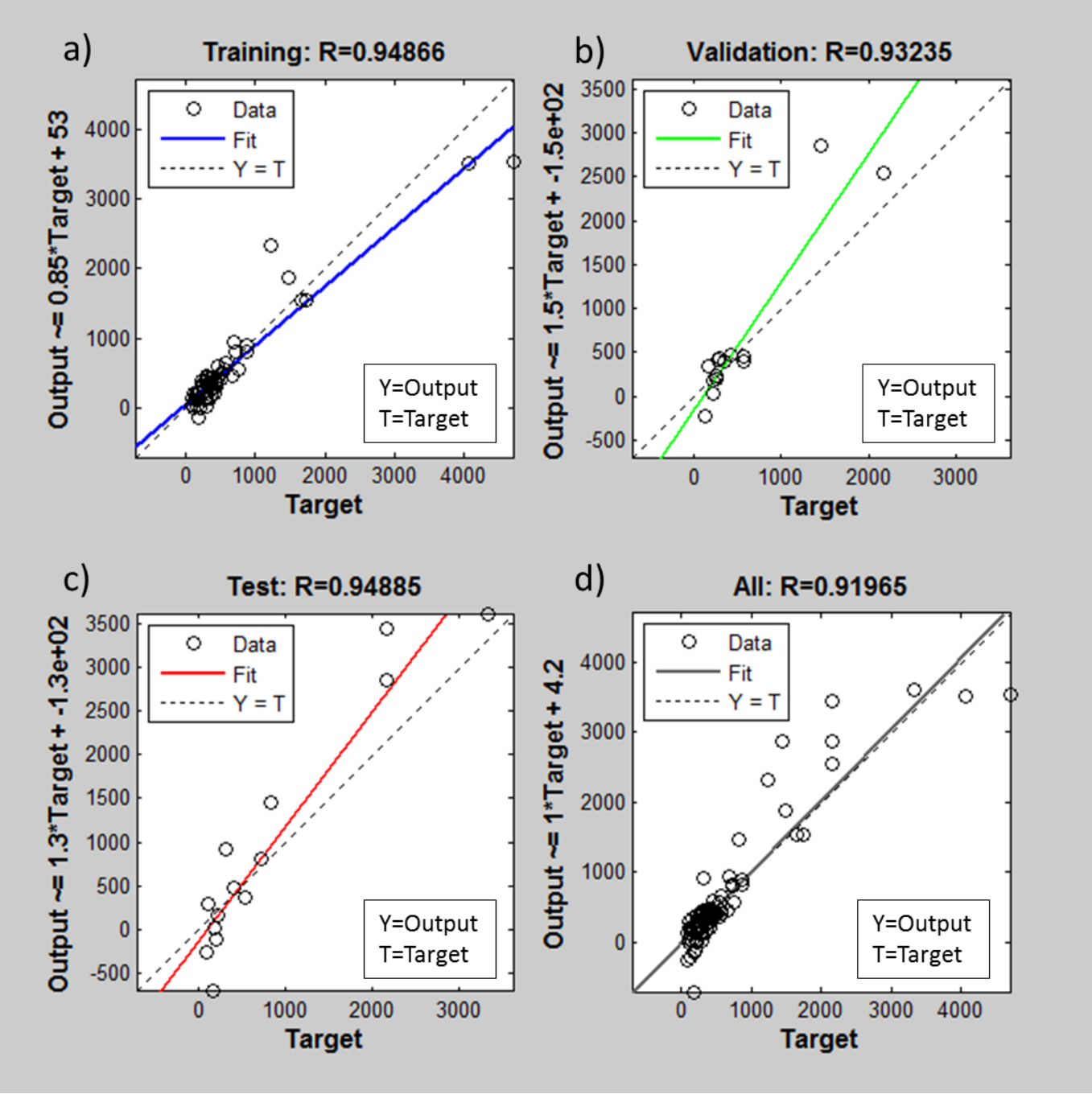

Figure 6-5: Training results generated by the neural network toolbox in Matlab. The curve fit for the output of the network and the target produced R values above 90% for the training, validation, network testing and the overall network performance.

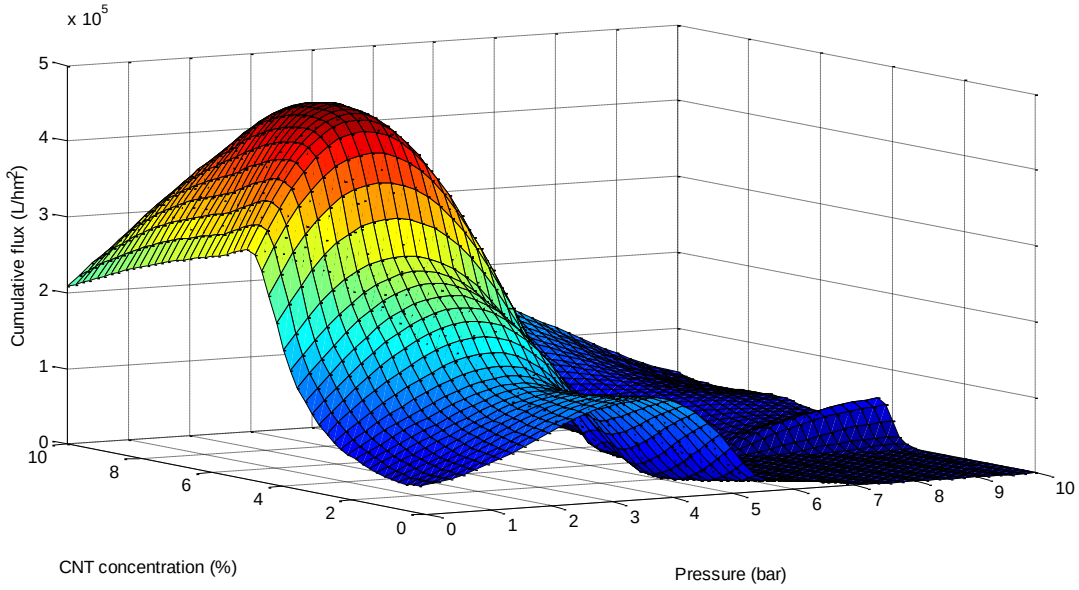

Figure 6-6: Surface plot of the cumulative flux achieved by a grid search of CNT concentration and pressure.

6.4. Conclusion

The aim of chapter 5 was to design an artificial neural network that can describe the membrane separation process taking place in chapter 4. A neural network is generated in order to give a representation of a dead end filtration system using a nanofiltration membrane to separate oil and water. The network is a 3 layer feedfoward network with 1 output, 13 hidden neurons and 3 input neurons. The training error of the network is found to be 0.99% and the evaluation error is 0.92% which means this network can approximate the system quite closely. The network was transferred to Matlab where it was trained using another method and the results obtained also showed that the network describes the data well. A grid search method was then implemented to determine the best combination of CNT concentration and pressure. It was found that

the best range to operate is at CNT concentrations between 5 and 8% and pressures between 1 and 4 bar.

References

Abbas, A. & Al-Bastaki, N., 2005, ‘ Modeling of an RO water desalination unit using neural networks’, Chemical Engineering Journal 114, 139–143.

Darwish, N.A., Hilal, N., Al-Zoubi, H. & Mohammad, A.W., 2007, ‘Neural networks simulation of the filtration of sodium chloride and magnesium chloride solutions using nanofiltration membranes’, Chemical Engineering Research & Design 85, 417–430.

Hagan, M. T. & Menhaj, M. B., 1994, ‘Training Feedforward Networks with the Marquardt Algorithm’, IEEE TRANSACTIONS ON NEURAL NETWORKS 5, 989-993.

Holmqvist, A., Wallberg, O. & Jönsson, A. S., 2005, ‘Ultrafiltration of Kraft black liquor from two Swedish pulp mills’, Chemical Engineering Research & Design 83, 994–999.

Niemi, H., Bulsari, A. & Palosaari, S., 1995, ‘Simulation of membrane separation by neural networks’, Journal of Membrane Science 102, 185-191.

Razavi, M. A., Mortazavi, A. & Mousavi, M., 2003, ‘Dynamic modelling of milk ultrafiltration by artificial neural network’, Journal of Membrane Science 220, 47-58.

CHAPTER 7

7. Conclusion and Recommendations

7.1. Conclusion

The aim of this study was to produce a membrane with increased mechanical properties that are provided by the addition of CNTs to the membrane and that is capable of separating synthetic oil from water. Carbon nanotubes were produced using the CVD technique and ferrocene as both a carbon source and catalyst and a thin film composite membrane comprising of a polysulfone bottom layer and a polyvinyl alcohol separation layer was produced. The mechanical properties of the bottom layer were enhanced by the addition of CNTs and the membrane was analysed by microscopy, mechanical, flux and rejection testing. Concentration polarization was reduced by the addition of a twisted tape to a tube housing an ultrafiltration membrane by inducing a rotational flow through the tube. A neural network model was developed using Encog to derive the structure of the network and Matlab for the utilization of the model to extrapolate data to determine the optimum operating conditions for high cumulative flux through the membrane.

Chapter 3 dealt with the production of CNTs using ferrocene as both a carbon source and a catalyst in a CVD reactor. MWCNTs were produced at temperatures between 800^{o}C and 950^{o}C but the TEM images very clearly showed the presence of catalyst particles within the nanotubes. The study also showed that there were fewer adherences of CNTs to the reactor wall at higher temperatures. In chapter 4 CNTs were added to the polysulfone support layer through ultra-sonication mixing with the polymer solution. The mechanical strength of the polysulfone support increased with increasing

CNT addition until 7.5% w/w CNT concentration was reached where mechanical properties began to decline due to factors linked with CNT agglomeration. This agglomeration effect of CNTs also led to the increase in the pore sizes of the polysulfone membrane, with an increase in CNT concentration. The study also found that due to the effect of the CNTs on the pore size of the membrane support layer, the filtration rate and retention ability of the membrane were dependent on the CNT concentration (this means that the higher the CNT concentration the higher the membrane flux but the lower the retention of oil particles). The pressures across the membrane also had an effect on the retention and flux of the membrane, the higher the pressure the higher the flux but the lower the retention ability of the membrane. Permeate oil concentrations lower than 10 mg/L were achieved at low CNT concentrations and low transmembrane pressures. Chapter 5 was a study on the possibility of reducing concentration polarisation by the addition of a helical insert in a tube. The study found that the addition of the insert increased the Reynold's number of the fluid in the tube and thus there is increased turbulence which decreases CP during filtration. This means that the fouling on the membrane was less (as seen with the reduced fouling resistance of the membrane) and that the lifetime of the membrane is increased (as periods between cleaning will increase). In chapter 6 a neural network was setup to model the membrane filtration process in chapter 4. The network gave a close approximation of the complex filtration process with a limited amount of data. This was made possible by the training methods used in both Encog and the neural network toolbox in Matlab. This network can be improved by simply continuing its training with new data but it may still struggle with some of the data generated at low time and flux

(because of the large variances) and if any condition (which cannot be measured) changes during filtration.

7.2. Recommendations

An observation that can be made from the TEM images in chapter 3 is that the nanotubes are not all uniform in size or shape or amount of structural defects. Therefore as a step forward, uniform CNTs should be produced without sacrificing the ease, speed and volume of production of the CVD production method. It is worth investigating what the effect of adding purified CNTs to the membrane would be, as it may be possible to get better mechanical strength results with “purer” CNTs. CNTs can be modified and certain chemical groups added to them to change their properties and therefore it would be interesting to see whether the addition of hydrophilic groups to the CNTs has any effect on the hydrophobic nature of the polysulfone membrane and if it does, is this effect positive or negative to both the filtration and mechanical integrity of the membrane. Another topic that can be investigated is the possibility of using melt extrusion to create the support membrane. If CNTs are added to the extruded membrane the chances of them being aligned are higher as CNTs tend to align in a polymer when a shear force if introduced. This means the mechanical strength of the membrane support could be increased since aligned CNTs accept more force from the polymer matrix than misaligned ones. It would be helpful if a multivariate analysis of the filtration data is done and the data “smoothed” into data with less “outliers” which cause the neural network to either require more training data or to give results that are not desirable. It would be of interest to investigate how an entire tubular module would behave with the added twisted tapes. Different twisting patterns on the twisted tape can

also be investigated to determine the effect changing the twisting pattern has on the flow through the tube.

Appendix A

To analyse the pore sizes of the membranes used in Chapter 3, the Tristar 3000 is used with the settings as per Table A-1.

Table A - 1: BET settings used for the analysis of membrane pores.

Sample Tube	
Sample Tube:	Sample Tube
Stem Diameter:	1/2 inch
Physical volume below mark:	1.0000 cm^3
Use Isothermal Jacket:	Yes
Use Filler Rod:	Yes
Analysis Conditions	
Preparation	
Fast evacuation:	Yes
Evacuation time:	0.10 h
Leak test:	Yes
Leak test duration:	120 s
Free Space	
Free-space type:	Measured
Lower dewar for evacuation:	Yes
Evacuation time:	0.50 h
Outgas test:	Yes
Outgas test duration:	180 s
Po and Temperature	
Po and T type:	Measure Po at intervals during analysis. Enter the Analysis Bath Temperature below.
Po and T type:	Measure Po at intervals during analysis. Enter the Analysis Bath Temperature below.
Temperature:	-195.800 °C
Measurement interval:	120 min
Dosing	
Use first pressure fixed dose:	No
Use maximum volume increment:	No
Target tolerance:	5.0% or 5.000 mmHg
Equilibration	
Equilibration interval:	10 s
Minimum equilibration delay at P/Po >= 0.995:	600 s

Adsorptive Properties	
Adsorptive:	Nitrogen
Maximum manifold pressure:	1050.00 mmHg
Non-ideality factor:	0.0000620
Density conversion factor:	0.0015468
Molecular cross-sectional area:	0.162 nm²

The nanotensile tests are done using the Hysitron Nanotensile 5000 Tester. The images and results shown below are specifically for the membrane with 7.5% CNT loading.

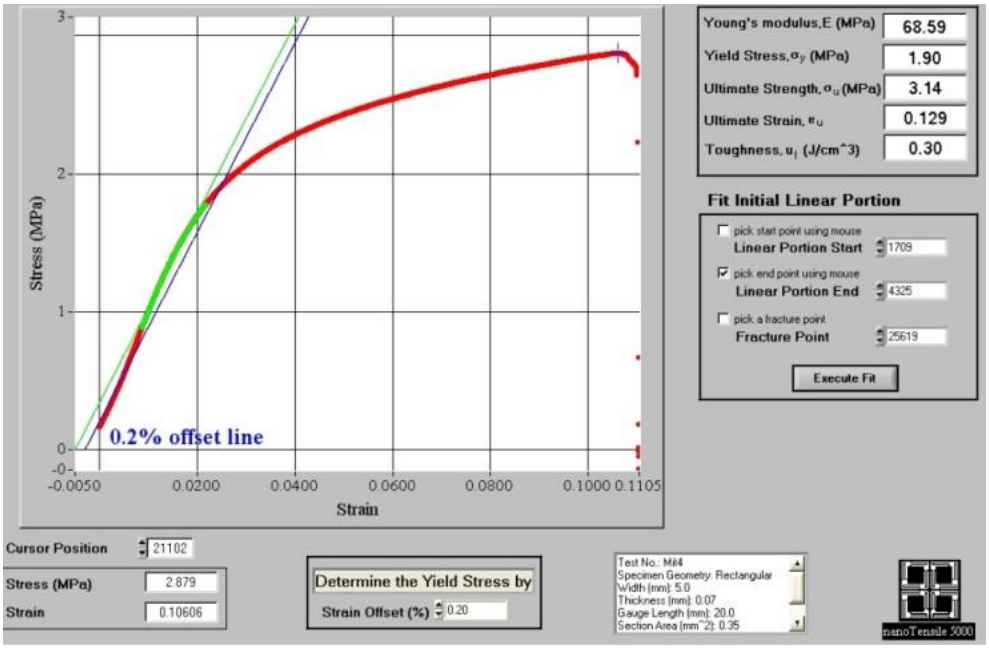

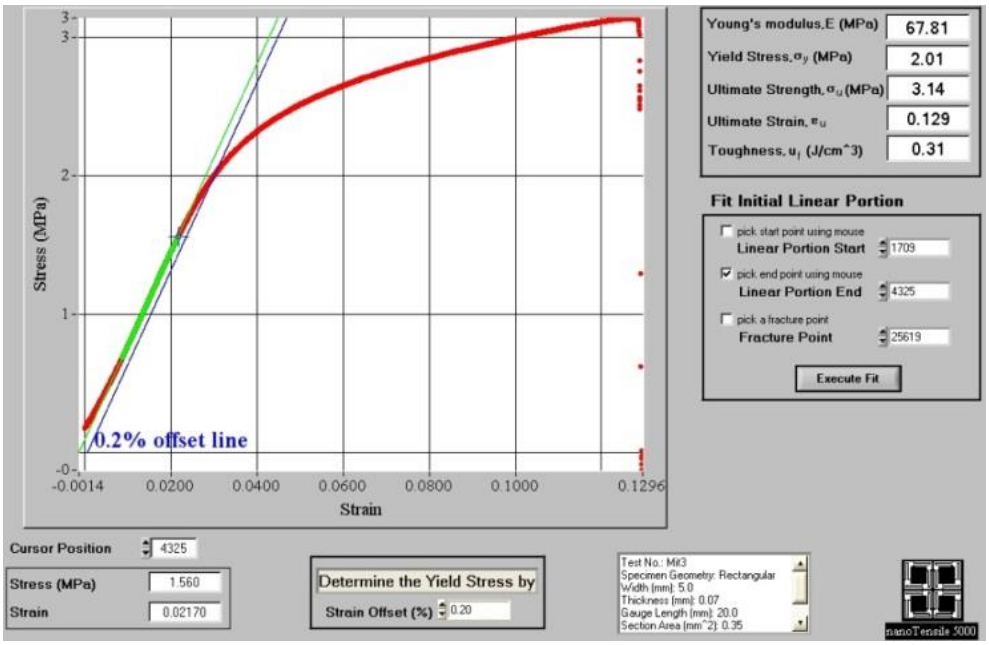

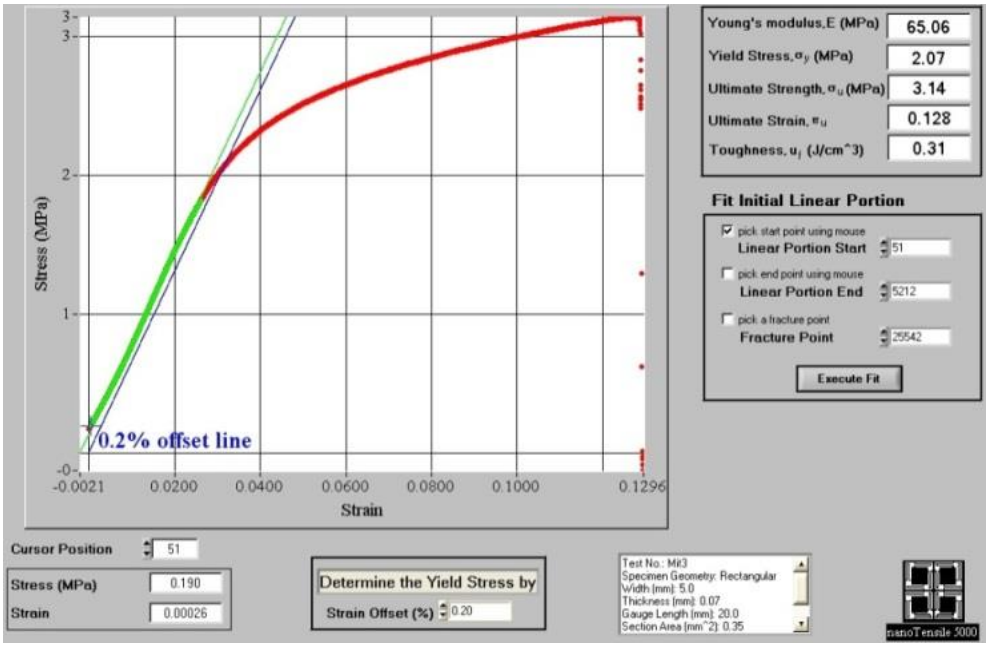

Figure A - 1: The stress strain graphs and data generated for a single test case by the Hystrion Nanotensile tester.

Appendix B

The data that is used to create the neural network in chapter 5 is given in table B-1.

Table B - 1: Filtration data from dead end filtration of oil in water.

Time (min)	Pressure (bar)	CNT (%)	Flux (L/m^{3}h)
10	4	0	270.77
20	4	0	171.49
30	4	0	135.39
40	4	0	108.31
50	4	0	90.26
10	4	5	451.29
20	4	5	266.26
30	4	5	192.55
40	4	5	150.43
50	4	5	129.37
60	4	5	108.31
10	4	10	829.98
20	4	10	539.91
30	4	10	416.91
40	4	10	279.46
50	4	10	187.33
60	4	10	125.57
10	5	0	315.90
20	5	0	230.16
30	5	0	162.46
40	5	0	120.34
50	5	0	102.29
60	5	0	96.28
10	5	5	451.29
20	5	5	288.83
30	5	5	216.62
40	5	5	180.52
50	5	5	156.45
60	5	5	132.38
10	5	10	577.65
20	5	10	406.16
30	5	10	342.98
40	5	10	288.83
50	5	10	270.77

60	5	10	216.62
10	6	0	558.07
20	6	0	306.27
30	6	0	236.15
40	6	0	155.16
50	6	0	112.67
60	6	0	66.99
10	6	5	885.42
20	6	5	457.63
30	6	5	359.98
40	6	5	231.84
50	6	5	180.56
60	6	5	85.29
10	6	10	722.07
20	6	10	424.21
30	6	10	415.19
40	6	10	361.03
50	6	10	324.93
60	6	10	306.88

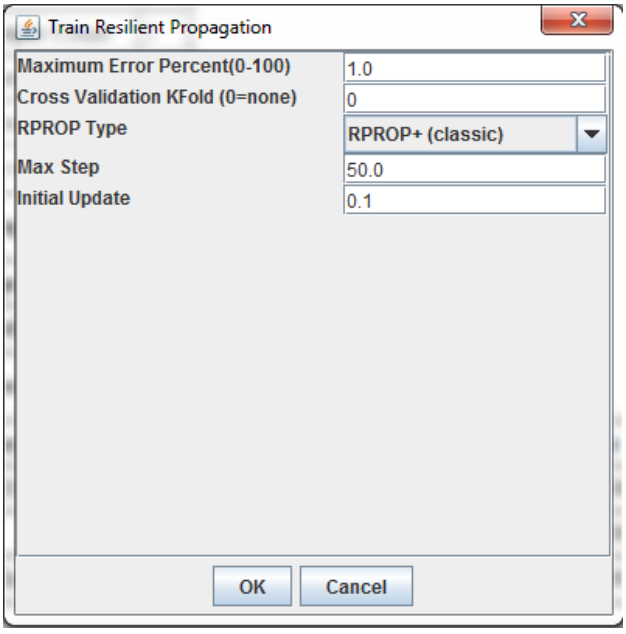

Figure B - 1: Window used to begin neural network training.

Table B - 2: Normalized training data.

Input 1	Input 2	Input 3	Ideal
-0.2	0	0	-0.634
-0.2	0	-1	-0.767
-0.6	0	-1	-0.601
0.2	0	0	-0.723
1.0	1	0	-0.955
0.6	-1	-1	-0.943
-0.6	1	0	-0.045
1.0	0	0	-0.840
1.0	-1	0	-0.899
-1.0	0	0	-0.061
1.0	1	1	-0.414
-1.0	0	-1	-0.392
-1.0	-1	1	0.865
-1.0	-1	-1	-0.502
-0.2	-1	0	-0.693
0.2	-1	0	-0.796
1.0	0	-1	-0.928
0.6	0	-1	-0.914
0.2	-1	1	-0.481
-0.6	0	1	-0.116
-0.6	-1	-1	-0.745
0.6	1	1	-0.370
-0.6	1	1	-0.127
-1.0	-1	0	-0.061
0.2	0	-1	-0.870
-0.2	1	0	-0.284
0.6	0	0	-0.781
-0.2	1	-1	-0.587
-0.2	-1	-1	-0.833
0.2	1	-1	-0.785
0.2	0	1	-0.458
-0.2	0	1	-0.326
0.6	1	-1	-0.888
1.0	-1	1	-0.857
0.6	-1	1	-0.706
-1.0	1	1	0.601
-0.2	-1	1	-0.145
-1.0	1	0	1.000

The resilient training method is used and the Encog window is shown in Figure B-1.

The training progression and the results of the training of the network are presented in figure B-2. The graph depicts the decrease in the different errors as the number of iterations increase.

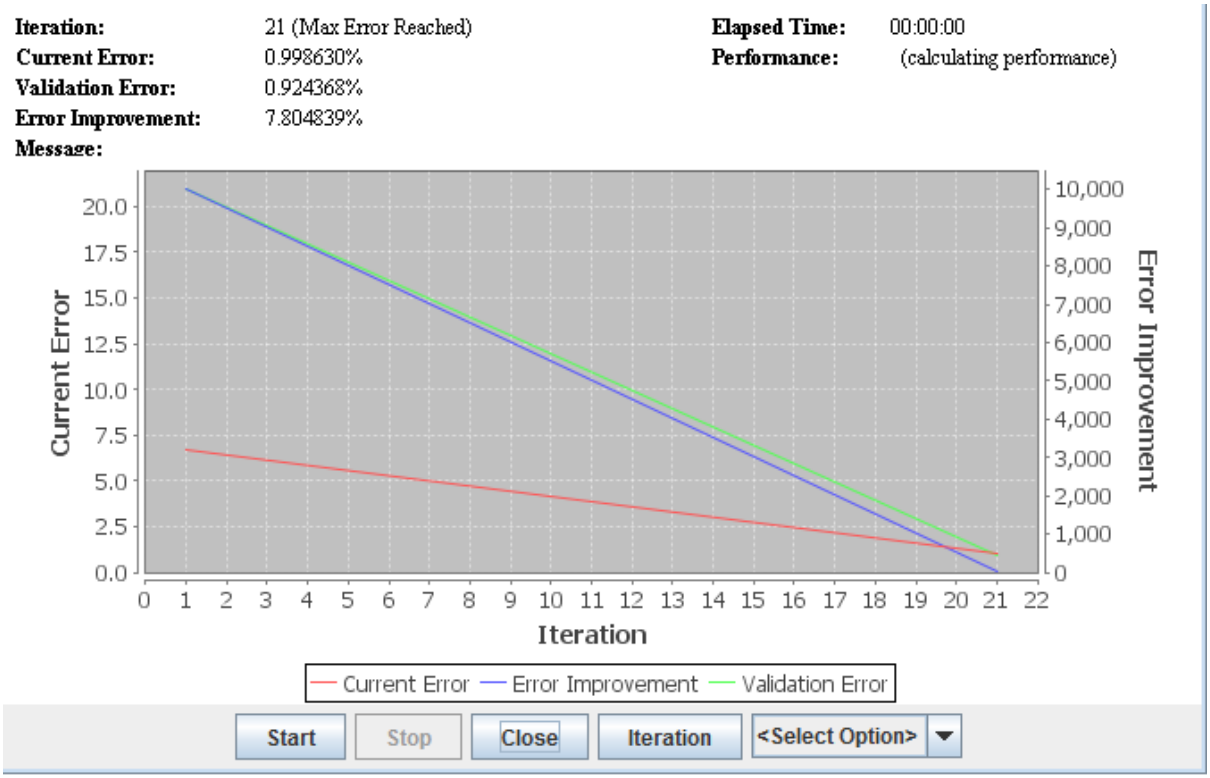

Figure B - 2: Resilient training results showing a decrease in the different errors.

The C# code used to generate the network is given below:

```
using Encog.ML;

using Encog.ML.Factory;

using Encog.Persist;

using Encog.Neural.Networks.Training

using Encog.Neural.Networks.Training.Propagation.Resilient
```

```
namespace EncogGenerated

{

public class EncogExample

    {

public static readonly double[][] INPUT_DATA = {

new double[] { -0.6,0,-1 },

new double[] { -1,0,1 },

new double[] { 1,-1,0 },

new double[] { 0.6000000000000001,1,-1 },

new double[] { -0.6,0,1 },

new double[] { 0.6000000000000001,0,1 },

new double[] { 1,0,0 },

new double[] { 0.6000000000000001,0,-1 },

new double[] { 0.19999999999999996,1,0 },

new double[] { -0.19999999999999996,-1,-1 },

new double[] { -1,1,-1 },
```

new double[] { 1,1,0 },

new double[] { 0.6000000000000001,-1,1 },

new double[] { -1,0,0 },

new double[] { 0.19999999999999996,0,0 },

new double[] { 1,1,-1 },

new double[] { 0.19999999999999996,1,1 },

new double[] { -0.6,0,0 },

new double[] { -0.19999999999999996,-1,1 },

new double[] { -0.19999999999999996,1,0 },

new double[] { 1,0,-1 },

new double[] { 0.6000000000000001,1,1 },

new double[] { 0.6000000000000001,0,0 },

new double[] { -0.6,-1,0 },

new double[] { 0.19999999999999996,0,-1 },

new double[] { 0.6000000000000001,1,0 },

new double[] { -1,1,0 },

new double[] { 0.19999999999999996,1,-1 },

```
new double[] { -1,-1,0 },

new double[] { 0.6000000000000001,-1,0 },

new double[] { 0.19999999999999996,-1,1 },

new double[] { 1,0,1 },

new double[] { -0.6,-1,-1 },

new double[] { -0.19999999999999996,-1,0 },

new double[] { -0.6,1,-1 },

new double[] { 0.19999999999999996,0,1 },

new double[] { -0.19999999999999996,0,-1 },

new double[] { -1,-1,-1 },

new double[] { -0.6,1,0 },

        };



public static readonly double[][] IDEAL_DATA = {

new double[] { -0.6012561529526717 },

new double[] { 0.24791374735661753 },

new double[] { -0.8990170271220077 },
```

new double[] { -0.8883566026194383 },

new double[] { -0.17115711267591827 },

new double[] { -0.5020025283110163 },

new double[] { -0.840200064271839 },

new double[] { -0.9137212677734574 },

new double[] { -0.5971396253100125 },

new double[] { -0.8328479439461142 },

new double[] { 0.200058525007192 },

new double[] { -0.955269888387464 },

new double[] { -0.7059131662528897 },

new double[] { -0.06087530730130575 },

new double[] { -0.7225661385715016 },

new double[] { -1 },

new double[] { -0.28143891780616104 },

new double[] { -0.45788980611229724 },

new double[] { -0.14488480294577466 },

new double[] { -0.2840012866625389 },

new double[] { -0.9284255084493441 },

new double[] { -0.36966436195922914 },

new double[] { -0.7813831014216703 },

new double[] { -0.5130307087996036 },

new double[] { -0.8696085455747384 },

new double[] { -0.7224608674931208 },

new double[] { 1 },

new double[] { -0.7845194670240283 },

new double[] { -0.06087530730130575 },

new double[] { -0.8475521845975639 },

new double[] { -0.4807655609421232 },

new double[] { -0.6343406944184335 },

new double[] { -0.744622499793046 },

new double[] { -0.6931576572686022 },

new double[] { -0.4152504567399379 },

new double[] { -0.45788980611229724 },

new double[] { -0.7666788607702206 },

```
new double[] { -0.5020025283110163 },
new double[] { -0.04538555930969135 },
        };

public static MLDataSet createTraining() {
            IMLDataSet result = new BasicMLDataSet(INPUT_DATA,IDEAL_DATA);
return result;
        }
public static IMLMethod createNetwork()
        {
            MLMethodFactory methodFactory = new MLMethodFactory();
            IMLMethod result = methodFactory.Create("feedforward","3:B->TANH->13:B->TANH->1", 0, 0);
            ((IMLEncodable)result).DecodeFromArray(WEIGHTS);
return result;
        }

static void Main(string[] args)
```

```
        {
            IMLDataSet trainingData = createTraining();
            IMLMethod method = createNetwork();
            ITrain training = new ResilientPropagation(method, trainingData);
for (int epoch = 0; epoch < 10000; epoch++)
              {
training.Iteration();
if (training.Error < 0.01) break;
        }
    }
}
```

The Matlab code used to train, validate and test the neural network is given below:

```
% Solve an Input-Output Fitting problem with a Neural Network
% Script generated by NFTOOL
% Created Sun Mar 16 13:17:51 CAT 2014
%
% This script assumes these variables are defined:
%
%   inputdata - input data.
%   outputdata - target data.
inputdata =  [0 5   0;
4   5   0;
8   5   0;
12  5   0;
16  5   0;
20  5   0;
24  5   0;
28  5   0;
32  5   0;
```

```
0   5   0;
4   5   0;
8   5   0;
12  5   0;
16  5   0;
20  5   0;
24  5   0;
28  5   0;
32  5   0;
0   5   10;
4   5   10;
8   5   10;
12  5   10;
16  5   10;
20  5   10;
24  5   10;
28  5   10;
32  5   10;
0   5   5;
4   5   5;
8   5   5;
12  5   5;
16  5   5;
20  5   5;
24  5   5;
28  5   5;
32  5   5;
0   5   7.5;
4   5   7.5;
8   5   7.5;
12  5   7.5;
16  5   7.5;
20  5   7.5;
0   5   7.5;
4   5   7.5;
8   5   7.5;
12  5   7.5;
16  5   7.5;
20  5   7.5;
24  5   7.5;
28  5   7.5;
0   6   0;
10  6   0;
20  6   0;
30  6   0;
40  6   0;
0   6   5;
10  6   5;
20  6   5;
30  6   5;
40  6   5;
50  6   5;
60  6   5;
0   6   10;
10  6   10;
20  6   10;
30  6   10;
```

```
40  6   10;
50  6   10;
60  6   10;
0   4   5;
10  4   5;
20  4   5;
30  4   5;
40  4   5;
50  4   5;
60  4   5;
0   4   10;
10  4   10;
20  4   10;
30  4   10;
40  4   10;
50  4   10;
60  4   10;
0   4   5;
10  4   5;
20  4   5;
30  4   5;
40  4   5;
50  4   5;
60  4   5;
];

outputdata = [1660.749744
866.4781274
577.652085
433.2390637
361.0325531
288.8260425
281.6053914
252.7227872
225.6453457
1732.956255
722.0651062
505.4455743
433.2390637
342.9809254
297.8518563
270.7744148
252.7227872
225.6453457
4693.42319
1227.510681
830.3748721
685.9618509
577.652085
523.497202
469.342319
433.2390637
397.1358084
4061.616222
1480.233468
866.4781274
667.9102232
```

541.5488297
469.342319
415.1874361
370.0583669
342.9809254
541.5488297
342.9809254
270.7744148
234.6711595
216.6195319
198.5679042
758.1683615
433.2390637
324.9292978
288.8260425
252.7227872
225.6453457
207.593718
189.5420904
270.7744148
171.4904627
135.3872074
108.3097659
90.25813828
3321.499489
722.0651062
424.2132499
415.1874361
361.0325531
324.9292978
306.8776701
2166.195319
451.2906914
288.8260425
216.6195319
180.5162766
156.4474397
132.3786028
1444.130212
577.652085
406.1616222
342.9809254
288.8260425
270.7744148
216.6195319
2166.195319
315.903484
230.1582526
162.4646489
120.3441844
102.2925567
96.27534749
2166.195319
451.2906914
266.2615079
192.550695
150.4302305

```
129.3699982
108.3097659
];
inputs = inputdata';
targets = outputdata';

% Create a Fitting Network
hiddenLayerSize = 13;
net = fitnet(hiddenLayerSize);

% Choose Input and Output Pre/Post-Processing Functions
% For a list of all processing functions type: help nnprocess
net.inputs{1}.processFcns = {'removeconstantrows','mapminmax'};
net.outputs{2}.processFcns = {'removeconstantrows','mapminmax'};


% Setup Division of Data for Training, Validation, Testing
% For a list of all data division functions type: help nndivide
net.divideFcn = 'dividerand';  % Divide data randomly
net.divideMode = 'sample';  % Divide up every sample
net.divideParam.trainRatio = 70/100;
net.divideParam.valRatio = 15/100;
net.divideParam.testRatio = 15/100;

% For help on training function 'trainlm' type: help trainlm
% For a list of all training functions type: help nntrain
net.trainFcn = 'trainlm';  % Levenberg-Marquardt

% Choose a Performance Function
% For a list of all performance functions type: help nnperformance
net.performFcn = 'mse';  % Mean squared error

% Choose Plot Functions
% For a list of all plot functions type: help nnplot
net.plotFcns = {'plotperform','plottrainstate','ploterrhist', ...
  'plotregression', 'plotfit'};


% Train the Network
[net,tr] = train(net,inputs,targets);

% Test the Network
outputs = net(inputs);
errors = gsubtract(targets,outputs);
performance = perform(net,targets,outputs)

% Recalculate Training, Validation and Test Performance
trainTargets = targets .* tr.trainMask{1};
valTargets = targets  .* tr.valMask{1};
testTargets = targets  .* tr.testMask{1};
trainPerformance = perform(net,trainTargets,outputs)
valPerformance = perform(net,valTargets,outputs)
testPerformance = perform(net,testTargets,outputs)
```

```
% View the Network
view(net)

% Plots
% Uncomment these lines to enable various plots.
%figure, plotperform(tr)
%figure, plottrainstate(tr)
%figure, plotfit(net,inputs,targets)
%figure, plotregression(targets,outputs)
%figure, ploterrhist(errors)
```

The neural network created by the above code is trained using the Levenberg-Marquardt training algorithm and the iteration termination condition is determined by the mean squared error.

The code used to do a grid search for the highest cumulative flux output for a given time period is found below:

```
InputSave = [0 0];
CNTLoopCount = 0;
for CNT = 0:0.2:10
    CNTLoopCount = CNTLoopCount + 1;
    LoopCount = 0;
    for Pressure = 0:0.2:10
        LoopCount = LoopCount + 1;
        SumY = 0;
        for Time = 1:1:100
            Y = net([Time; Pressure; CNT]);
            if Y < 0
                Y = 0;
            end
            SumY = SumY + Y;
        end
        InputSave(LoopCount,1) = Pressure;
        OutputSave(LoopCount, CNTLoopCount) = SumY;
    end
        InputSave(CNTLoopCount,2) = CNT;
end
```

Appendix C

The tables calculating the Reynold's number of the flow of the oil/water mixture in a tube with and without a twisted tape added is given below.

Table C - 1: Reynold's number calculation for no twisted tape.

No twisted tape				
Q	4.71×10^{-5}	m^3/s		
v	0.267	m/s		
D	15	mm	0.015	m
ρ	1	kg/L		
μ	1	cP		
kine μ	0.801	mm^2/s	8.01×10^{-7}	m^2/s
area	1.77×10^{-4}	m^2		
Re	4001			

where Q is the flowrate, v is the velocity, D is the tube diameter, ρ is the density, μ is the viscosity, kine μ is the kinematic viscosity and Re is the Reynold's number.

Table C - 2: Reynold's number calculation for twisted tape.

Twisted tape				
D_{tp}	15	mm	0.015	m
L_e	18	mm	0.018	m
O_{tp}	1.2			
K_L	1.323631			
D	0.015			
δ_{tp}	0.7	mm	0.0007	m
K_a	0.940582			
v_{ac}	0.375417			
Re	5631			

where D_{tp} is the tape diameter, L_e is the twist length of the tape, O_{tp} is the ratio of the tape diameter and L_e, K_L is the description of a particle travelling along the edge of the tape, δ_{tp} is the tape thickness, K_a is the finite element of the helical area of the tape and v_{ac} is the actual velocity.

Table C - 3: Values used to calculate fouling resistance.

	Tape		No Tape
Rw	117665.0547	m^{-1}	117665.0547
Rp	142725.8351	m^{-1}	246195.0554
Rf	25060.78043	m^{-1}	128530.0008
TMP	100	kPa	100
μ_w, μ_p	0.000798	Pas	0.00798

where R_w is the membrane resistance, R_p is the resistance of the membrane in relation to the permeate, R_f is the fouling resistance, TMP is the trans-membrane pressure and μ_w and μ_p is the viscosity of water and permeate respectively.

Appendix D

Creative Commons

The request you have made is considered to be non-commercial/educational. As the article you have requested has been distributed under a Creative Commons license (Attribution-Noncommercial 2.5), you may reuse this material for non-commercial/educational purposes without obtaining additional permission from Nature Publishing Group, providing that the author and the original source of publication are fully acknowledged.

For full terms and conditions of the Creative Commons license, please see the attached link http://creativecommons.org/licenses/by-nc/2.5